11-21-2022

Synthetic Amphiphiles as Antibiotic Potentiators

Helena Spikes
University of Missouri-St. Louis, helenaspikes@gmail.com

Synthetic Amphiphiles as Antimicrobial Potentiators

Helena J. Spikes

M.S. Biochemistry and Biotechnology, UMSL 2019

B.S. Biochemistry and Biotechnology, UMSL 2019

A dissertation submitted to the Graduate School at the

University of Missouri-St. Louis

in partial fulfillment of the requirements for the degree

Doctor of Philosophy

in

Chemistry

December 2022

Advisory Committee

George W. Gokel, Ph.D.

Chairperson

Bruce Hamper, Ph.D.

Michael R. Nichols, Ph.D.

Wendy Olivas, Ph.D.

ABSTRACT OF THE DISSERTATION

Synthetic Amphiphiles as Antimicrobial Potentiators

By

Helena J. Spikes

Doctor of Philosophy in Chemistry

University of Missouri-St. Louis 2022

Dr. George W. Gokel, Advisor

Antibiotic resistance has become a massive threat to modern medicine. Bacteria acquire resistance either through genetic mutations or mobile genetic elements, such as plasmids. The growing resistance crisis is exacerbated by over-prescription of antibiotics and improper use. As antimicrobial resistance becomes more widespread, superbugs (bacteria resistant to more than one class of drug) have evolved. Since few new drugs reach clinical trials and even fewer are approved by the FDA, we must find a way to make existing drugs more potent. One technique to accomplish this is by using combination therapy. By administering two or more drugs at a time, their combined effect can be greater than that of the individual drugs.

Lariat ethers (LEs) and their salts have shown activity against a variety of bacteria, including multi-drug resistant pathogens such as *K. pneumoniae* and methicillin-resistant *S. aureus* (MRSA). LEs have also been shown to reverse resistance in tetracycline-resistant *E. coli*. Their intrinsic bactericidal activity and resistance reversal ability are mainly thought to occur by enhanced membrane permeability and disrupted ion homeostasis. However, neutron reflectometry suggests that a supramolecular complex may form between tetracycline and the LE.

In this work, a set of LEs and their salts were examined for supramolecular complexation of clinically relevant drugs using nuclear magnetic resonance (NMR) and dynamic light scattering (DLS). Additionally, the same combinations were screened for *in vitro* combination activity.

(Bis)-Tryptophans are a class of amphiphile prepared by the Gokel Lab, which are composed of an alkyl or phenylene spacer that links two terminal tryptophan residues. These compounds have shown activity against Gram +/- bacteria, as well as the eukaryote *Saccharomyces cerevisiae*, in the low micromolar range and have been demonstrated to be non-cytotoxic. For these reasons, a variety of structures have been proposed to expand the library of (Bis)-Tryptophans.

Summary and Contributions

The majority of the work reported herein was completed by the author. This section details contributions to the experimental work undertaken as part of this dissertation.

Chapter 2. I performed all NMR and DLS studies, with the assistance of Baylor Smith, an undergraduate in the Gokel Lab. I performed all checkerboard experiments.

Chapter 3. I performed all chemical syntheses and NMR. Dr. Rensheng Luo, in the mass spectrometry facility at UMSL, assisted with collecting mass spec data. Biological screening was conducted with the aid of Bobby Bailey, a coworker in the Gokel Lab.

Acknowledgements

Many people have helped me on this long academic journey, and there isn't enough space to adequately express my gratitude to all of them for their advice and encouragement. I would like to thank them all.

First, I am tremendously grateful to my advisor Dr. George W. Gokel. From the moment I joined his lab, he has never been anything but encouraging. Words cannot express the depths of my appreciation for him. He has been a compassionate mentor in both my professional and personal life. I am honored to have worked with him, and I owe a great deal of my professional and scientific development to this man. I would not have the scientific perspective and understanding that I have today, if not for Dr. Gokel.

Next, I would like to thank the members of my committee, Dr. Bruce Hamper, Dr. Mike Nichols, and Dr. Wendy Olivas. With these professors, I have had many enlightening conversations about my research. At times, they have donated materials to further my research, and other times they've given me their expertise about techniques with which I was unfamiliar. Additionally, many members of the Gokel Lab have contributed significantly to this process. I am grateful to my coworkers Michael R. Gokel, Dr. Mohit Patel, Dr. Saeedeh Negin, Bobby Bailey, and Baylor Smith.

I dedicate this Ph.D. dissertation to my father. Although he is no longer here, his unwavering faith in me has inspired me to persevere in the face of many obstacles. I would be remiss in not mentioning the enduring love and encouragement from my grandfather, aunt, and uncle, which have proved essential to my success and happiness.

Table of Contents

Page

Dissertation Abstract.....ii

Summary and Contributions.....iv

Acknowledgements.....v

Table of Contents.....vi

List of Figures and Tables.....viii

Chapter 1. Introduction.....1

Antimicrobial resistance and mechanisms.....2

Crown ether functionality.....8

Bis-Tryptophans.....30

Resensitization to antibiotics.....36

Chapter 2. Supramolecule Formation Between LEs and Antibiotics.....39

Introduction.....40

Experimental Design.....47

Results and Discussion.....48

Complexation of tetracycline derivatives by LEs.....49

Complexation of other antibiotic classes.....59

Aggregation of dialkyl LEs.....63

Antimicrobial activity against resistant bacteria.....72

Mechanistic Information and Speculation.....76

Conclusion.....78

Chapter 3. Structure Activity Relationship of Bis-Tryptophans.....81

Introduction.....82

Target Structures and Experimental Details.....90

Results and Discussion.....93

Aliphatic BTs.....94

Aromatic BTs.....99

Conclusion.....102

Chapter 4. Further Research.....108

Chapter 5. Experimental Details.....115

Dynamic Light Scattering (DLS).....115

Synthesis and Characterization.....115

Bacterial Cultures and MIC Determination.....119

Checkerboard Experiments.....120

Chapter 6. References.....122

Appendix 1. Group 14 Metallafluorenes as Sensitive Luminescent Probes of Surfactants in Aqueous Solution.....132

Appendix 2. Group 14 Metallafluorenes for Lipid Structure Detection and Cellular Imaging.....142

List of Figures and Tables

Chapter 1

Figure 1-1 ..... Decline in antibiotic development.....2

Figure 1-2 ..... Distribution of resistant isolates of MRSA.....4

Figure 1-3 ..... Distribution of resistant isolates of *K. pneumoniae*.....4

Figure 1-4 ..... Mechanisms of antibiotic resistance 6

Figure 1-5 ..... Cation complexation with an LE 9

Figure 1-6 ..... Cation complexation with crown ethers and cryptands 10

Table 1-1 ..... Bind and release kinetics for 18-crown-6 ether and potassium.....12

Figure 1-7 ..... Structure of valinomycin 11

Figure 1-8 ..... Structures of carbon- and nitrogen-pivot lariat ethers.....13

Figure 1-9 ..... Two-armed vs one-armed LE complexation of KI.....14

Figure 1-10 ..... MICs of dialkyl LEs against Gram -/+ bacteria and yeast.....15

Figure 1-11 ..... Ion transport of LEs 16

Figure 1-12 ..... An efflux pump within a bilayer membrane 17

Figure 1-13 ..... Ion channel activity of C_8LE and C_{11}LE.....18

Figure 1-14 ..... Potential orientation of LEs in a membrane.....19

Figure 1-15 ..... 3-, 4-, or 5-membered aggregates of LEs.....20

Table 1-2 ..... Combination activity between LEs and antibiotics in DH5α.....21

Figure 1-16 ..... Structures of LE freebases and salts.....22

Table 1-3 ..... MICs of Les against DH5α.....23

Table 1-4 ..... MICs of LEs and antibiotics against K12, *S. aureus*, and Tet^R.....24

Figure 1-17 ..... MICs of LE freebases and salts against DH5α *E. coli*.....23

Figure 1-18 ..... Effect of LEs on membrane permeability.....26

Figure 1-19 ..... Effect of LEs on membrane depolarization.....26

Figure 1-20 ..... Hydraphile structure.....27

Figure 1-21 ..... Polarity regimes of a bilayer membrane.....28

Figure 1-22 ..... Original hydraphile design concept.....29

Figure 1-23 ..... Actual channel structure of hydraphiles.....30

Figure 1-24 ..... Ribbon structure of KcsA channel.....31

Figure 1-25 ..... Structures of *n*-alkylindoles.....32

Figure 1-26 ..... Bis-tryptophan template.....32

Figure 1-27 ..... Initial bis-tryptophan structures.....33

Table 1-5 ..... MICs of BTs against K12.....35

Figure 1-28 ..... Ion channel activity of m-phenylene BT.....36

Figure 1-29 ..... Structures of amoxicillin and clavulanic acid.....37

Chapter 2

Figure 2-1 ..... Structure of 15-crown-5 and 18-crown-6 ethers.....40

Figure 2-2 ..... U-tube for ion transport studies.....44

Figure 2-3 ..... Crystal structure of NaI complexation by C_{12}LE.....44

Figure 2-4 ..... Same as Figure 1-10, duplicated for convenience.....45

Figure 2-5 ..... Structure of tetracycline and C_{10}LE.....47

Figure 2-6 ..... Solubilization of tetracycline by C_{10}LE.....49

Figure 2-7 ..... NMR complexation of tetracycline by C_{10}LE in $CDCl_3$.....50

Figure 2-8 ..... NMR complexation of tetracycline by C_{10}LE in D_2O.....51

Figure 2-9 ..... FTIR complexation of tetracycline by C_{10}LE.....52

Figure 2-10 ..... Structures of tetracycline derivatives.....53

Table 2-1 ..... Complexation ratios between C10LE and tetracycline derivatives.....54

Figure 2-11 ..... Crystal structure of tetracycline hydrochloride.....56

Figure 2-12 ..... Tetracycline numbering.....57

Figure 2-13 ..... Crystal structures of tetracycline and chlortetracycline.....57

Table 2-3 ..... Complexation of tetracycline and minocycline by *n*-alkyl LEs.....58

Figure 2-14 ..... Structures of various antibiotics.....59

Table 2-2 ..... Complexation ratios between *n*-alkyl LEs and antibiotics.....60

Figure 2-15 ..... Duplicated from Figure 1-16 for convenience.....61

Table 2-4 ..... MICs of LE freebases and salts against DH5α.....61

Table 2-5 ..... Complexation ratios of LE salts and antibiotics.....62

Figure 2-16 ..... Aggregation of C_{12}LE and tetracycline in MQ H_2O.....65

Figure 2-17 ..... Aggregation of C_{12}LE in MQ H_2O and buffer.....66

Figure 2-18 ..... Aggregation of C_{12}LE with tetracycline.....67

Figure 2-19 ..... Complexation of NaI by C_{12}LE.....68

Figure 2-20 ..... Particle size analysis of C_{12}LE with tetracycline derivatives.....69

Figure 2-21 ..... Particle size analysis of C_{14}LE with tetracycline derivatives.....70

Figure 2-22 ..... Particle size analysis of C_{12}LE with antibiotic suite.....71

Figure 2-23 ..... Particle size analysis of C_{14}LE with antibiotic suite.....71

Figure 2-24 ..... Comparison between NMR complexation and aggregation inhibition.....73

Table 2-6 ..... MICs of antibiotics against resistant bacteria.....74

Table 2-7 ..... MICs of LEs against resistant bacteria.....75

Table 2-8 ..... Combination activity between LE methiodides and antibiotics.....76

Figure 2-25 ..... Proposed hydrogen bonding between C_{10}LE and tetracyclines.....78

Figure 2-26.....Framework structure of Crown:Tet complex.....80

Chapter 3

Figure 3-1 ..... Duplicated from Figure 1-25 for convenience.....83

Table 3-1 ..... Particle sizes of *n*-alkylindoles.....84

Figure 3-2 ..... Structures of original BTs.....86

Table 3-2 ..... MICs of initial BT library.....87

Figure 3-3 ..... Cytotoxicity of BTs against three mammalian lines.....88

Table 3-3 ..... Recovery of tetracycline potency in Tet^R by BTs.....89

Figure 3-4 ..... Membrane permeabilization by BTs.....90

Figure 3-5 ..... Channel behavior of m-phenylene BT.....91

Figure 3-6 ..... Proposed BT structures to expand library.....92

Scheme 3-1 ... Coupling reaction of Boc-protected tryptophan and diamines.....93

Scheme 3-2 ... Deprotection of Boc-protected product.....93

Figure 3-7 ..... Particle size analysis of short aliphatic BTs.....96

Figure 3-8 ..... Particle size analysis of long aliphatic BTs.....97

Figure 3-9 ..... Correlation of aggregation with antibacterial activity.....98

Table 3-4 ..... Log Ps, aggregate sizes, and MICs of aliphatic BT.....99

Figure 3-10 ..... Particle size analysis of phenylene BTs.....101

Figure 3-11 ..... Particle size analysis of poly-ring BTs.....102

Table 3-5 ..... Log Ps, aggregate sizes, and MICs of aromatic BTs.....103

Chapter 4

Figure 4-1.....Proposed structure of tetrasubstituted crown ether for FRET.....112

Figure 4-2.....Proposed structure of redox tetrasubstituted crown ether.....113

Chapter 1

Introduction

1.1 Antimicrobial Resistance

Statistics The overarching theme of this dissertation concerns the worldwide antimicrobial resistance (AMR) crisis. After the Second World War when penicillin saw widespread use, it seemed that microbial infections had become a thing of the past. By the 1960s declarations appeared in the popular press suggesting that the war on microbes had been won.[1,2] Sadly, however, the emergence of antibiotic resistance has significantly reversed the trend of this battle.[2] At present, there is some form of resistance by some organism to all commercial antimicrobials. The need for new antibiotics is critical and the rate of development has diminished in recent decades. A table adapted from the monograph *Antibiotics: The Perfect Storm* is shown in Figure 1-1.[1]

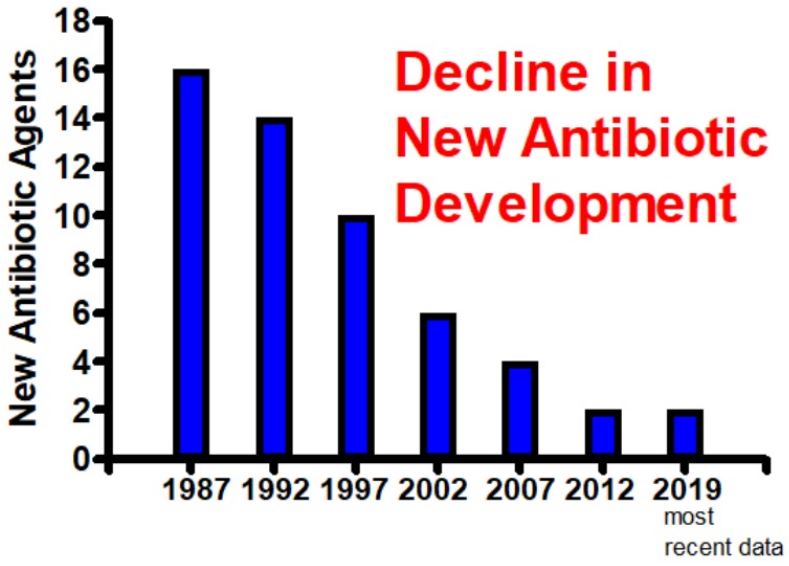

Figure 1-1. Graph depicting the decline in antibiotic development during the past three decades.[1]

A biological arms race with bacteria was unavoidable; humans want to treat and cure bacterial infections, while the bacteria simply want to live.[3,4] However, this race is accelerated by the excessive and overuse of antibiotics. We have entered a

post-antibiotic era, where an infection may be deadly due to a lack of suitable treatment.[5–7] Environments such as hospitals present a breeding ground for resistance and multi-drug resistant "superbugs". Highly susceptible individuals are concentrated in one location, which enables bacteria to swiftly move from one host to the next. Additionally, antibiotics are commonly prescribed in hospitals, even for nonbacterial infections, which simply selects for resistant bacteria. Finally, bacteria can easily share plasmids containing multiple resistance genes. This results in the evolution of superbugs, which are resistant to at least three classes of antimicrobial agents.

Although caused by a viral infection, this was recently highlighted during the Covid-19 pandemic which took the lives of over six million people.[8] During this pandemic, hospitalization rates soared along with the duration of the hospital stay. While hospitalized, the rates for patients who required catheters and ventilators also increased.[9] Combined with global supply chain issues which reduced the availability of personal protective equipment, it comes as no surprise that "resistant hospital-onset infections and deaths increased **at least** 15% during the first year of the pandemic," according to a special report by the CDC in 2022.[10] In some cases, such as carbapenem-resistant *Acinetobacter*, infection rates have increased about 80%.[10] Global health threats, like the Covid-19 pandemic, put additional pressure on resistant bacteria to spread and set back efforts to combat AMR.

The effects of antibiotic resistance, in terms of public health and economic costs, are difficult to quantify, especially in rural areas with limited access to healthcare.[7] Most studies are limited to a region or demographic; however, a global analysis was conducted in 2019 and recently published. They showed that 4.95 million deaths were attributed to antimicrobial resistance in 2019, making AMR a leading cause of death.[11] Additionally, they found that roughly 3.57 million of these deaths were attributed to just six pathogens: *Escherichia coli, Staphylococcus*

aureus, Klebsiella pneumoniae, Streptococcus pneumoniae, Acinetobacter baumannii, and *Pseudomonas aeruginosa*. To further emphasize the extensive threat of antimicrobial resistance, a world map designating percent resistance in *S. aureus* and third-generation *K. pneumoniae* found in clinical isolates are shown in Figure 1-2 and Figure 1-3, respectively.

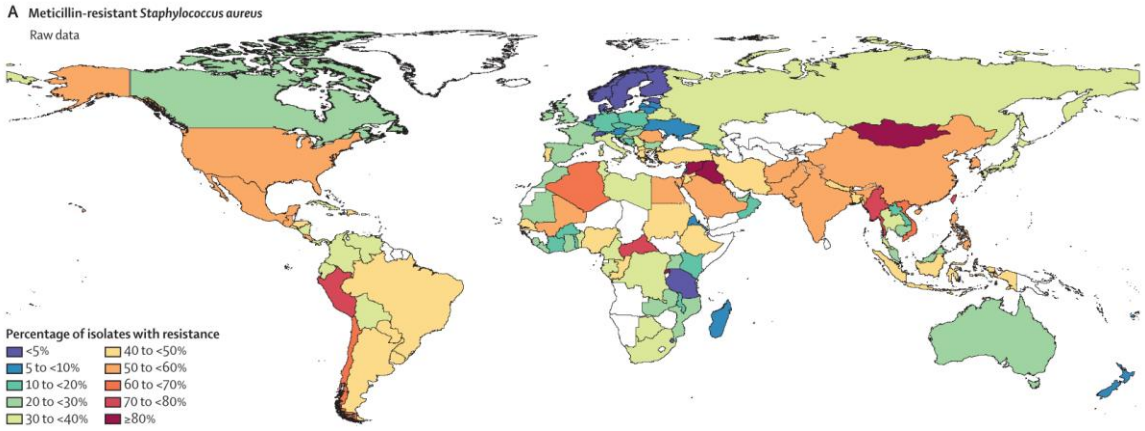

Figure 1-2. Map showing the distribution of resistant isolates of methicillin-resistant *S. aureus*. [11] Adapted from Figure 7 in reference 9.

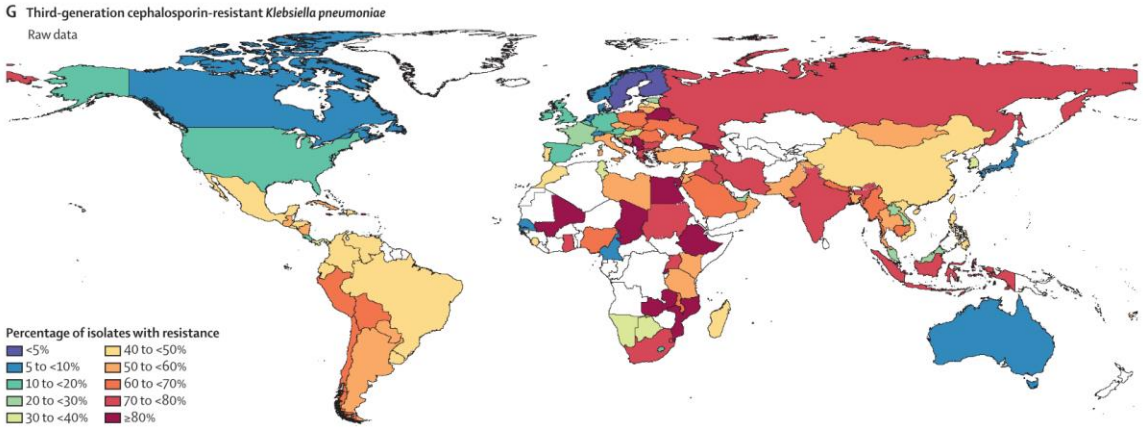

Figure 1-3 Map showing distribution of resistant isolates of cephalosporin-resistant *K. pneumoniae*.[11] Adapted from Figure 7 in reference 9.

Both Figure 1-2 and Figure 1-3 clearly show that resistance rates appear to be globally at least 20% for each species. Particularly for *K. pneumoniae,* rates commonly exceed 70% resistance in clinical isolates.[11]

In 2017, the World Health Organization (WHO) published a list of resistant bacteria to help focus research efforts.[12] The species were subsequently ranked based on priority; the highest priority species are referred to as ESKAPE pathogens. ESKAPE is an acronym of the six highest priority species: ***E****nterococcus faecium,* ***S****taphylococcus aureus,* ***K****lebsiella pneumoniae,* ***A****cinetobacter baumannii,* ***P****seudomonas aeruginosa,* and ***E****nterobacter* species.[13] In fact, the species' responsible for about 70% of AMR-related deaths in 2019 were ESKAPE pathogens, except AMR-*E. coli* which has been separately recognized as a threat to public health.[13] More than ever, global health is in dire need of a new strategy to fight against AMR.

Mechanisms of Resistance Bacteria have many ways in which they can become resistant to antibiotics, but these can generally be described in four categories: 1) prevention of cell entry, such as the formation of a biofilm; 2) inactivation of antibiotic, usually through hydrolysis; 3) mutation of antibiotic target, such as penicillin binding proteins; 4) expulsion of the antibiotic from the cell using efflux pumps. Examples of these mechanisms are depicted in Figure 1-4.[13,14]

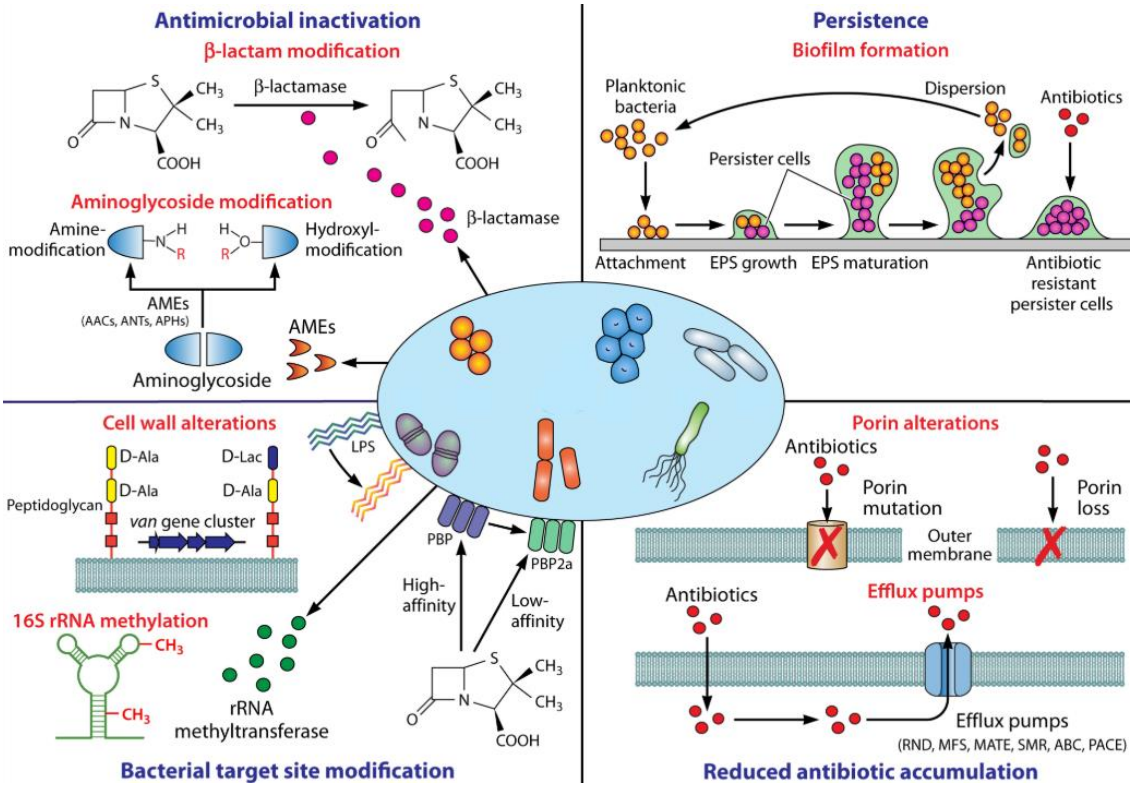

Figure 1-4 Mechanisms of antimicrobial resistance.[13]

Although single-celled, bacteria can associate with each other to form biofilms. In biofilms, the cells stick to each other within an extracellular matrix composed of proteins, nucleic acids, and other polymers.[15] It has been noted that bacteria in a biofilm are markedly less susceptible to antibiotics than planktonic bacteria, which could be due to several reasons.[16,17] This extracellular matrix that makes up part of the biofilm makes it more difficult for antimicrobial agents to reach the target cells. The bacteria may also be able to secrete antibiotic-modifying enzymes into the matrix. Differences in metabolic state and gene expression may also contribute to persistence of biofilms because cells on the interior of the biofilm will be in a starkly different environment than those along the periphery. It is also possible for multiple species of bacteria to exist within one biofilm. This increases the frequency of horizontal gene transfer, increasing the transmission of resistance genes between bacteria.[15]

Antimicrobial activity is dependent on structure. When the structure changes, so does the activity. Resistant bacteria frequently express antibiotic-modifying enzymes, such as beta-lactamases and aminoglycoside-modifying enzymes (AMEs).[13] Beta-lactamases are enzymes which cleave the four-membered beta-lactam ring found in penicillin and its derivatives. Extended-spectrum beta-lactamases show activity against other beta-lactam antibiotics, such as cephalosporins and carbapenems.[18,19] These enzymes are more common in Gram negative bacteria and localize in the periplasm. This allows the penicillin to be degraded before reaching its target, the penicillin binding protein. [20,21]

Rather than destroy their target, AMEs covalently modify the antibiotic. Aminoglycosides affect their activity by binding to the A site of the ribosome and promoting mistranslation.[22] By acylating free amines and free hydroxyl groups on the aminoglycoside, ribosome binding is inhibited or diminished. [23] These examples are shown in the upper left panel of Figure 1-4.

Much like antimicrobial activity is dependent on the structure of the antimicrobial agent, it is also dependent on the structure of the biological target. When the antibiotic can no longer bind its target, it ceases to have any activity. This mechanism of resistance is most common for penicillin derivatives, fluoroquinolones, and macrolides.[13]

Penicillin derivatives bind to penicillin-binding proteins, which are transpeptidases essential for cell wall synthesis.[18] Alterations of these proteins prevent binding of penicillin, leading to resistance. Fluoroquinolones inhibit DNA synthesis and repair by binding to DNA-bound topoisomerases and preventing their progression along the replication fork.[24] Increased mutations along the quinolone-binding domain confer resistance to this class of antibiotic.

Limiting the residence time of an antibiotic in the cell will reduce its ability to damage the bacteria, which is why many bacteria possess efflux pumps. These pumps are transmembrane proteins which eject antibiotics from the cells, by coupling this process with ATP hydrolysis or generation of an ion gradient.[25,26] This mechanism of resistance will be the most significant, given the context of this dissertation. It is also diagrammed in the lower right panel of Figure 1-4.

The sensitivity of cells to changes in their ion balance is particularly important in the regulation of tetracycline resistance. Tetracycline enters cells by simple diffusion; in sensitive cells, it binds to the ribosome and inhibits protein synthesis.[27] Very often, clinically relevant strains of Gram-negative bacteria achieve resistance using a TetA efflux pump, which is an $H^+/[Tet•M]^+$ antiporter.[28] This protein pumps protons into the cell, while simultaneously ejecting a tetracycline-metal complex, typically a divalent cation such as magnesium. Expression of this protein is highly regulated because overexpression is detrimental to the cell. There is a fine balance where the cell must quickly detect tetracycline and produce the TetA efflux pump before the tetracycline builds up and begins to inhibit protein synthesis. Once the tetracycline is removed from the cell, the pump must be quickly degraded to avoid enhanced osmotic sensitivity.[29]

This section has briefly described a handful of examples of antimicrobial resistance. There are countless more that could have been included, which highlights the need for creativity when approaching this global problem.

1.2 Crown Ether Functionality

Conception, Design, and Cation Binding Ions play several essential roles in living cells, but their concentrations must be closely regulated. For example, the sodium-potassium pump is a membrane-bound protein found in all mammalian cells.[30] This pump is an ATPase; for every hydrolyzed ATP, three Na+ are pumped

out and two K+ are pumped into the cell. This generates a membrane potential of about 60 mV.

This example, along with the TetA efflux pump, highlights how proper ion balance is essential for life processes but can also play a role in mediating antibiotic resistance. This presents a good strategy for the development of a novel class of antibiotic. Initial interest in the Gokel Lab in developing a new antimicrobial derived from earlier work with a broad range of macrocycles known as crown ethers. The crown ethers were developed by Charles Pedersen in the 1960s.[31] They proved to be excellent binding agents for a variety of cations, most notably the alkali metal cations. The importance of this work is reflected in the fact that Pedersen shared the 1987 Nobel Prize in Chemistry for his work.[32]

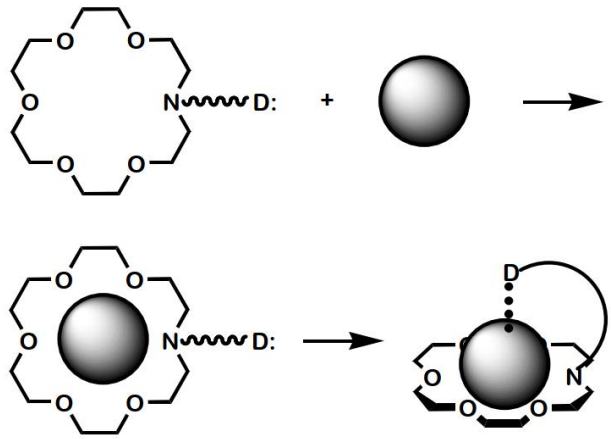

Figure 1-5. Schematic representation of a lariat ether complexing a ring-bound cation.

Work in the Gokel Lab focused initially on compounds they named lariat ethers. These compounds incorporated macrocycles connected to side arms.[33] The side arms incorporated oxygen donor groups. The hypothesis that drove this development was that if the side arms were appropriately placed, they would add additional solvation and stabilization to a cation that was bound within the

macroring.[34,35] In the schematic representation shown in Figure 1-5, "D" represents the side arm donor group or groups such as ether or carbonyl.

At the time the lariat ethers were developed, most crown ethers incorporated monocycles of various sizes. Often, various residues were incorporated within the ring structure. Probably the best known and studied of these compounds is dibenzo-18-crown-6, prepared originally by Pedersen.[31] Simultaneous with Pedersen's report of crown ethers, Jean-Marie Lehn in France revealed related structures that added a third dimension. Lehn's compounds encapsulated alkali metal cations and were named cryptands.[36] Both dibenzo-18-crown-6 and [2.2.2] cryptand are shown in Figure 1-6 along with their cation bound counterparts. Complexes of cryptands are called cryptates. A systematic, but rarely used, nomenclature calls crown ethers coronands and their cation complexes coronates.[37]

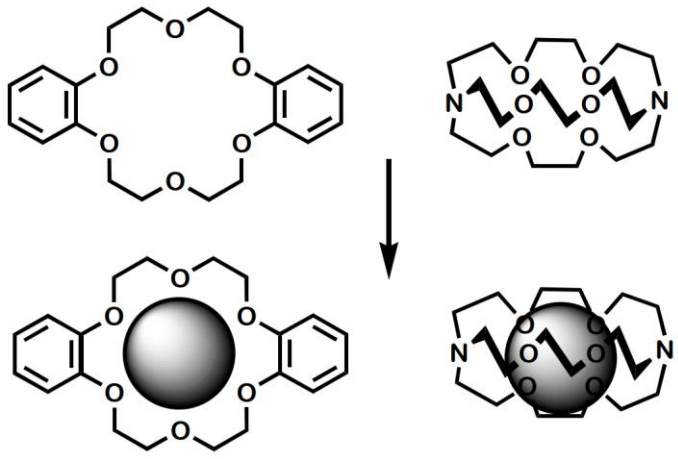

Figure 1-6. Top: Structures of dibenzo-18-crown-6 and [2.2.2] cryptand. Bottom: The crown and cryptand binding a potassium cation.

An important difference in how the cation is bound is revealed in Figure 1-6. The K^+ cation is bound by six oxygen atoms essentially within a plane. The apical positions of the complex are unoccupied. Crystal structures of such complexes show that the apical positions are typically occupied by an anion or by water linked to an

anion.[31] In contrast, the cryptand forms a three-dimensional cryptate complex in which octahedral solvation of the cation is provided by the six oxygen atoms in the three sidearms.[36] The nitrogen atoms also contribute but are weaker donors for alkali metals than are the oxygen atoms.

An early application for crown ethers was as ion carriers for alkali metal cations. Natural ion complexers such as valinomycin bind K^+ with remarkable selectivity over Na^+ and also function as carriers.[38] The structure of valinomycin is shown in Figure 1-7. It is a 36-membered ring and seems far too large to complex a K^+ ion. It is a cyclododecadepsipeptide. The stereochemistry of the amino and hydroxy acids alternate from D,D to L,L which permits the compounds to adopt an enveloping binding conformation that has been characterized as a tennis ball seam conformation.[38]

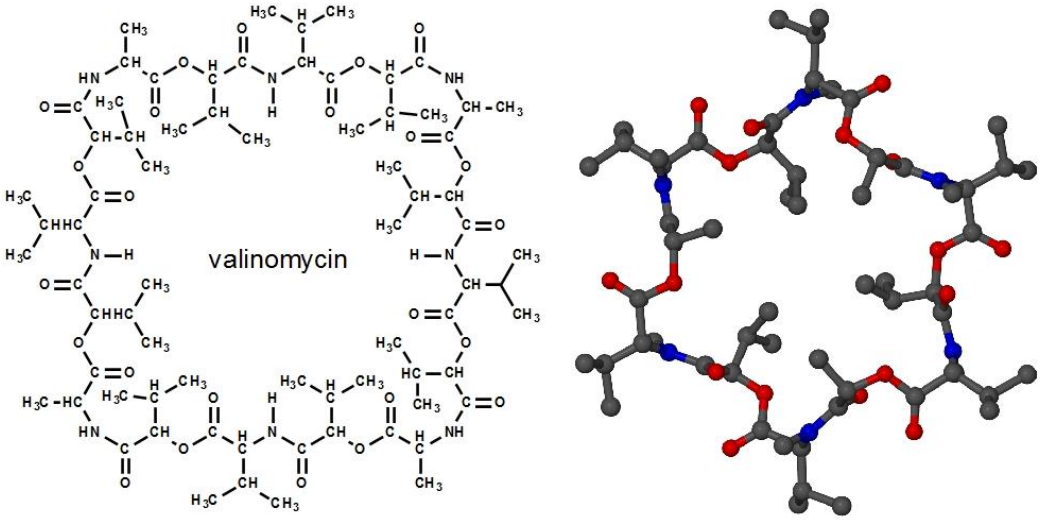

Figure 1-7. Chemical (left) and solid-state (right) structures of the natural carrier valinomycin.

A second goal in the development of lariat ethers was to mimic the dynamics of valinomycin. Simple crown ethers bind cations very rapidly, but they also release them easily.[39] Since the binding constant, K_S is equal to the binding rate divided by

the decomplexation rate: $K_S = k_{complex}/k_{release}$, slower release kinetics were desired Data for a typical crown ether, 18-crown-6, are shown in Table 1-1 for complexation in water.[40]

Table 1-1. Complexation and release kinetics of sodium and potassium ions by 18-crown-6 in water.[40]

Ion	$\mathbf{K_{complex}}$	$\mathbf{K_{release}}$	$\mathbf{K_S}$
Na^+	$2.2 * 10^8 M^{-1}$	$3.4 * 10^7 s^{-1}$	6.5
K^+	$4.4 * 10^8 M^{-1}$	$3.7 * 10^6 s^{-1}$	118

The data show clearly that binding and release for 18-crown-6 with sodium or potassium cations is rapid. The binding constants, however, are modest at best. The enveloping cryptand molecules are far stronger binding agents. The K^+ binding constant for [2.2.2] cryptand is 2.0 x 10^5 in water. The greater binding strength results from a binding rate (7.5 x 10^6 M^{-1}) and a release rate of 38 s^{-1}. The binding and release rates for valinomycin with K^+ cation are 4.0 x 10^7 M^{-1} and 1.3 x 10^3 s^{-1}, respectively. This leads to a substantial binding constant, K_S, of 3.1 x 10^4. The valinomycin values were determined in methanol and are therefore higher than they would be in water. Nevertheless, binding is strong, and dynamics are high.[40] It was the combination of high dynamics and good binding that lariat ethers were designed to emulate.

Crown ethers with sidearms Two classes of lariat ethers were prepared. In each of these, the central scaffold was a macrocycle.[41] In the first systems prepared, the side arm(s) was attached at one of the macroring carbon atoms. These were called carbon-pivot lariat ethers.[41] In the second family, the side arm(s) was linked to a nitrogen heteroatom within the cycle – *i.e.,* nitrogen pivot lariat ethers.[42] By far, the largest number of examples prepared fell into the latter category. The advantage

of *N*-pivot compounds is that nitrogen is readily invertible, so side arm stereochemistry is not an issue as it might be with C-pivot compounds. Examples of the structures prepared are illustrated in Figure 1-8.

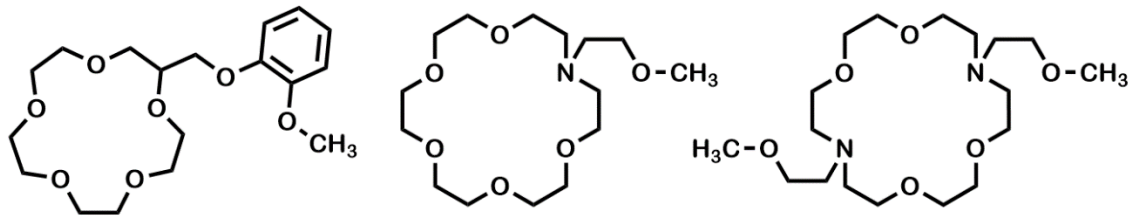

Figure 1-8. A carbon-pivot lariat ether (left) and single and twin-armed nitrogen-pivot lariat ethers (center and right, respectively).

Numerous complexes of *N*-pivot lariat ethers and varioius cations were obtained and examined by X-ray crystallography. As anticipated, cations such as sodium and potassium were bound within the macroring and the side arm or arms provided additional, usually apical, solvation. When a single side arm was present, the opposite apex was occupied either by an anion or water or water linked to an anion. Solid state structures of two complexes are shown in Figure 1-9.[40,41]

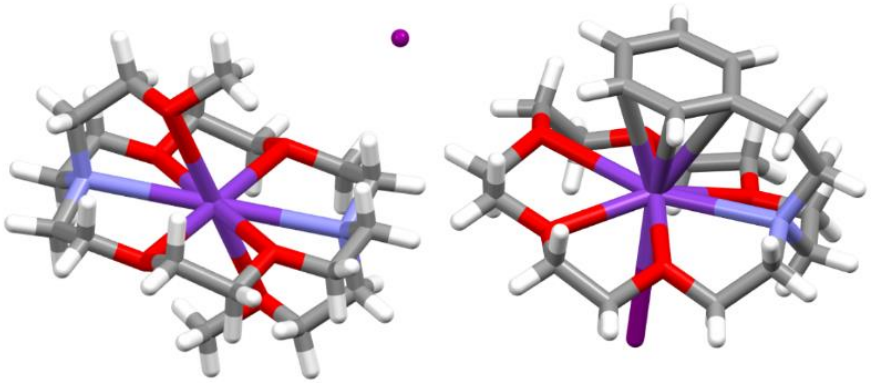

Figure 1-9. A two-armed oxygen donor lariat ether complex of KI (left, CSD: FIRYAG) and a single-armed lariat ether complex of KI in which the apical donor is a benzene ring (right, CSD: DUGHUI).

The structures shown in Figure 1-9 illustrate several different points. First, potassium cation fits well in the 18-membered ring, which provides medial solvation. The oxygen donor groups present in each of the two sidearms solvate the ring-bound cation, but not in a perfect hexagonal pyramid. Still, the cation is fully solvated and the iodide ion shown at the upper right of the left hand structure is separated from the cationic complex. In the structure on the right, iodide occupies that lower apical position and the side arm donor is a benzene ring. Side arms incorporating heteroatoms double bonds, triple bonds, arenes, and heterocycles all afforded encapsulating complexes.

The lariat ethers possessing side arm donors functioned as complexing agents as well as carriers. When side arms were present, but donor groups were absent, the lariat ethers still functioned as carriers.[43] Absent the the side arm donors, however, cation binding strength was diminished. A survey of biological activity showed that the dialkyl lariat ethers were toxic to bacteria, while the lariats possessing donors showed little biological activity.[44,45] Further discussion will be limited to the sidearms without donors.

Lariat Ethers A group of *N,N'*-di-*n*-alkyl-4,13-diaza-18-crown-6 compounds (lariat ethers, LEs) was prepared. The macrocycle was identical in each case and the sidearms were comprised of *n*-octyl, *n*-decyl, *n*-undecyl, *n*-dodecyl, *n*-tetradecyl, *n*-hexadecyl, and *n*-octadecyl chains. These compounds were initially screened for antibacterial activity against *E. coli*, *Bacillus subtilis,* and *Saccharomyces cerevisiae* which revealed that sidearms from n-octyl to n-dodecyl were active. These results are depicted graphically in Figure 1-10.[43,46]

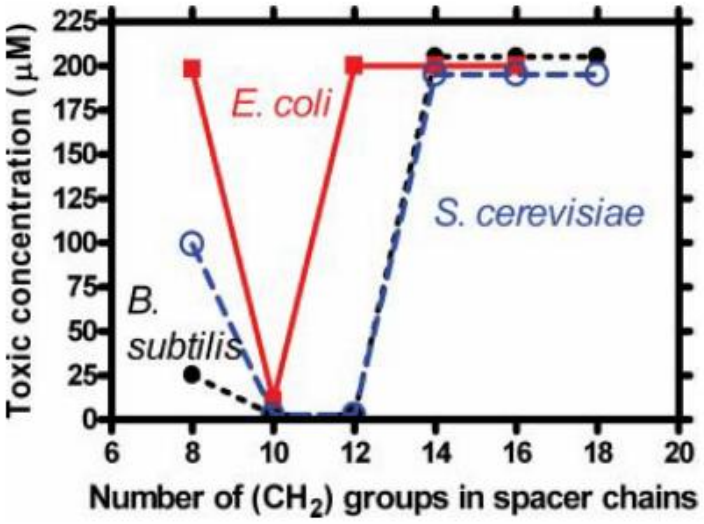

Figure 1-10. MICs of *n*C_8-nC_{18}LEs against Gram negative/positive bacteria and yeast.[46]

The capacity for crown ethers to bind cations is well established, and our group has previously reported that LEs form stable aggregates.[47,48] Taken together, we hypothesized that the LEs likely associate with the microbial membrane and disrupt ion homeostasis. For this reason, the library of LEs was assessed for their ability to transport sodium ions across a membrane. Synthetic vesicles were prepared according to the thin-film hydration method and loaded with sodium chloride. Next, the LE was added and sodium release was monitored over time using an ion-selective electrode (Figure 1-11).[46]

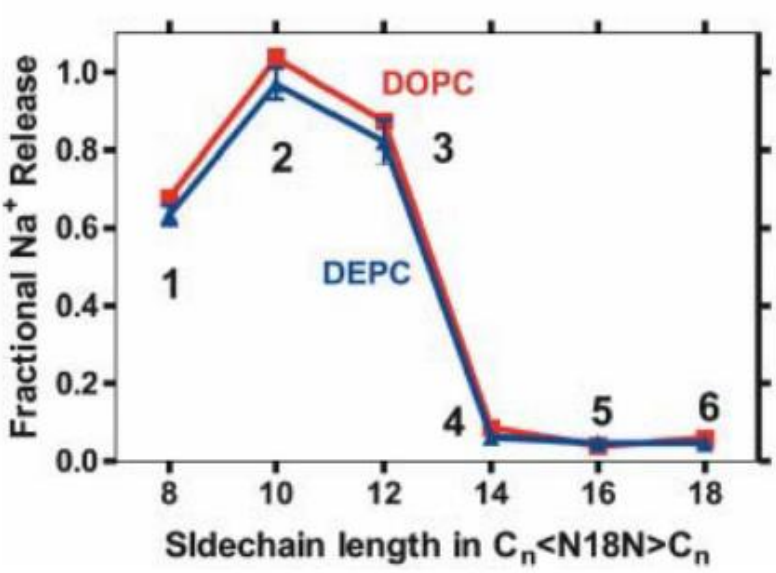

Figure 1-11. Ion transport of lariat ethers. Vesicles were prepared with 1,2-dioleoyl-*sn*-glycero-3-phosphochloline (DOPC) or 1,2-dierucoyl-*sn*-glycero-3-phosphocholine (DEPC).[46]

Clearly, there is a correlation between ion transport and antimicrobial activity. The longer sidearms, like *n*-tetradecyl, *n*-hexadecyl, and *n*-octadecyl, show no ability to transport ions or to inhibit bacterial growth. Contrarily, the *n*-decyl LE is the most potent biologically and the most efficient ion transporter. This data suggests that the LEs must be altering ion homeostasis to affect their toxicity, but were they doing that as ion carriers or channels?

Planar bilayer conductance is a technique commonly used to study ion gradients across synthetic membranes. Two chambers are connected by a small window, which contains a synthetic membrane. Into one chamber, a solution of the ionophore is added along with a known concentration of cation. Next, the ionic current into the remaining chamber is measured following applied potential, often in picoAmperes.[49] A cartoon graphic of this process is shown in Figure 1-12.

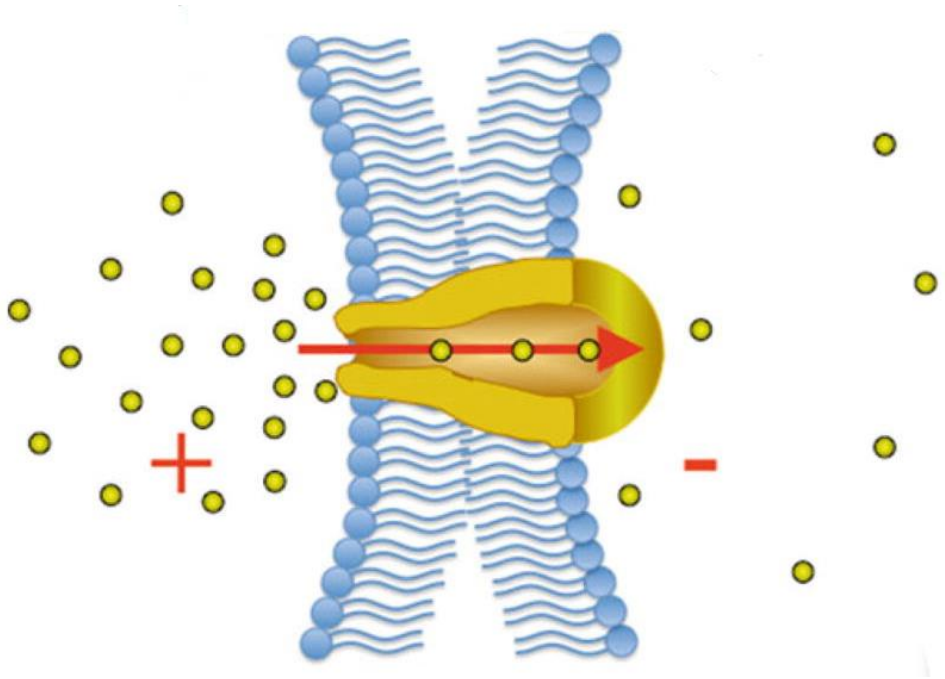

Figure 1-12. Diagram of a bilayer membrane with an ion channel.[49]

The *n*-octyl and *n*-undecyl sidearmed LEs were examined for channel activity at 3 and 24 μM, respectively. The traces generated are shown in Figure 1-13. Traces A and C were following an applied potential of ±50 mV, while traces B and C were following an applied potential of ±70 mV.[43] These traces show that, while varied, both LEs form stable and well-behaved pores. Analysis of the conductance data suggests that there are three primary states: 11 pS, 18 pS, and 27 pS.[43] However, the nature of the pore formed by the LEs was unclear. Various orientations of LE were proposed, and they are shown in Figure 1-14.

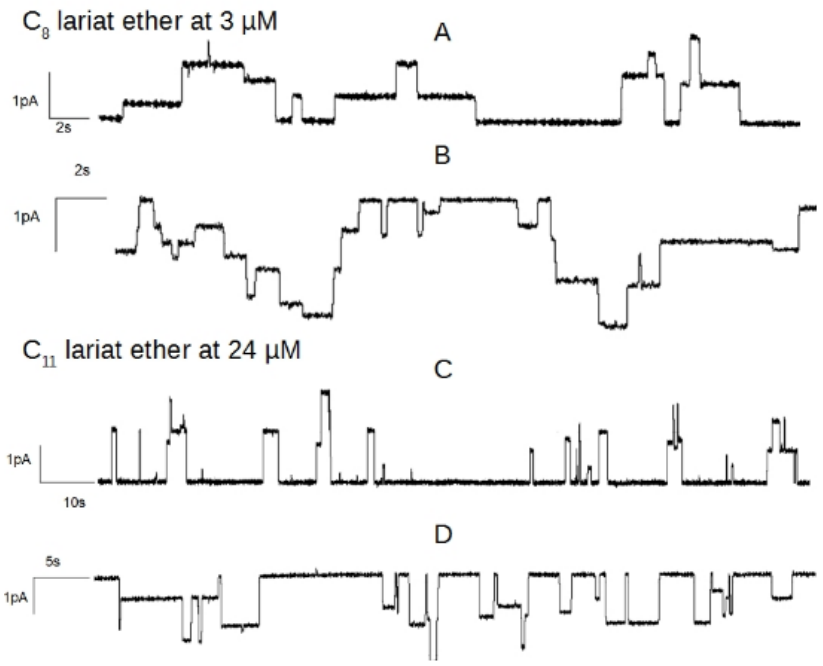

Figure 1-13. Planar bilayer conducatance data for C_8LE and C_{11}LE. Soybean asolectin membrane, 450 mM KCl (HEPES, 10 mM, pH 7).[43]

The potential mechanisms for pore formation by LEs are shown in Figure 1-14. Panel A shows the LE in an extended conformation with the sidearms pointing to either side of the membrane. While this arrangement could comprise an effective membrane disruptor, it is unlikely because it requires the most polar part of the LE to be at the most nonpolar part of the membrane. Panel B shows the long alkyl sidearms interdigitating among the hydrocarbon slab of the membrane, while the crowns may stack to form a pore through which ions could pass. This configuration seems plausible, although it does not account for the reproducible detection of three states. Panel C shows the LE adopting the same conformation as a lipid monomer; however, this structure would require one LE molecule to flip to the inner leaflet, which is energetically disfavored. Panel D suggests the formation of a single molecule toroidal pore, which would avoid the flipping issue of panel C. If this is the mechanism, it would not explain why the longer chain LEs are inactive.

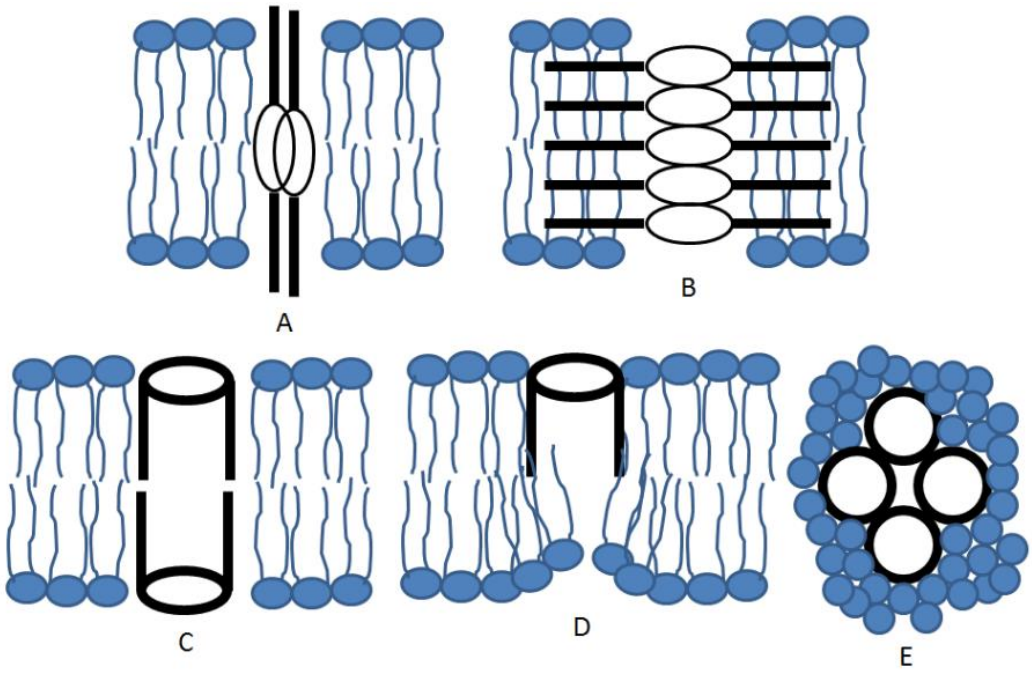

Figure 1-14. Potential orientations of LE in a bilayer membrane.[43]

Finally, panel E depicts pore formation according to a barrel-stave mechanism. In this option, LE molecules would aggregate and then insert into the bilayer. Instead of passing through the crown, ions would pass through the central cavity of the aggregated crowns. This seems to be the most viable option. It is logical that the three states observed (11 pS, 18 pS, and 27 pS) correspond to the size of the opening through which they pass. CPK models of 3, 4, or 5- membered aggregates were made and are shown schematically in Figure 1-15. The internal cavity of the CPK models were measured and found to be 3 Å, 4.5 Å, and 6.5 Å when scaled appropriately. Although not confirmatory, the conductance data strongly support a barrel-stave mechanism of pore formation.

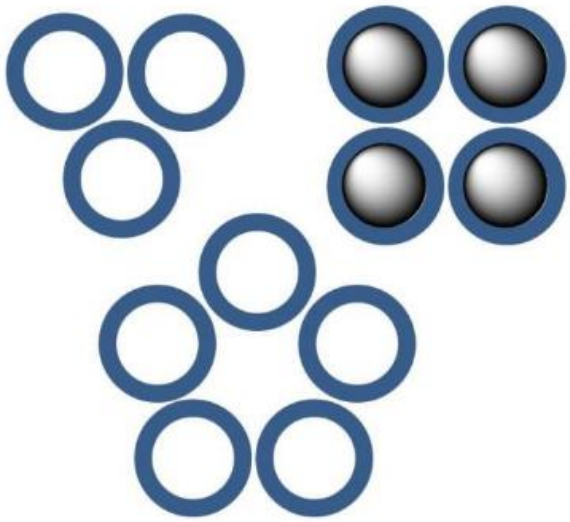

Figure 1-15. Diagram of 3, 4, or 5-membered aggregates of LEs which could refer to the three observed conductance states. The 4-membered aggregate is shown with cations bound, which would increase the rigidity of the structure.[43]

In addition to their individual activity, the LEs also enhance the potency of clinically relevant antibiotics, such as tetracycline and rifampicin, when co-administered (Table 1-2). In these experiments, the LE is administered at sub-lethal concentrations. Impressively, the LEs reduce the MIC of tetracycline up to 48-fold (12 μM down to 0.25 μM). The enhancement is more modest for rifampicin at 21-fold; however, it is still a dramatic improvement in the potency of these antibiotics. As described in Section 1-1, there is an urgent need to recover potency in existing antibiotics. This data supports the lariat ethers as novel adjuvants for antimicrobials.

Table 1-2. Combination activity between LEs and antibiotics against DH5α *E. coli*.

LE	Fraction of LE MIC	Antibiotic	Enhancment
C_8LE	0.67	Rifampicin	21x
C_8LE	0.50	Rifampicin	21x
C_8LE	0.33	Rifampicin	21x
C_8LE	0.67	Tetracycline	48x
C_8LE	0.50	Tetracycline	24x
C_8LE	0.33	Tetracycline	6x
C_8LE	0.25	Tetracycline	6x
C_8LE	0.17	Tetracycline	4x
C_{11}LE	0.75	Rifampicin	20x
C_{11}LE	0.67	Rifampicin	10x
C_{11}LE	0.5	Rifampicin	10x
C_{11}LE	0.33	Rifampicin	4x
C_{11}LE	0.67	Tetracycline	48x
C_{11}LE	0.50	Tetracycline	12x

For reasons such as stability and solubility, it is desirable for oral medications to be administered as their salts. This inspired us to examine the activity of the hydrochloride and methiodide salts for two alkyl sidearms: nC_{10}LE and nC_{12}LE. In both cases, protonation occurs at the 4,13-diaza groups. The structures are shown in Figure 1-16.

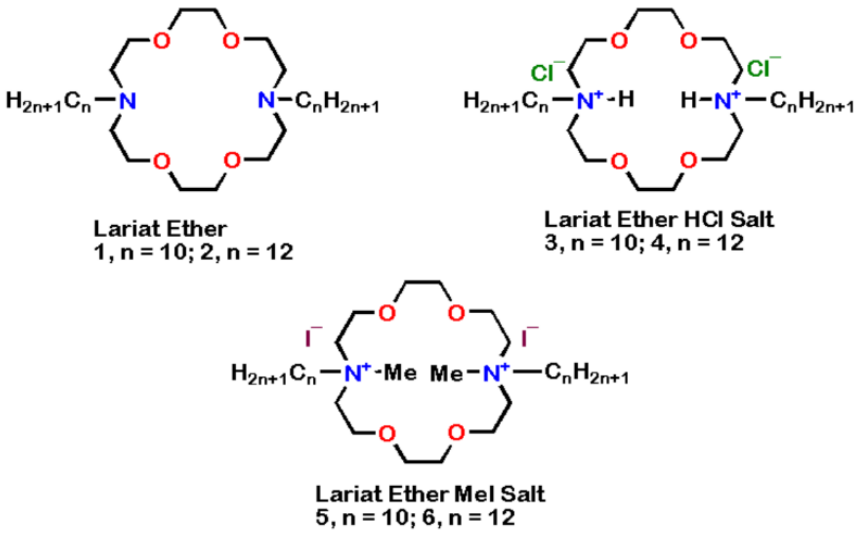

Figure 1-16. Structures of di-*n*-alkyl-18-crown-6 ethers and their hydrochloride and methiodide salts.

All six compounds were screened for their minimum inhibitory concentration (MIC) against gram positive and negative bacteria, *S. aureus* and *E. coli* respectively. Although the focus of further mechanistic studies were the n-decyl and n-dodecyl sidearms, salts for the n-octyl and n-tetradecyl lariat ethers were also prepared and screened for antimicrobial activity against the Gram negative *E. coli*. These results are shown graphically in Figure 1-17 and tabulated in Table 1-3.

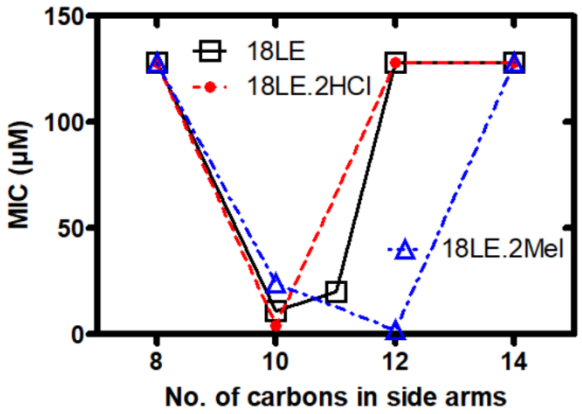

Figure 1-17. Potency of lariat ethers, lariet ether hydrochlorides, and lariat ether methiodides against DH5α *E. coli*. MIC values were capped at 128 μM regardless of their actual value.

Table 1-3. MICs of Lariat Ethers[a] against DH5α *E. coli*.

Chain Length	[LE] μM	[LE.2HCl] μM	[LE.2MeI] μM
C_8	120	>128	>128
C_{10}	11	4	24
C_{11}	24	nd[b]	nd[b]
C_{12}	>128	>128	2
C_{14}	>128	>128	>128

[a]4,13-diaza-18-crown-6, [b]not determined.

Figure 1-17 shows that the salts are more potent than the freebase; however, there is a striking difference between the methiodide salts and the freebase and hydrochloride. In the two latter cases, the n-decyl sidearm is most potent. In the case of the methiodide salt, the n-dodecyl has the lowest MIC. This change in trend could suggest a difference in mechanism. Notably, the methiodide salts possess a permanent positive charge, whereas the protons in the hydrochloride salt are dissociable. Previously, we found that the pKas of the macrocycle's nitrogens are

pKa_1= 9.40 and pKa_2= 7.97. Given that these biological studies are done at physiological pH, the hydrochlorides may exist as a mixture of the mono- and diprotonated species.

Biological activity was assayed for the n-decyl and n-dodecyl lariat ether freebases and salts against *S. aureus* 1199B, which expresses the NorA efflux pump. This bacterial strain is resistant to norfloxacin, and is reported to have a MIC of 64 μM. Additionally, our lab transformed *E. coli* to express the TetA efflux pump. This bacterial strain is designated Tet^R *E. coli*. Sensitivity of each strain to their respective antibiotic was assessed in the presence and absence of lariat ethers and their salts. The results are shown below in Table 1-4.

Table 1-4. MICs (μM) of LEs and antibiotics.

Compound	*E. coli* K12	*S. aureus* 1199B	Tet^R *E. coli*
Norfloxacin	0.125	64	-
Tetracycline	2	-	1000
C_{10}LE	32	8	8
C_{10}LE.2HCl	8	2	8
C_{10}LE.2MeI	4	1-2	32
C_{12}LE	>128	32	>64
C_{12}LE.2HCl	>128	4	>64
C_{12}LE.2MeI	4	1	16

Comparing the data in Table 1-3 and Table 1-4, it is clear that the LEs are more potent against Gram positive than Gram negative bacteria. This is not unusual, because of differences in the membrane structure between Gram negative and positive bacteria. Whereas Gram positive bacteria have one cell membrane covered by a thick layer of peptidoglycan, Gram negative bacteri have an additional outer

membrane.[50] This presents an extra layer through which drugs must traverse, which generally makes them slightly more resilient.[51]

There does not appear to be much of a difference in potency against the Tet^R and wildtype *E. coli* for the freebase and hydrochloride salt. To determine a MIC, the compound of interest is serially diluted two-fold. Although the values may differ, it is by only one dilution factor, so it is considered within error. However, the methiodide salts, particularly for the n-dodecyl sidearms, we see an increase in potency against Tet^R *E. coli*.

The current hypothesis is that lariat ethers penetrate bacterial membranes. This would lead to two possible consequences: alterations in membrane permeability and membrane depolarization. Association of the LE with the bacterial membrane may alter the local environment resulting in a loss of integrity. This altered permeability could affect ion homeostasis. Both of these effects can be measured usign fluorescent dyes.

The effects of the LEs on membrane permeability were examined using the nuclear stain propidium iodide (PI). This dye fluoresces following intercalation into DNA; however, it is impermeable to cells. *S. aureus* was treated with the six lariat ether derivatives shown in Figure 1-16, then stained with PI. The cells were imaged and their fluorescence quantitated to yield the results shown in Figure 1-18. The hydrochloride salts showed the greatest increase in permeability, while there was nearly no change for the methiodide salts. The freebases appear to cause an intermediate increase in permeability.

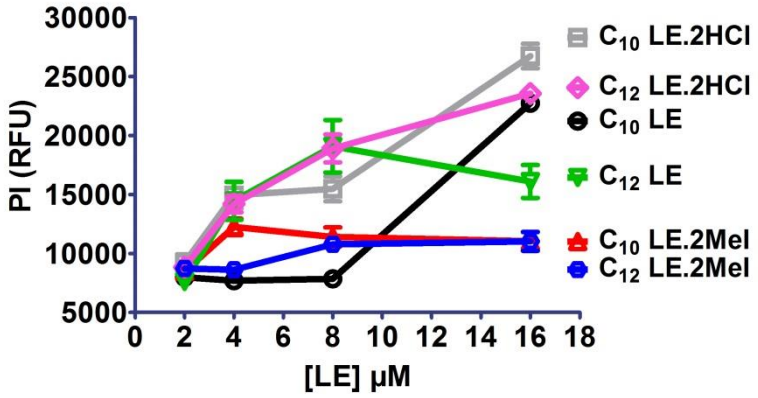

Figure 1-18. Increase in membrane permeability of *S. aurus* in the presence of lariat ethers and salts. Error bars represent standard deviation in three independent trials.

Membrane depolarization was also examined using the fluorophore DiBAC4(3) (bis-1,3-dibutylbarbituric acid)trimethine oxonol). This dye readily enters cells, due to their negative internal potential. Depolarization results in increased fluorescence, while hyperpolarization decreases the fluorescent signal. These results are shown in Figure 1-19.

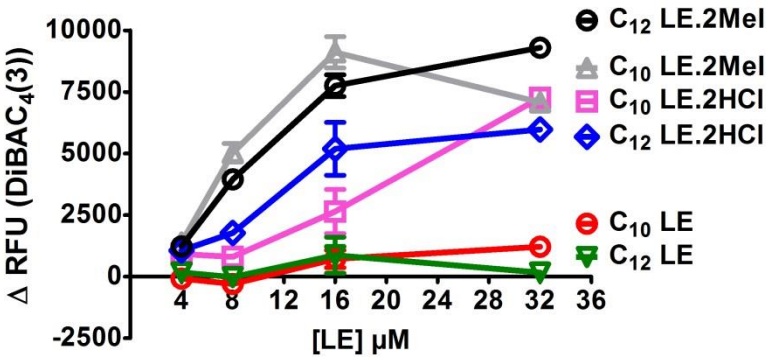

Figure 1-19. Increase in membrane depolarization of *S. aureus* in the presence of lariat ethers and salts. Error bars represent standard deviation in three independent trials.

It is no surprise that the hydrochloride salts increase membrane depolarization, given that they caused the largest increase in membrane permeability. However, it is shocking that the methiodide salts cause an even larger increase in depolarization and there is no depolarization observed for the freebases. Once again, this highlights the difference mechanism. The freebase appears to function by only altering the cell's permeability, while the methiodide salts increase depolarization. Unsurprisingly because of the dissociable protons, the hydrochloride salts appear to function with some kind of hybrid mechanism.

Hydraphiles Simultaneous with the biological activity studies of dialkyl lariat ethers, studies in the Gokel Lab were focused on synthetic ion channel forming compounds.[52] The most relevant of these to the present thesis are the hydraphiles. These molecules are characterized by linked macrocycles reminiscent of the lariat ethers.[53] The structures of two of the membrane-active pore-formers are shown in Figure 1-20.

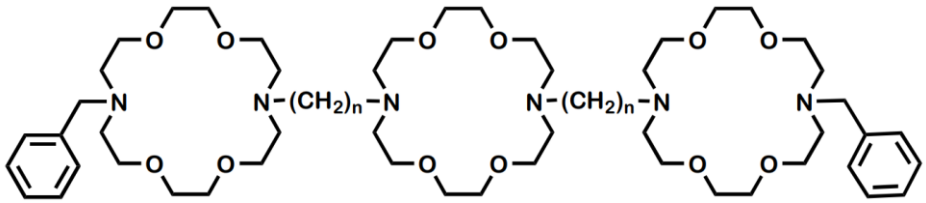

Figure 1-20. A family of benzyl hydraphiles having connector chains ranging from octylene to eicosylene.

It is apparent from the structure shown in Figure 1-20 that the central macrocycle and linker chains resemble the dialkyl lariat ethers. The hydraphiles were designed with a completely different intention than were the dialkyl lariat ethers. Although valinomycin is a dynamic cation carrier that shows a high selectivity for K^+ over Na^+, carriers are far less common ion transporters than channels in biological

systems. The goal was to prepare a compound that could insert into a bilayer membrane and conduct ions through it by forming a pore.

The initial concept was that the two distal macrocycles would create entry and exit portals in a bilayer. The system was modeled on a phosphatidyl ethanolamine bilayer membrane (see Figure 1-21). At the time the compounds were designed, no crystal structure of a protein channel had been solved. The hydraphiles were reported in 1990 and the structure of the KcsA voltage gated potassium channel of *Streptomyces lividans* did not appear until 1998.[54,55] Estimates had to be made concerning the overall span required of the synthetic channel and whether the principal interactions would be with the membrane's polar head groups or with the midpolar regime. The span was estimated to equal the width of the insulator regime and the decision was made to focus head group interactions on the midpolar regime.

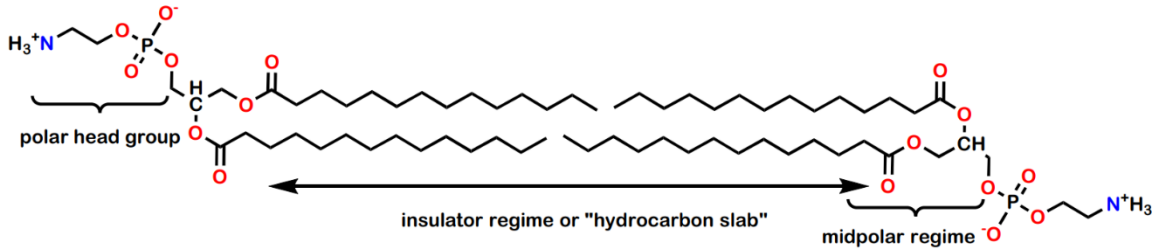

Figure 1-21. The three regimes of a phosphatidylethanolamine bilayer membrane.

As noted above, the distal macrocycles were designed to be entry and exit portals for the channel. The medial macrocycle was envisioned as a relay station through which the transient ion would pass. It was thought that the presence of this medial macrocycle would serve as a "central relay" station in the least polar part of the macrocycle. The initial concept is illustrated in Figure 1-22.

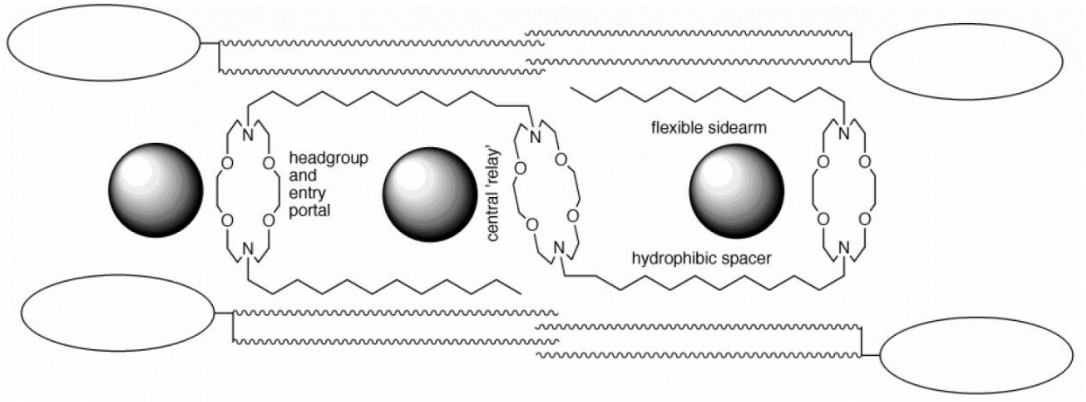

Figure 1-22. Schematic of the initial design concept for hydraphile channels. The ovals represent the combined midpolar and polar head group regimes. The wavy lines represent the hydrocarbon tails of the membrane monomers.

As the work evolved, it became apparent that the medial macrocycle was not in the proposed conformation. If so, it's ion-binding ability would have been an impediment to the rapid passage of ions. When analogous compounds were prepared in which the medial macrocycle was a 15- or 12-membered ring, the channel functioned, although the transport rate was diminished some. When an open-chain ethyleneoxy was substituted, the channel still functioned.[43] When the crystal structure of the KcsA channel appeared, it confirmed the conclusion that the medial macrocycle was in an extended conformation, likely perpendicular to the distal macrocycles. Mackinnon *et al*. showed that the KcsA channel had a "water and ion capsule" at its center that served as a central relay.[55] The central relay served as an energy-reducing element as was originally envisioned, but the conformation was wrong. The active conformation, deduced from extensive biophysical studies is shown in Figure 1-23.

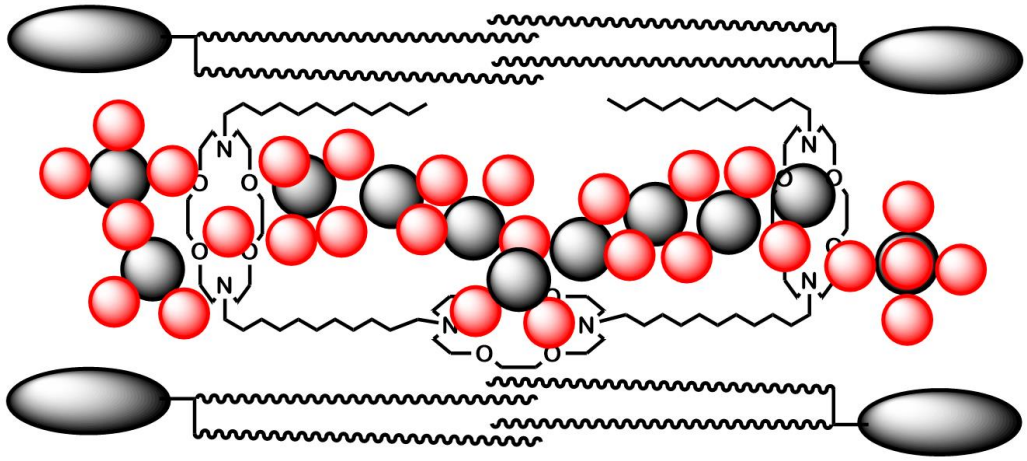

Figure 1-23. Schematic of the hydraphile unimolecular pore.

The schematic representation of the hydraphile shows that a column of water and ions likely is within the pore. The conformation was established by FRET studies and by fluorescence depth quenching.[56] The compounds shown in Figure 1.10 were studied for transport function and the peak was found for the compound having tetradecylene (14 carbon) spacers. The initial design incorporated dodecylene (12 carbon) spacers.[57] Interestingly, a computational study reported by another group had predicted the maximum at 14 carbons shortly before the length study was published.[58]

1.3 Bis-Tryptophans

Tryptophan in Membranes One of the intriguing aspects of the KcsA voltage channel is that a number of tryptophan residues are present in the primary structure. When folded into the active conformation, the tryptophans are found only at the membrane boundaries.[55] Figure 1-24 illustrates this fact. It is a ribbon diagram taken from the Protein Data Base, code 1bl8. The inference drawn from this is that the tryptophan amino acids, their indole groups are serving as membrane anchors.[59]

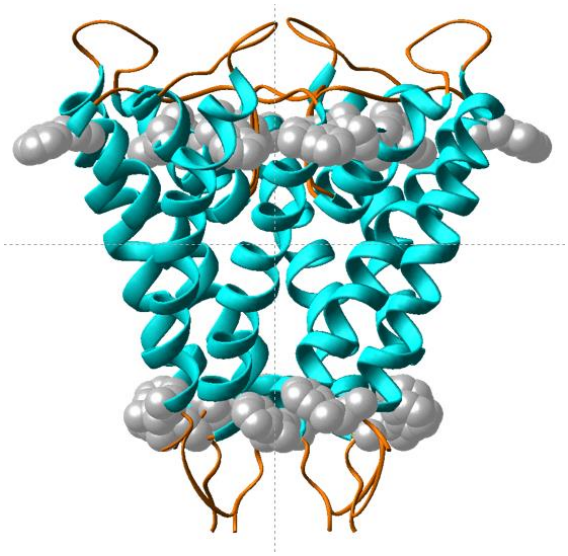

Figure 1-24. Ribbon structure of the KcsA voltage gated potassium channel showing all tryptophan molecules in the space-filling metaphor.

Previous studies undertaken in the Gokel Lab involved the preparation of *N*- and 3-*n*-alkylindoles (Figure 1-25).[60] Several of these molecules were synthesized and tested for aggregation behavior. When the alkyl side chains were *n*-decyl, *n*-octadecyl, and cholestanyl, stable vesicles were formed. No aggregates could be detected for the methyl or *n*-hexyl derivatives. Stability was confirmed both by dye inclusion and by freeze fracture electron microscopy.[61] It was anticipated that the formation of aggregates would be more favorable for the 3-substituted compounds because indole's free N—H was expected to interact more effectively with the surrounding aqueous environment. In fact, it was the *N*-substituted indoles that formed more stable aggregates, although aggregates were formed in both cases.

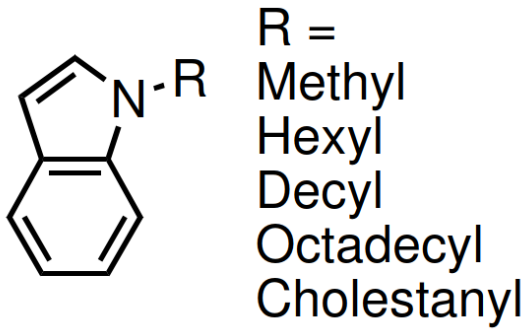

Figure 1-25. *N*-Substituted indole derivatives studied for aggregation behavior.

Early (Bis)-Tryptophans and Their Biological Activity *N*-substitution on indole does not best represent the indole in tryptophan, which has a free NH. Still, the combination of the aggregation results and the solid-state structure of the KcsA channel suggested the compounds of the form Trp-spacer-Trp might have interesting properties. Thus, a family of compounds was prepared by coupling Boc-protected tryptophan with various α,ω-diamines and then deprotecting. The result was the generalized compound shown in Figure 1-26.[62,63]

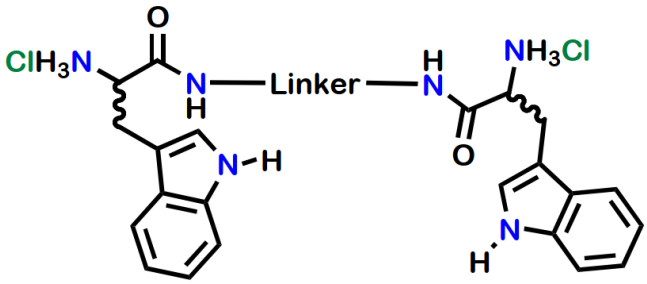

Figure 1-26. Schematic of the family of compounds called bis(tryptophan)s or BTs.

The linkers in these compounds were *n*-alkyl and various aromatics, especially *ortho*-, *meta*-, and *para*-phenylene. These compounds were screened for antimicrobial activity against three organisms. They were *Escherichia coli* K-12, *Staphylococcus aureus*, and a strain of *E. coli* developed in the Gokel Lab that is

called *E. coli* Tet^R. This organism was prepared by transforming a competent *E. coli* strain with a plasmid coding for the tetracycline efflux pump. The minimum inhibitory concentration for this strain was ~1,000 μM, compared to a more typical value for *E. coli* of about 10 μM.

The biological activity revealed an interesting profile among the various derivatives that were prepared initially. The linkers indicated in Figure 1-26 were either phenylene or alkylene. All three isomeric phenylene derivatives were prepared, those substituted ortho, meta, or para. In addition, the D,D-isomer of the meta isomer was prepared so that the effect of chirality could be assessed. The alkylene derivatives that were prepared included propylene, butylene, hexylene, and dodecylene. Among the alkylene derivatives, only dodecylene was active as an antimicrobial. The structures of these compounds are illustrated in Figure 1-17.

By far, the greatest antimicrobial potency was exhibited by Trp-C_{12}-Trp. It was screened against *E. coli* K12, *E. coli* Tet^R, and *Staphylococcus aureus*. The minimum inhibitory concentrations (MICs) ranged from 4-10 μM. Although such potency was encouraging, it was felt that other alkylene derivatives should be explored as well.

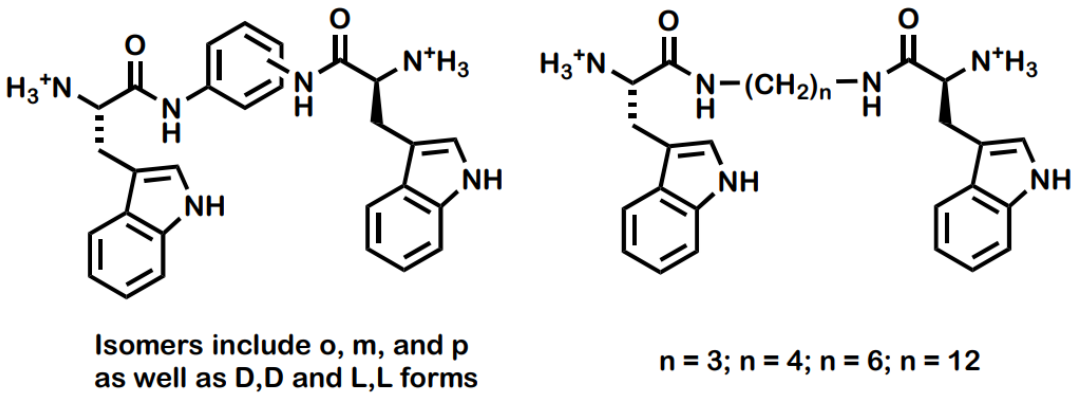

Figure 1-27. The *bis*(tryptophan) structures that were prepared initially.

Four additional questions were raised by this early effort. First, which, if any, other amino acids could show antimicrobial activity in the form of Aaa-linker-Aaa, where Aaa refers to any other amino acid. Second, would other alkylene derivatives show greater antimicrobial potency? Third, are the *bis*(tryptophan) [BT] structures surface active? For example, do they form aggregates in aqueous solution? Do they insert in membranes and show channel-like activity? Fourth, when co-administered with antibiotics of known potency, do they serve as potency-enhancing adjuvants?

In order to address the first of these questions, a range of BTs was prepared with different amino acids. The spacer chosen for this effort was meta-phenylene. Although Trp-*m*-C_6H_4-Trp was not the most potent compound in the family, it did show activity, it was simple to prepare, and it was crystalline. The amino acids present in the compounds H_2N-Aaa-*m*-C_6H_4-Aaa-NH_2 were alanine, leucine, lysine, proline, threonine, and tyrosine. None of these compounds showed antimicrobial activity.

The second question was addressed by preparing the octylene (C_8), decylene (C_{10}), tetradecylene (C_{14}) derivatives to augment the previously prepared butylene (C_4), hexylene (C_6), and dodecylene compounds (C_{12}). These compounds were prepared by Michael McKeever, who examined them for antimicrobial potency.[64] A summary of the minimum inhibitory concentrations against the general lab strain *Escherichia coli* K12 are shown in Table 1-5.

Table 1-5. Summary of antimicrobial potency of existing BTs

BT Linker	MIC against K12 (μM)
nC_3	>128
nC_4	>128
nC_6	>128
nC_8	16
nC_{10}	8
nC_{12}	4
nC_{14}	2
o-phenylene	64
m-phenylene	32
p-phenylene	32

The third question embodies issues including surface activity, aggregation, and the possibility of pore formation. The family of C_8-C_{14} BTs was studied by dynamic light scattering and found to form aggregates to a greater or lesser extent. It was found that aggregation and antimicrobial potency appeared to correlate. When the aggregation in aqueous solution (or suspension) was significant, greater – but not necessarily significant – antimicrobial potency was observed. This issue was further pursued as part of the work described in this dissertation.

Additional confirmation of lipophilicity and membrane interaction resulted from a previous planar bilayer voltage clamp experiment. In this experiment, a bilayer membrane is formed in a pinhole between two salt solutions. There is no detectable ion current if the membrane is intact. If a pore forms within the bilayer, current may pass with a regularity referred to as “open-close” behavior. Such behavior was observed for several of the BTs and one trace has already been

published. It is shown in Figure 1-28. The active compound in this case is Trp-*m*-C_6H_4-Trp.[62]

Figure 1-28. Trace taken from a previous lab publication.[62]

The data show that when the channel is in an open state, ions pass readily through the membrane. If the channel is closed, only baseline is recorded. In this case, both sustained openings of single channels and the simultaneous opening of two channels are apparent. Other BTs showed evidence for pore formation while still others showed what is often referred to as spiking behavior. This profile indicates interaction with a membrane, but not the presence of an organized pore.

1.4 Resensitization to Antibiotics

Given that we are now in a post-antibiotic world, there is great pressure either to develop new antibiotics or to make existing antibiotics work better. In the past 30 years, there have been only two new classes of antibiotics approved by the FDA while the number of deaths due to antibiotic-resistant bacteria has raised dramatically.[5,10] This highlights the importance of recovering antibiotic potency against resistant bacteria. One way to accomplish this is by administering the antibiotic alongside a drug which inactivates the mechanism of resistance. For example, one of the most prescribed antibiotics is Augmentin, which is a combination of amoxicillin and clavulanic acid (the structures of which are shown below).

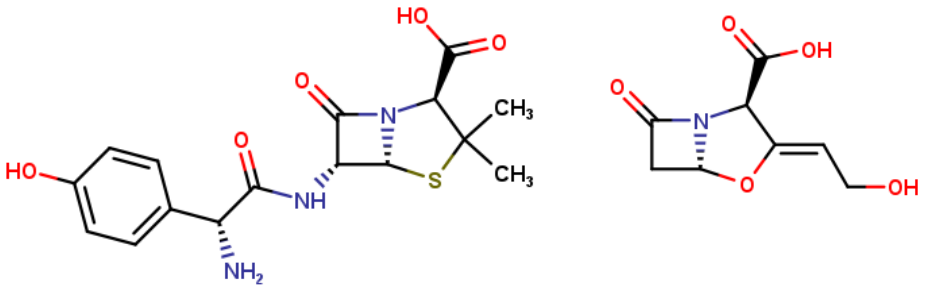

Amoxicillin Clavulanic acid

Figure 1-29. Structures of amoxicillin (left) and clavulanic acid (right).

Amoxicillin (Figure 1-29, left) is a broad-spectrum antibiotic in the penicillin class. It kills bacteria by inhibiting the synthesis of peptidoglycan for their cell wall. Most commonly, resistance to penicillin antibiotics is mediated by beta-lactamases. These are enzymes which cleave the 4-membered beta-lactam ring. Clavulanic acid (Figure 1-29, right) is a competitive, irreversible beta-lactamase inhibitor, which is administered alongside amoxicillin to mitigate resistance. The clavulanic acid competes with amoxicillin to bind the lactamase, which permanently inactivates the enzyme. This saves the amoxicillin and allows it to reach its target without being hydrolyzed.

Amphiphilic compounds that enter membranes and function as antimicrobials may also enhance the potency of other antimicrobials. Combination antibiotics are well known. For example, Augmentin® is a combination of amoxicillin and a β-lactamase that prevents enzymatic disabling of the penicillin within the bacterium. The fourth question concerns whether the BTs can function as adjuvants that enhance antimicrobial potency. In principle, this would occur by BT-based disruption of membrane organization. This, in turn, would lead to altered ion homeostasis. To the extent membranes were disrupted and ion balance was deregulated, more antimicrobial could penetrate the boundary membranes and less

would be ejected by efflux pumps. This is another issue that is addressed in this dissertation.

Another, more general, issue is also addressed in this thesis. We have noted that amphiphilic molecules may assist the entry of antimicrobials into bacteria. Two mechanisms have been mentioned: membrane disruption and deregulation of ion homeostasis. We speculated that it might be possible for the amphiphiles to directly interact with the drugs. This would, in essence, be the formation of supramolecular complexes. Evidence for this phenomenon is also presented in this dissertation.

Chapter 2

Supramolecule Formation between Lariat Ethers and Antibiotics

2.1 Introduction

Lariat ethers are a class of macrocycles related to simple crown ethers such as 18-crown-6. The lariats possess side arms that may include within them various functional groups.[35,40] The original design for lariat ethers was to incorporate one or more side arms into (onto) either a 15- or 18-membered macrocycle. Figure 2-1 shows lariat ether structures which were initially of interest.

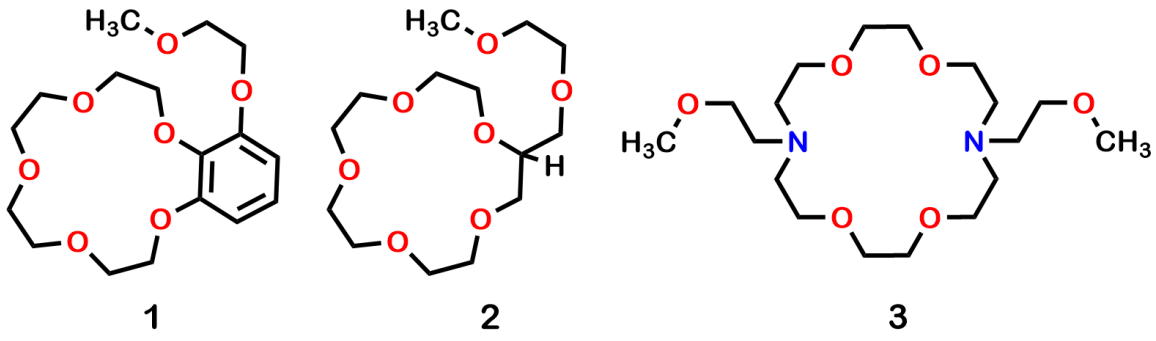

Figure 2-1. Structures of 15-crown-5 and 18-crown-6 lariat ethers with varying sidearms.

An important design goal of the lariat ethers in addition to dynamically enhancing complexation strength was to foster ion transport. Ion transport across various membrane boundaries is of fundamental interest. It is studied in cellular systems and in the membranes used for desalination. For many years, complexing agents effective for transporting alkali metal cations were unavailable and crown ethers presented a solution. The ability of various macrocycles to transport cations was extensively studied, albeit generally less than simple complexation.[66–68]

A device for studying transport was developed by Pressman who used it to study ion transport with the cyclododecapepsipeptide valinomycin, the structure of which appears in the introduction.[69] It is a U-shaped tube into which is placed a solvent not miscible with, and denser than, water. Such a solvent is a membrane mimic, and the most frequently used ones are dichloromethane and chloroform. The solvent is added to an extent sufficient to cover the "U". Water is added to one arm of the U-tube and an aqueous solution of salt is placed in the other. A crown ether or other potential transporter is added to the second arm. The transporter in the membrane solvent diffuses back and forth between the two aqueous phases until an equilibrium concentration is reached. The amount of salt transported into the water phase is usually reported as a percentage of available salt per unit time. A schematic of the U-tube device is shown in Figure 2-2.

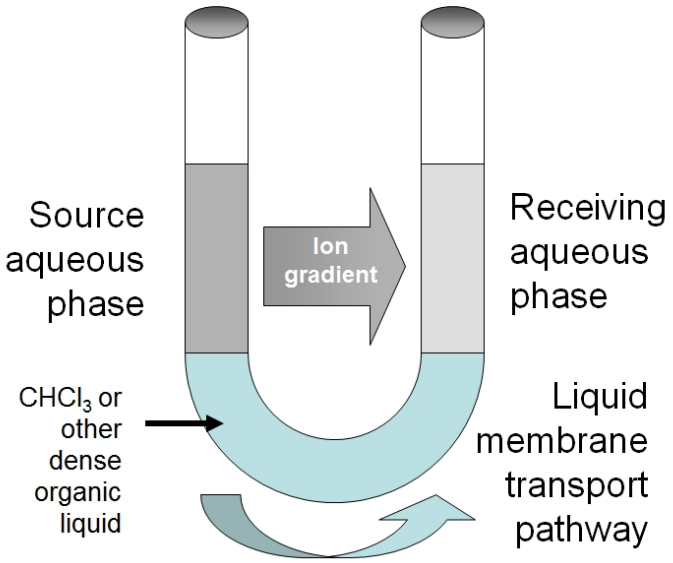

Figure 2-2. A U-tube device used to assess ion transport.

After investigating the cation binding properties of these donor group containing sidearms, the focus shifted to dialkyl substituted lariat ethers. The behavior of simple dialkyl lariat ethers is quite different from similar ones that incorporate side arm donor groups. If we represent 4,13-diaza-18-crown-6 as

H<N18N>H, the crown moiety of **3** with *n*-dodecyl side arms can be represented as C_{12}<18>C_{12} or simply C_{12}LE. As expected, the dialkyl lariats function effectively as carrier molecules. In such a capacity and because they are hydrophobic, they can conduct cations through membranes.[70]

When an alkali metal cation is complexed, the sidearm does not participate. Rather than being enveloped, the two side arms align in a fashion reminiscent of the twin fatty acyl chains in phospholipids. A solid-state structure was obtained in the Gokel Lab and is shown in Figure 2-3.[41]

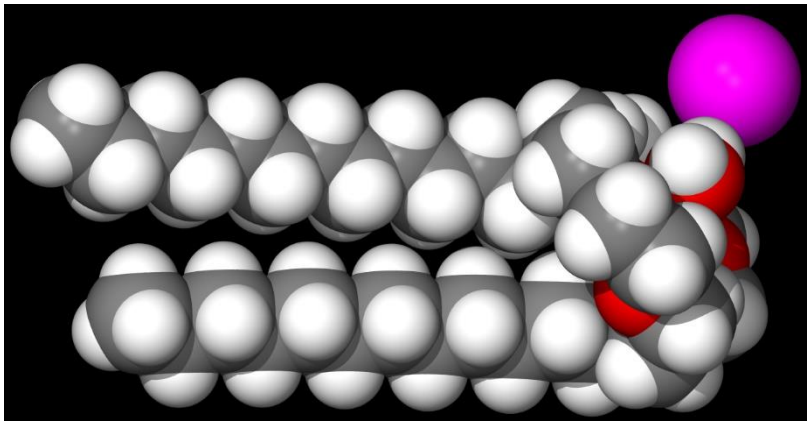

Figure 2-3. Solid-state structure of *N,N'*-didodecyl-4,13-diaza-18-crown-6 sodium iodide complex (CSD: HUTGUY).[41]

By penetrating membranes and conducting ions through them, the dialkyl lariat ethers disrupt ion balance and the functions of proteins that depend on ion homeostasis for successful reactivity.[46] As a result of membrane penetration and the ability to conduct ions through them, it was found that these simple lariats exhibited antimicrobial activity against DH5α *Escherichia coli* and *Saccharomyces cerevisiae*. The potency depended on the organism and the side chain lengths, as shown in the graph of Figure 2-4, below.

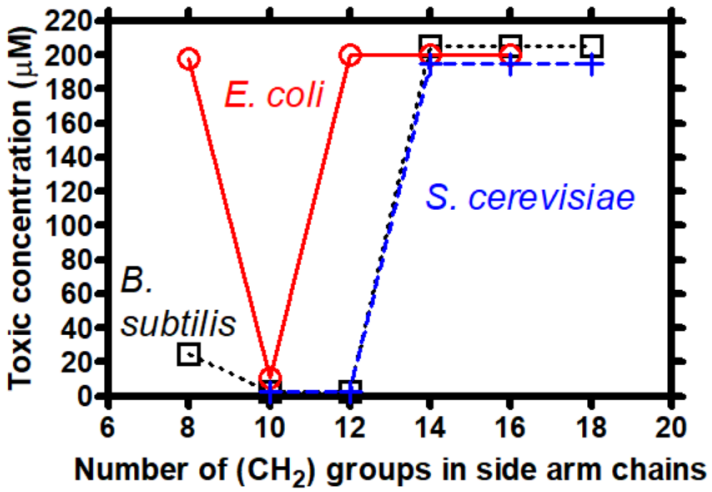

Figure 2-4. Graph showing the potencies of dialkyl lariat ethers against *E. coli* (Gram-), *Bacillus subtilis* (Gram+), and the fungus *Saccharomyces cerevisiae*. The ordinate is arbitrarily truncated at 200 μM, beyond which potency, if any, is insignificant.[46] This figure is identical to Figure 1-10; it is duplicated for the readers' convenience.

Further study showed that not only were the dialkyl lariat ethers effective as antimicrobials, but they could also function as adjuvants. Thus C_{10}<N18N>C_{10} or C_{10}LE exhibits a minimum inhibitory concentration (MIC) of 11 μM against *E. coli*, but when used at half of its MIC value in conjunction with another antimicrobial, the latter's potency is enhanced. For tetracycline and rifampicin, there was a range of potency enhancements from 4 to 48-fold.

It is interesting to note that *E. coli* DH5α is essentially inert to C_8LE. However, in its presence, the potencies of both rifampicin and tetracycline are enhanced. In the latter case, the enhancement is modest unless a significant amount of the adjuvant is used. It remains true, however, that significant potency increases are manifested when the alkyl lariat ethers are co-administered with various antibiotics.

Recent studies conducted in collaboration with the Laboratory of Professor Harshita Kumari at the University of Cincinnati School of Pharmacy have used the neutron reflectance technique to demonstrate that tetracycline hydrochloride penetrates a model bilayer membrane more effectively when a lariat ether is present. The structures of the lariat ethers and tetracycline hydrochloride are shown in Figure 2-5. It seemed reasonable to assume that some supramolecular interactions between the lariat ether and the antibiotic must occur to enhance the penetration of the drug.

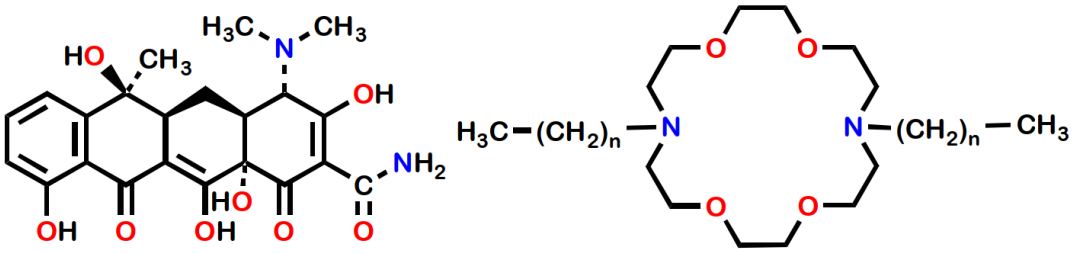

Figure 2-5. Chemical structures of tetracycline and 4,13-diaza-18-crown-6 [decyl (n = 10) and dodecyl (n = 12) side arms], both in their free base forms.

2.2 Experimental Design

NMR Complexation The neutron reflectance studies noted above were conducted by using a supported bilayer membrane. The interior of a bilayer membrane is dominated by hydrocarbon chains and is therefore hydrophobic. 1-Octanol is often used as a model for bilayers. Octanol contains a hydrophobic chain and a polar headgroup, which is conceptually like a phospholipid membrane

although obviously far simpler. When a compound favors octanol, membrane penetration is predicted.[71] The preference for octanol over water is assessed by using log P, which is simply the ratio of the affinities of a compound for water or the alcohol. Using octanol as a model, we undertook spectroscopic studies in dichloromethane (DCM, CH_2Cl_2) to determine if such an interaction could be documented. Dichloromethane was chosen because it is hydrophobic, and its dielectric constant is similar to that of 1-octanol (~10).[72]

The idea behind this experiment was that if the lariat ether could draw the tetracycline into the nonpolar solvent, this would be further evidence of a supramolecular interaction. It would also add weight to the results observed in the neutron reflectance experiments. A 5 mM solution of LE was prepared in either dichloromethane (CD_2CL_2) or chloroform ($CDCl_3$), then added to an equimolar mass of finely ground antibiotic. The resulting solutions were warmed and mixed thoroughly to encourage dissolution, then allowed to sit for two hours before being examined via NMR spectroscopy.

To calculate complexation ratios, integrals from the NMR spectrum of the LE:antibiotic solution are compared according to the following equation:

$$\frac{\text{Integral A}}{\text{Integral B}} * \frac{\text{\# of protons contributing to integral B}}{\text{\# of protons contributing to integral A}} = \text{complexation ratio}$$

For example, if a peak corresponding to a single aromatic proton has an integral of 0.9987 and a peak corresponding to 28 aliphatic protons has an integral of 27.8976, the complexation ratio would be 0.9976. Plugging these values into the above equation gives the following:

$$\frac{27.8976}{0.9987} * \frac{1}{28} = 0.9976$$

This calculation was done for each peak that could be identified as belonging to the antimicrobial agent, then averaged together to give the complexation ratio for a single trial. The NMR complexation experiments were conducted in at least triplicate.

Aggregation Studies Dynamic light scattering (DLS) was employed to assess the aggregation behavior of the C_{12}LE and C_{14}LE. Buffer conditions were selected to mimic those used in biological studies for consistency. The LEs were initially dissolved in DMSO and subsequently diluted into 1x PBS (phosphate buffered saline), pH 7.4 such that the DMSO was held constant at 0.5%. Concentrations were chosen across a range that produced biological activity: 2-128 μM. All solvents and buffers were filtered prior to use. Buffer conditions were kept the same for experiments involving a LE plus antibiotic.

Bacterial studies The bacterial strains utilized in this research were *E. coli* K12, methicillin-resistant *S. aureus* BAA-1720, and *K. pneumoniae* BAA-2146. They were all cultured in MHII (Mueller-Hinton) media, pH 7.24. Stock solutions of antibiotic or LE were prepared in DMSO, then diluted into 1x PBS with 2% DMSO. Following serial dilution with media and cells, the final DMSO concentration was ≤0.5%.[73] Plates were incubated overnight. The following morning their absorbances at 600 nm were measured, which reflected the extent of bacterial growth. The same technique was used to assess combination activity between LEs and antibiotics.[73]

2.3 Results and Discussion

Solubilization of tetracycline hydrochloride by C_{10}LE It was known, and we confirmed, that tetracycline hydrochloride, the form in which the drug is typically administered to humans, is insoluble in DCM. In contrast, *N,N*-didecyl-4,13-diaza-18-crown-6 (C_{10}LE) is freely soluble in the chlorocarbon solvent.

The intended experiment was to add tetracycline hydrochloride to a DCM solution of C_{10}LE to determine if the drug was drawn into the solution. The success of this experiment was obvious from a simple visual examination, shown in Figure 2-6.

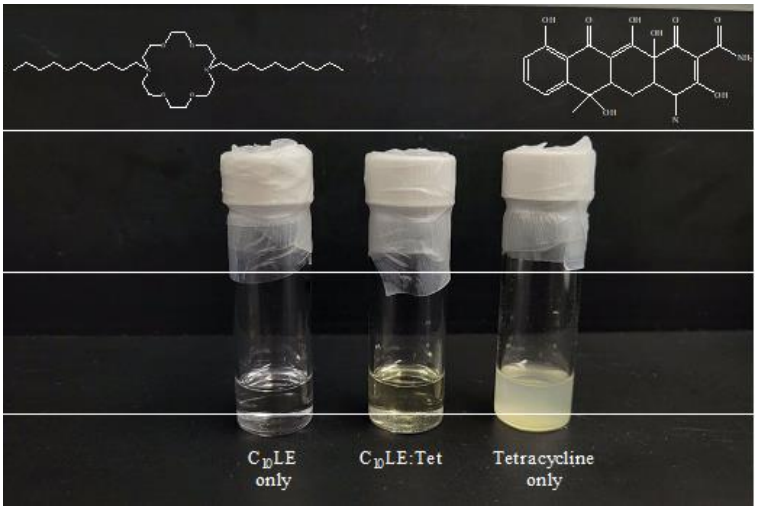

Figure 2-6. Photograph of three vials containing (left) C_{10}LE dissolved in dichloromethane, (right) DCM-insoluble tetracycline hydrochloride suspended in dichloromethane, and (center) a dichloromethane solution containing a 1:1 mixture of C_{10}LE and tetracycline hydrochloride.

In addition to visual confirmation, ^{1}H-NMR was used to monitor the dissolution process. The NMR spectrum of tetracycline hydrochloride was recorded in DMSO-d_6 so that new peaks in the combination spectrum could be identified. It was understood that differences in the chemical shifts of tetracycline hydrochloride protons might be observed simply based on the differences in DMSO vs. DCM-crown-solubilized drug. The results of the study conducted between tetracycline and C_{10}LE are shown in the stack plot of Figure 2-7.

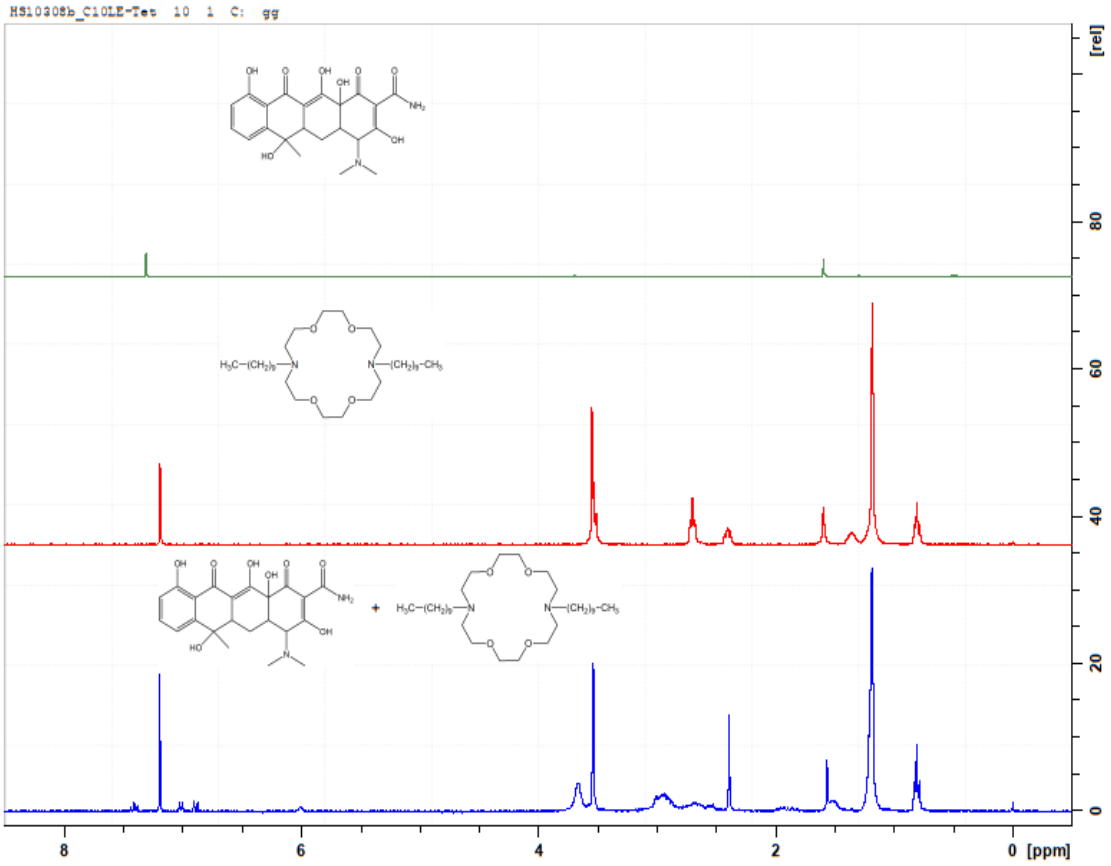

Figure 2-7. Stack plot showing the ^{1}H-NMR spectra of (top panel) tetracycline hydrochloride, (center panel) *N, N*-didecyl-4,13-diaza-18-crown-6, and (bottom panel) the combination of crown and drug. This particular experiment was conducted in $CDCl_3$ which gave identical results to experiments conducted in CD_2Cl_2 and was more economical to use for multiple experiments.

The initial experiment was conducted using stoichiometric quantities of crown and drug. Following successful dissolution of the insoluble drug, experiments were conducted with one equivalent of crown and various excesses of drug. The mixtures were filtered, and the resulting complexation ratios were determined from an analysis of the integrals. The experiment was conducted in triplicate and the ratio of drug to crown for this combination was 1.03 ± 0.02.

This experiment was repeated essentially in reverse. In this case, the tetracycline hydrochloride was dissolved in D_2O and added to finely ground C_{10}LE. The results were the same as the original experiment, and they are shown in Figure 2-8.

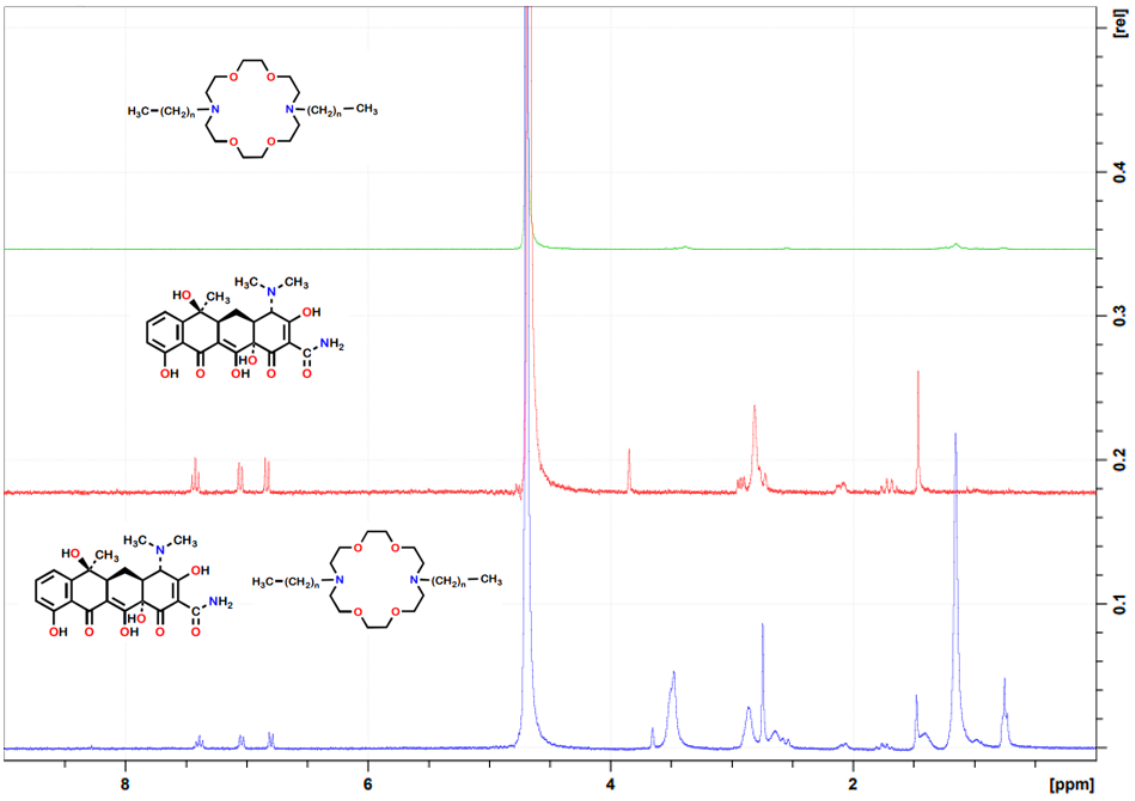

Figure 2-8. Stack plot showing the ^{1}H-NMR spectra of *N, N*-didecyl-4,13-diaza-18-crown-6 (top panel), tetracycline hydrochloride (middle panel) and (bottom panel) the combination of LE and drug.

An effort was made to obtain additional information about the complexation process by using Fourier transform infrared spectroscopy. An attempt using solutions was unavailing. Instead, the antimicrobial and macrocycle were ground together into a fine powder. If complexation was taking place, it was felt that this method would be satisfactory based on the work of Etter and others.[74] The results revealed little more information than did the NMR study. A stack plot showing the

IR spectra of tetracycline hydrochloride alone, didecyldiaza-18-crown-6 alone, and the two in combination is shown in Figure 2-9.

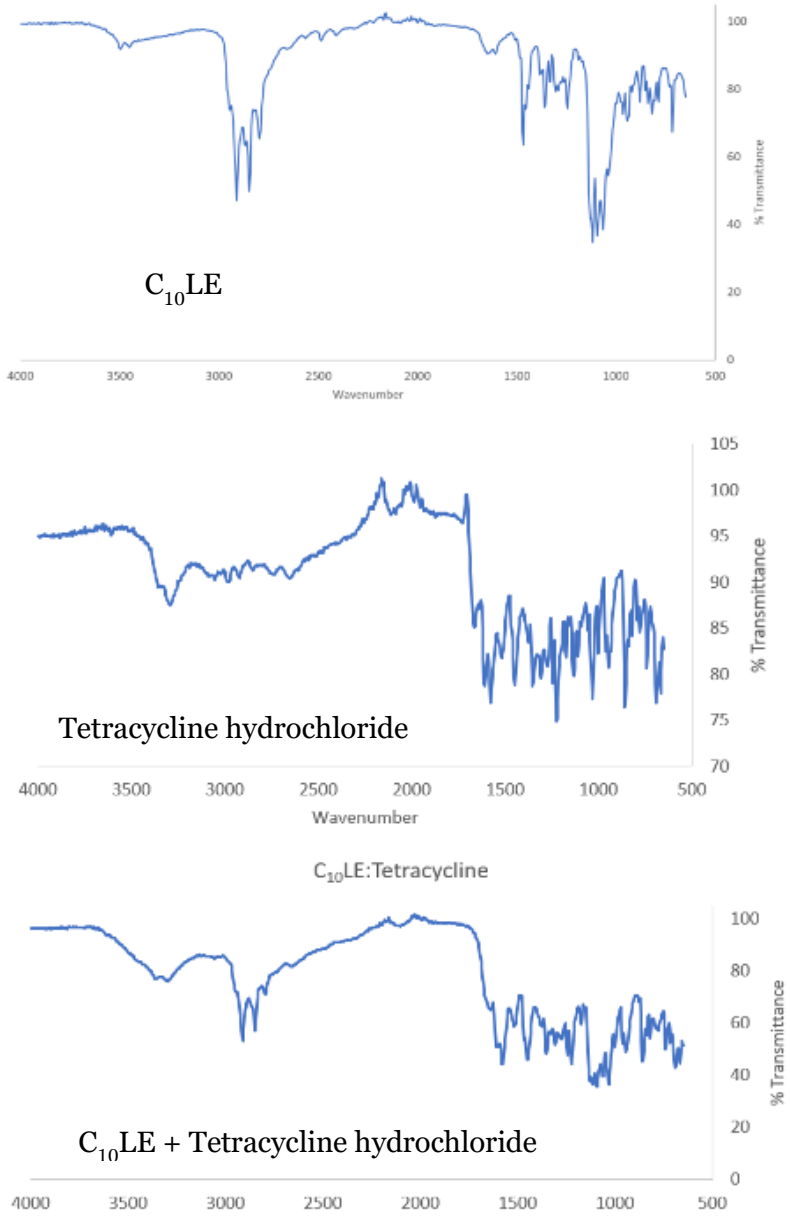

Figure 2-9. FT-IR study of tetracycline hydrochloride, C_{10}LE and the combination conducted between salts after fine grinding of each sample.

Studies of tetracycline derivatives complexed by LEs Five tetracycline derivatives were selected for further study. They were tetracycline•HCl,

minocycline•HCl, doxycycline•HCl, oxycycline•HCl, and chlortetracycline•HCl. These molecules are closely related and share the same arrangement of four fused six-membered rings. The compounds are illustrated below in their free base forms in Figure 2-10. Protonation occurs on the aliphatic dimethylamino group when acid is present.

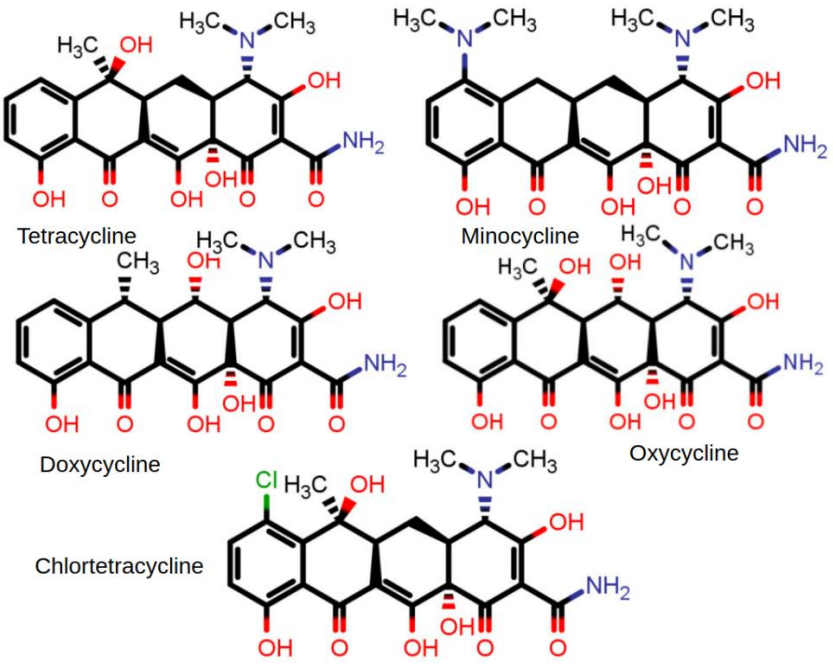

Figure 2-10. Chemical structures of (top) tetracycline and minocycline; (middle) doxycycline and oxycycline; and (bottom) chlortetracycline.[1]

The similarities among these five compounds are obvious both in terms of names and structures. The spectroscopic studies that were done with them paralleled the description of the tetracycline-lariat ether experiments described above. All five compounds were used as their hydrochloride salts. All were white or light-yellow powders. The melting points of all compounds were confirmed as were their ^{1}H-NMR spectra taken in DMSO-d_6. The results of the NMR complexation studies are

[1] Extensive discussions with PARATEK corporation led to an agreement to supply omadacycline for these studies, but ultimately no sample was obtained.

presented in Table 2-1.**Table 2-1**. Complexation ratios between tetracycline derivatives and C_{10}LE in $CDCl_3$ as determined by ^{1}H-NMR.

Antimicrobial	Complexation Ratio[a]
Tetracycline•HCl	1.03 ± 0.02
Minocycline•HCl	1.06 ± 0.05
Doxycycline•HCl	1.02 ± 0.04
Oxycycline•HCl	0.997 ± 0.01
Chlortetracycline•HCl	No complexation observed

[a]All ratios were determined in at least triplicate and variations from 1:1 did not exceed ± 5%.

Considering the observed 1:1 interaction and solubilization of tetracycline by C_{10}LE, similar behavior was anticipated for the other four antimicrobials. Indeed, four of the five antibiotics whose structures are shown in Figure 2-10 did behave identically. The surprising result is that chlortetracycline hydrochloride showed no dichloromethane solubility either in the absence or presence of C_{10}LE.

Our initial effort to understand why such a striking difference in complexation behavior would be observed centered around the solid-state structures available in the Cambridge Crystal Structure Database (CCSD). A search using the Conquest software revealed numerous tetracycline-related structures including at least one for each tetracycline derivative except minocycline. A structure has been obtained for minocycline hydrochloride dihydrate by powder X-ray methods and computational refinement. To our knowledge, however, there is no single crystal X-ray structure currently available for this antimicrobial.

The structures of tetracycline, oxytetracycline, and doxycycline are similar. Thus, the following analysis compares the structure of tetracycline with chlortetracycline. In both cases, the drugs subjected to the complexation study were

hydrochloride salts. It is in the hydrochloride form that the drugs are distributed commercially.

Figure 2-11 shows tetracycline hydrochloride in three views. The chemical structure is shown in the top panel. The middle and bottom structures are renderings of the solid-state structure reported in the CCSD under the index identifier XAYCAB. The structure was originally reported by Clegg and Teat. The stick and space-filling structures are identical views shown in different representations in an effort to enhance clarity.

In subsequent discussion, attention will be drawn to certain positions within the tetracycline framework. It is therefore useful to include a figure showing the tetracycline numbering system. This is shown in Figure 2-12.

In both Figures 2-10 and 2-11, the tetracyclines are represented in what might be called a front view. Figure 2-13 shows tetracycline hydrochloride (top) and chlortetracycline in a side view. The positions of the chloride anion are obviously different, but these solid-state structures may not reflect what is encountered by the lariat ether in solution. Of course, within a hydrophobic membrane, the tetracycline cations and chloride anions may not be well solvated ion pairs.

In any event, key differences are noted. The methyl group at the 6-position of the C-ring in tetracycline obtrudes from the more or less planar BCD portion of the framework. This congests the adjacent 7-position on the D-ring. In chlortetracycline, the chlorine atom at the 7-position in the D-ring congests the 6-position in the adjacent C-ring. The criticality of this steric congestion may be irrelevant to the complexation difference because minocycline has a dimethylamino group pendant to the 7-position of the D-ring. Unlike chlortetracycline, it is complexed on a 1:1 basis with C_{10}LE.

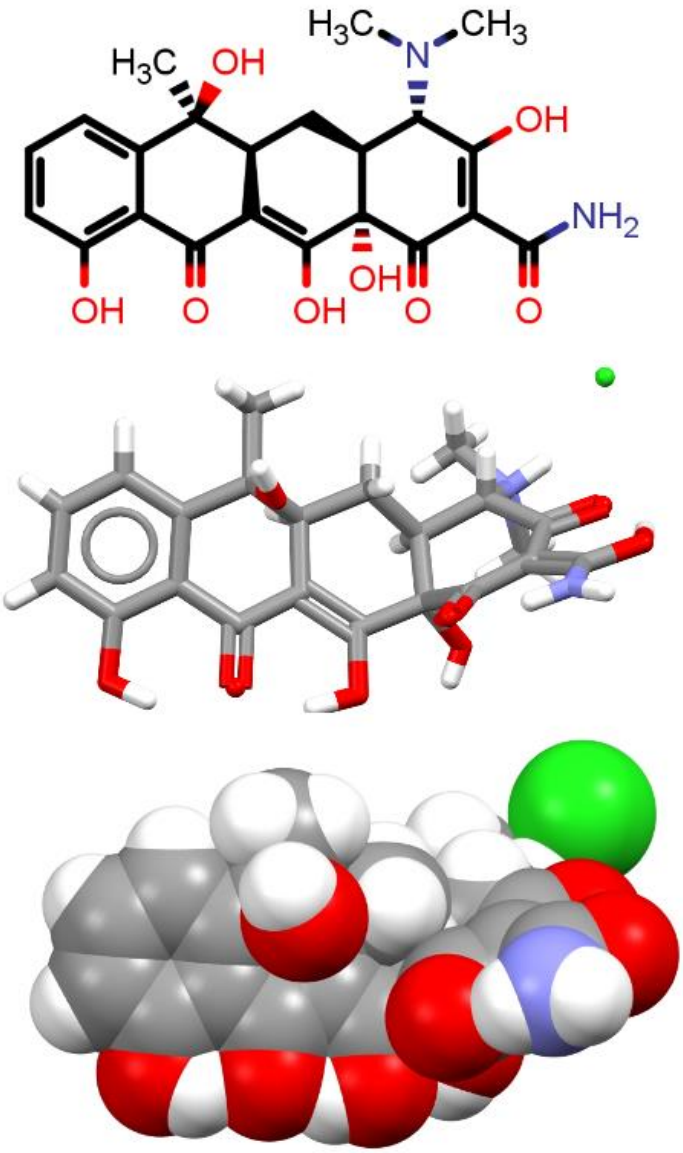

Figure 2-11. Structure of tetracycline. The free base is shown at the top in a structural drawing representation. The hydrochloride salt is shown in two representations from the solid-state structure (CCSD: XAYCAB).

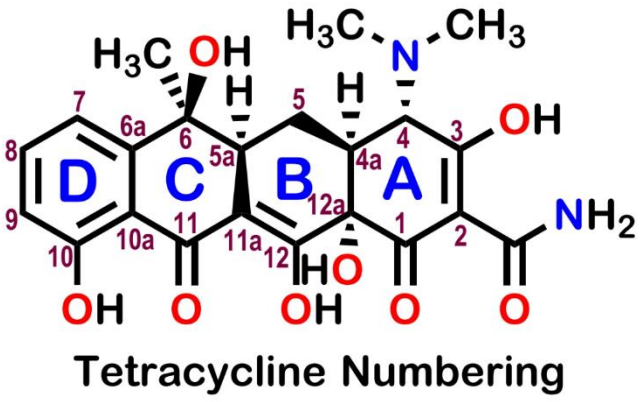

Figure 2-12. The standard numbering system for tetracycline derivatives.

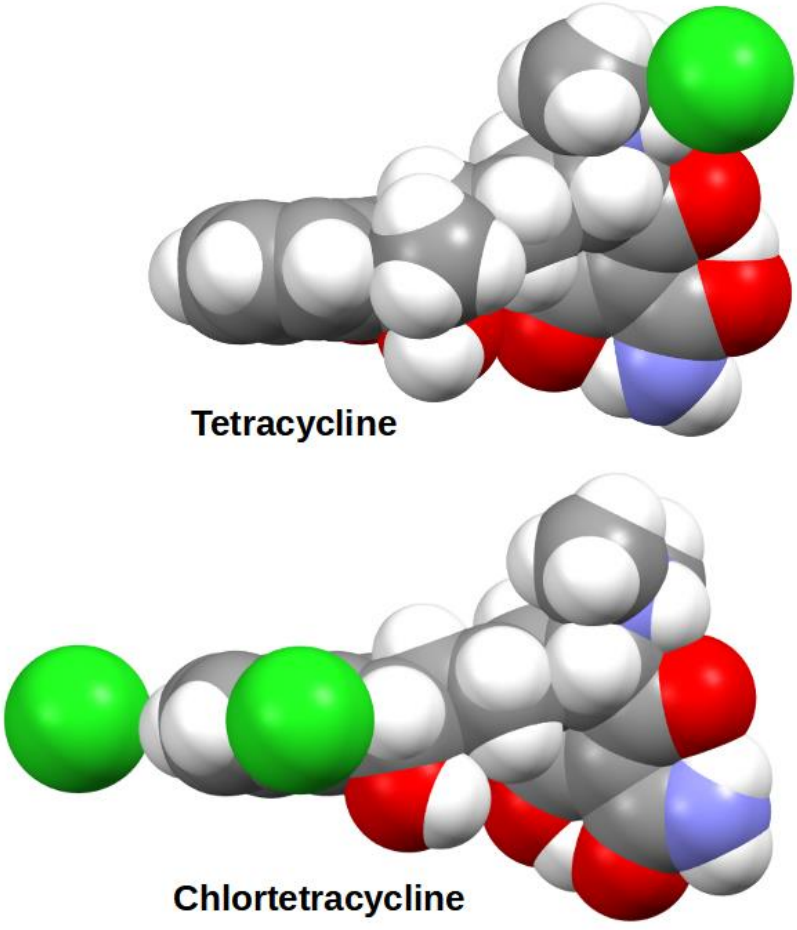

Figure 2-13. Figure showing the solid-state structures of tetracycline (CCSD: XAYCAB) and chlortetracycline (CCSD: CMTCYH10) in the space-filling metaphor in a side view perspective.

A point worth noting is that the amido group pendant to the 2-position of the A-ring occurs in different stereochemistries in the two molecules. This alters the overall hydrogen bonding pattern. The structures of Figure 2-13 also suggest that there is a slightly greater torsion angle in the AB regime in chlortetracycline. The potential effects of these structural variations on the complexation phenomenon remain unclear. *Complexation of Tetracycline and Minocycline by n-alkyl LEs* A comparison of C_{10}LE, C_{12}LE, and C_{14}LE in terms of their ability to complex and solubilize in dichloromethane (or chloroform) antimicrobials is presented in Table 2-2. Note that these data represent the average of at least three replicates in each case. Complexation on, within experimental error, a 1:1 basis was observed for C_{10}LE with both tetracycline and minocycline. Both antimicrobials required more than an equivalent of C_{12}LE and C_{14}LE to be solubilized. Because a larger amount of lariat ether was required for solubilization, we interpret the complexation interactions to be weaker. Weaker interactions also suggest, but do not confirm, that the interactions are less specific.

Table 2-2. Complexation of tetracycline or minocycline hydrochloride by dialkyl lariat ethers in dichloromethane as evaluated by ^{1}H-NMR.

Antimicrobial	**C_{10}LE**	**C_{12}LE**	**C_{14}LE**
Tetracycline	1:1	1:2.5	1:4
Minocycline	1:1	1:2	1:3.5

The NMR spectra shown in Figure 2-7 show significant broadening about the peaks corresponding to the crown protons. We can infer that the crown moiety is responsible for complexation, although the sidearms appear to affect the strength of this association.

Screening of Other Antibiotic Classes Several other antimicrobials were assayed for complexation by these freebase macrocycles. The structures are shown in Figure 2-14. The experiments were conducted as described above. The results are shown in Table 2-3.

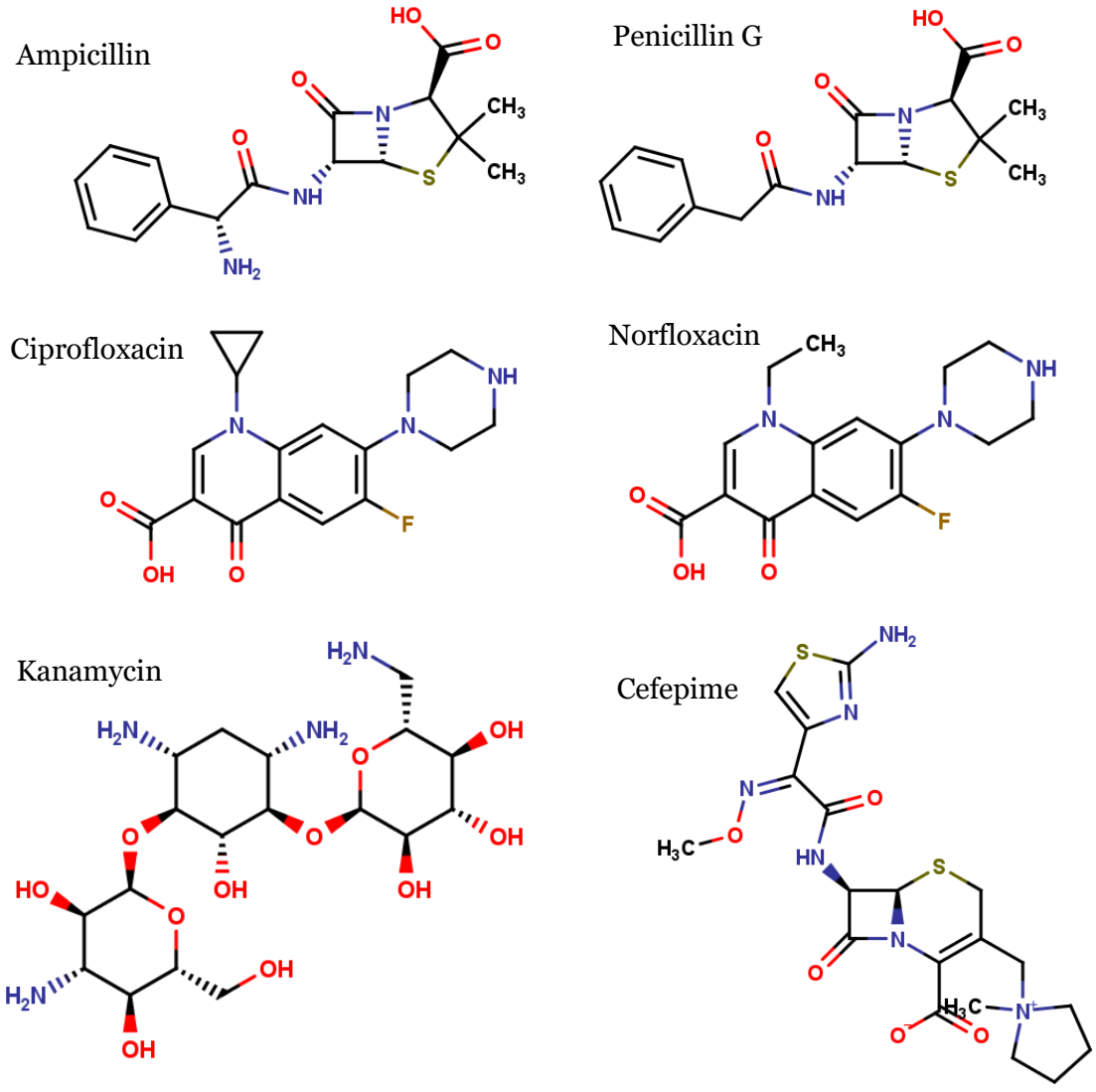

Figure 2-14. Structures of antibiotics surveyed for supramolecular complexation by C_{10}LE, C_{12}LE, and C_{14}LE.

Table 2-3. Complexation of a suite of antibiotics by C_{10}LE, C_{12}LE, and C_{14}LE

Antibiotic	C_{10}LE	C_{12}LE	C_{14}LE
Ampicillin	3.5 ± 0.2	7.1 ± 0.8	5.6 ± 0.6
Penicillin G	4.2 ± 0.1	5.1 ± 0.7	4.8 ± 0.5
Ciprofloxacin	3.7 ± 0.4	2.9 ± 0.3	none
Norfloxacin	none	none	none
Kanamycin	none	none	none
Cefepime	none	none	none

These results highlight the selectivity of lariat ethers for tetracycline derivatives. Although some complexation is observed for penicillin derivatives, and one fluoroquinolone (ciprofloxacin), it is not to the same extent observed for tetracyclines (see Table 2-1). This likely indicates a weaker and more transient interaction.

Complexation by Lariat Ethers in Different Charge States Lariat ethers having twin *n*-dodecyl side arms were also prepared and explored to a lesser degree. The focus on C_{10}LE was dictated by two factors. First, as shown in Figure 2-2, the greatest biological activity was realized with it. Second, the neutron reflectance study of bilayer membrane co-penetration of tetracycline used C_{10}LE, as recorded in the manuscript recently accepted for publication in *RSC Advances*. The structures of the two compounds, C_{10}LE and C_{12}LE, are shown in Figure 2-15 along with their charged variants.

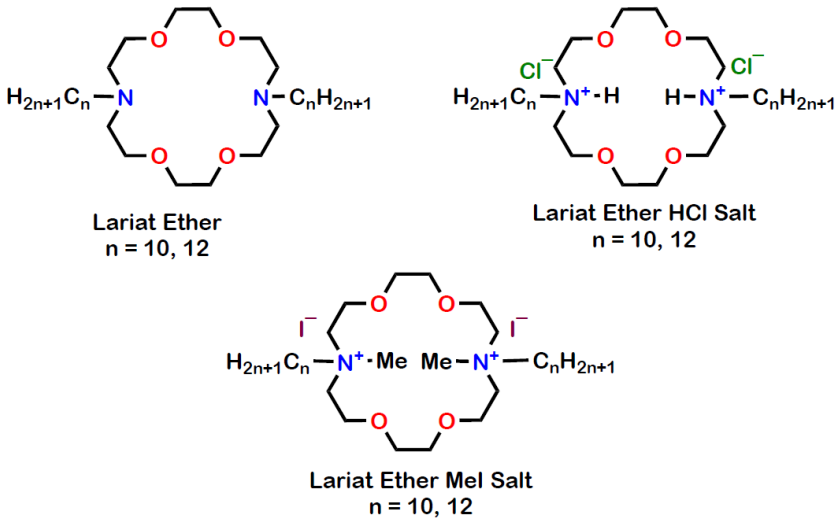

Figure 2-15. Bis(*n*-decyl)- and bis(*n*-dodecyl)-side armed lariat ethers as free bases, hydrochloride salts, and methiodide salts.[2] This figure is identical to Figure 1-16. It is duplicated for the reader's convenience.

These six compounds were tested for antimicrobial activity against the DH5α strain of *E. coli*. The data are shown as minimum inhibitory concentrations (MICs) for C_{10}LE and C_{12}LE as well as the two, bracketing series, C_8LE and C_{14}LE. The compounds in the latter series are inactive in this survey. The data are shown in Table 2-4. The most active compound is C_{12}LE•2CH_3I although C_{10}LE•2HCl is essentially as active. As a series, the *n*-decyl sidearms are the most active family.

[2] Several of these compounds were prepared by Shanheng "Andrew" Yin in the Gokel Lab.

Table 2-4. Minimum inhibitory concentrations (MICs) against DH5α *E. coli*

LE Sidearms	MIC (μM)		
	Freebase	**HCl salt**	**MeI salt**
n-octyl	>128	>128	>128
n-decyl	11	4	24
n-dodecyl	>128	>128	2
n-tetradecyl	>128	>128	>128

In the same fashion as previously described, the lariat ether salts were assessed for their ability to complex the library of selected antibiotics. Despite being charged, the LE salts were still soluble in both dichloromethane and chloroform. Table 2-5 compares the complexation results of the freebases with their salts for the *n*-decyl and *n*-dodecyl sidearms.

Table 2-5. NMR complexation by lariat ether freebases and salts.

Antibiotic	$C_{10}LE^a$			$C_{12}LE^a$		
	Freebase	2HCl	2MeI	Freebase	2HCl	2MeI
Tetracycline	1:1	none	none	2.5:1	none	none
Minocycline	1:1	none	none	2:1	none	none
Ampicillin	3.5:1	none	none	7.1:1	none	none
Penicillin G	4.2:1	1.4:1	none	5.1:1	1.4:1	none
Ciprofloxacin	3.7:1	none	none	2.9:1	none	none
Norfloxacin	none	none	none	none	none	none
Kanamycin	none	none	none	none	none	none
Cefepime	none	none	none	none	none	none

[a]Ratio reflects LE:Antibiotic.

The freebase lariat ether has six hydrogen bond acceptors. When the diaza-groups are protonated or methylated, they can no longer serve this function. Based

on the data shown in Table 2-5, it is clear that the presence of a charged nitrogen inhibits complexation. This is apparent from the lack of complexation observed for any of the dihydrochloride or dimethiodide salts, with one exception. Strikingly, penicillin G shows nearly 1:1 complexation for both the *n*-decyl and *n*-dodecyl LEs. The structures of ampicillin and penicillin G differ only in one amine. It is speculated that having one fewer hydrogen bond donor allows complexation to occur.

Aggregation of Dialkyl Lariat Ethers The first example of aggregation by any lariat ether was reported in 1988.[42] The steroidal side-chained azacrown formed non-ionic liposomes, also called niosomes. It was ultimately shown that aggregation was a common property of macrocycles that had side arms of sufficient length for their hydrophobicity to serve as a counterpoint for the crown's polarity.[75] In this study, it was shown that 18-crown-6 derivatives having one, two, or three nitrogen atoms could form aggregates. In the monoaza case, the successful side chains were tetradecyl and cholestanyl.[65]

Diaza-18-crown-6 derivatives of the type discussed herein were assayed for their ability to form stable niosomes.[42] The twin sidearms studied were *n*-butyl, *n*-nonyl, *n*-dodecyl, *n*-tetradecyl, *n*-octadecyl, and cholestanyl attached by two different linkers. For these experiments, aggregates were prepared according to a thin-film hydration method. Briefly, LEs were dissolved in a non-polar solvent, then dried onto the walls of a glass vessel by evaporating the solvent. Next, they were rehydrated in water and sonicated. In all cases, stable liposomes were formed. However, when the side chains were *n*-butyl, the concentration of the solution was increased to 15 mM from the typical 1 mM in order to observe aggregation.[47] In this reported study, C_{10}LE was not examined, but C_{12}LE formed liposomes of approximately 3000 Å in diameter. In this case, nearly identical results were obtained when an equivalent of KCl was added.[47] This suggests that the interaction

of water with the salt prevailed over the crown's interaction so that no effect was observed.

Dynamic light scattering (DLS) is a well-known and widely used technique that allows nanometer particles to be sized. Typically, a laser beam is passed through an aqueous solution that contains a dispersion of amphiphiles. If the amphiphiles aggregate to form particles within the suspension, they deflect light in proportion to their size. The scattering profile is mathematically deconvoluted to afford an average diameter.[76] As noted above, C_{12}LE was found to aggregate in aqueous solution to form particles having an average diameter of 300 nm.[47] The bis(tetradecyl) lariat ether (C_{14}LE) formed aggregates of 220-250 nm but a cumulant distribution by signal intensity showed the formation of two types of particles, 79% ~230 nm and 21% ~590 nm.[47] In some cases, aggregation may continue to increase over time and the average diameter recorded will change.

It seemed possible that if any complexation occurred between and antimicrobial and a lariat ether, aggregation behavior could be affected or even impeded completely. We therefore undertook a study using dynamic light scattering to assess this possibility. The first step was to prepare suspensions of C_{12}LE and tetracycline in distilled water and evaluate their ability to aggregate. The solutions were prepared by diluting a stock solution in DMSO into either 18 MΩ H_2O (MQ) or phosphate buffered saline (PBS, details concerning this solution can be found in Chapter 5), then vortexing and allowing the solutions to rest at room temperature for 2 hours. These two control experiments were conducted with the results shown in Figure 2-16.

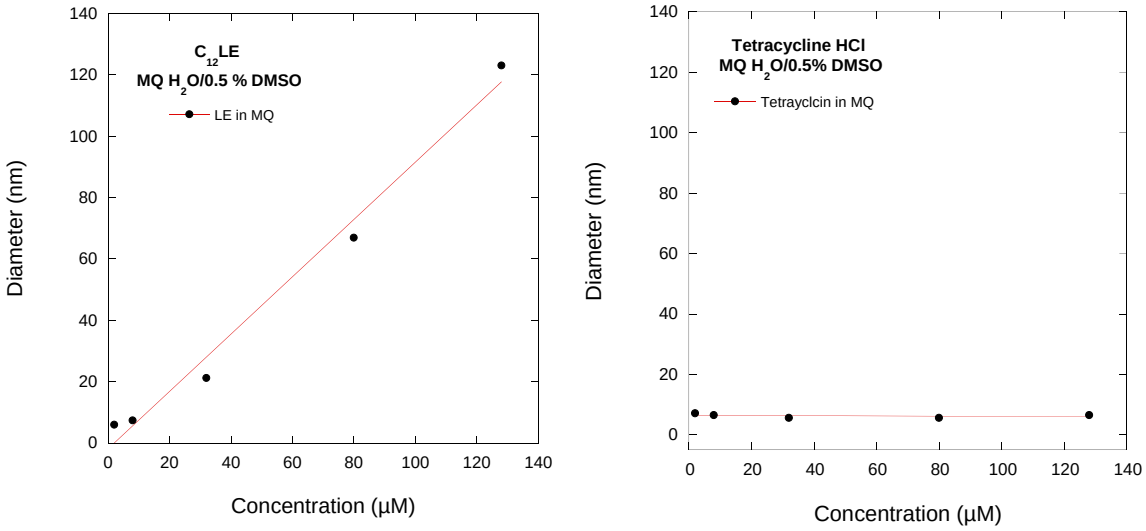

Figure 2-16. Particle size analysis of C_{12}LE and tetracycline hydrochloride in milli-q water.

The lariat ether forms aggregates that increase in size in a linear fashion as concentration increases. Water soluble tetracycline hydrochloride is expected to be dispersed isotropically in aqueous solution. Since each tetracycline molecule will be solvated by water, the observed absence of aggregation was anticipated. Similar results were observed for C_{12}LE and tetracycline when the studies were conducted in phosphate buffered saline (PBS), shown in Figure 2-17, although C_{12}LE formed larger aggregates in buffer than in pure water.

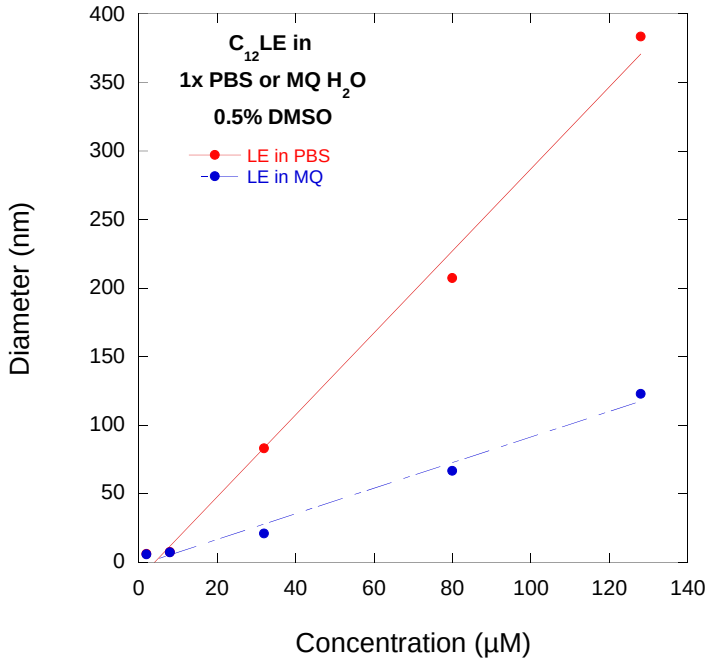

Figure 2-17. Comparison of aggregate sizes of C_{12}LE in buffer versus pure water.

The latter system replaced distilled water because many of the biological studies also reported in this dissertation were conducted therein. The aggregation of the lariat ether shows clear evidence for aggregation to afford particles that exhibit sizes proportional to the amphiphile concentration. This trend was observed in all experiments with dialkyl lariat ethers when aggregation was observed.

Although PBS is more complex than distilled water, sodium chloride and phosphate buffer are not present at concentrations sufficiently high to significantly alter the aggregation behavior. This was anticipated and confirmed by the data shown graphically below. In the case of tetracycline hydrochloride and C_{12}LE, the latter compound exhibits the expected linear concentration dependent behavior (red circles) observed in pure water. When an equivalent of tetracycline is added to C_{12}LE (blue line), no aggregation at all is observed. This was consistent in both buffer and pure water, shown in Figure 2-18.

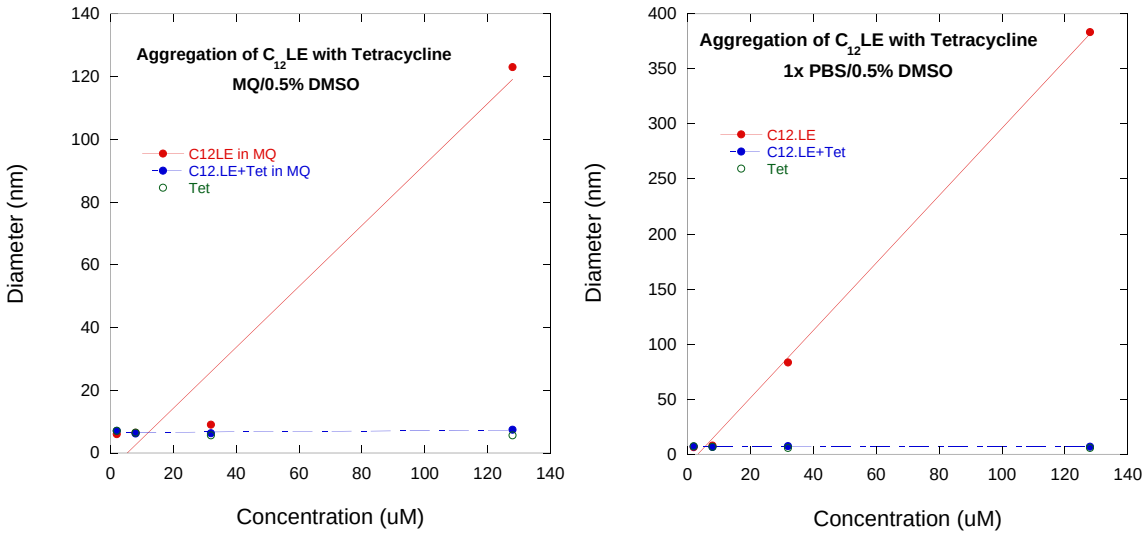

Figure 2-18. Effect of tetracycline on C_{12}LE aggregation in MQ water and 1x PBS.

We interpret the lack of C_{12}LE aggregation occurring in the presence of tetracycline hydrochloride to mean that complexation interaction observed in non-polar solvent takes place here, as well. To the extent that complexation alters the conformation or overall structure by forming a supramolecule, the amphiphilicity will be diminished. This can easily be seen by considering the solid-state structure of C_{12}LE•NaI obtained in the Gokel Lab previously. The twin alkyl side chains are aligned with each other in the solid state as they do bilayer membranes. In this structure, sodium cation is bound in the macroring as would likely be the case in PBS. Attachment of tetracycline to or insertion of it within the ring or chains would significantly alter the amphiphilicity of the resultant complex.

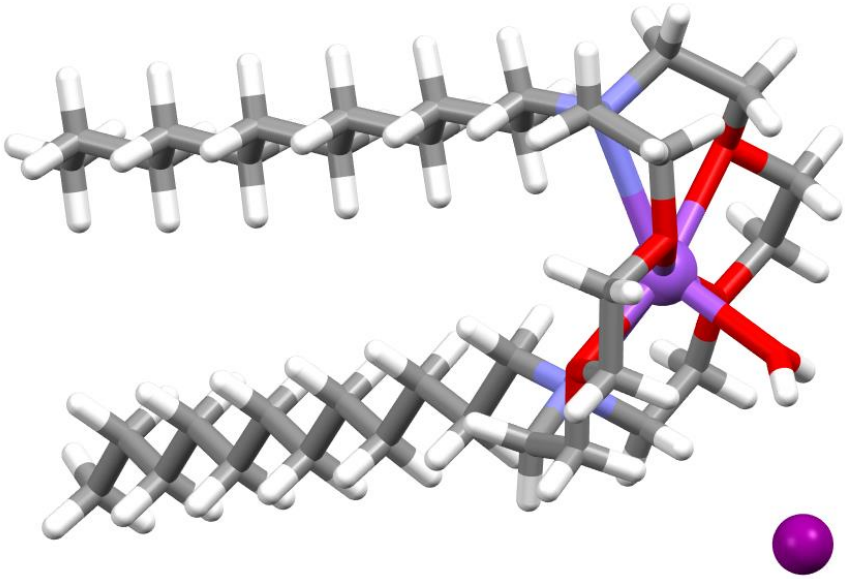

Figure 2-19. Solid-state structure of *N,N'*- *bis*(*n*-dodecyl)-4,13-diaza-18-crown-6 complexing sodium iodide.[41]

Based on the selectivity of lariat ethers for tetracycline derivatives, this particle size analysis was repeated for the other tetracylines: minocycline, doxycycline, oxycycline, and chlortetracycline. The results from these experiments are shown in Figure 2-20, and they confirm that the supramolecule formed between tetracyclines and lariat ethers alters the amphiphilicity in such a way that aggregation is completely inhibited.

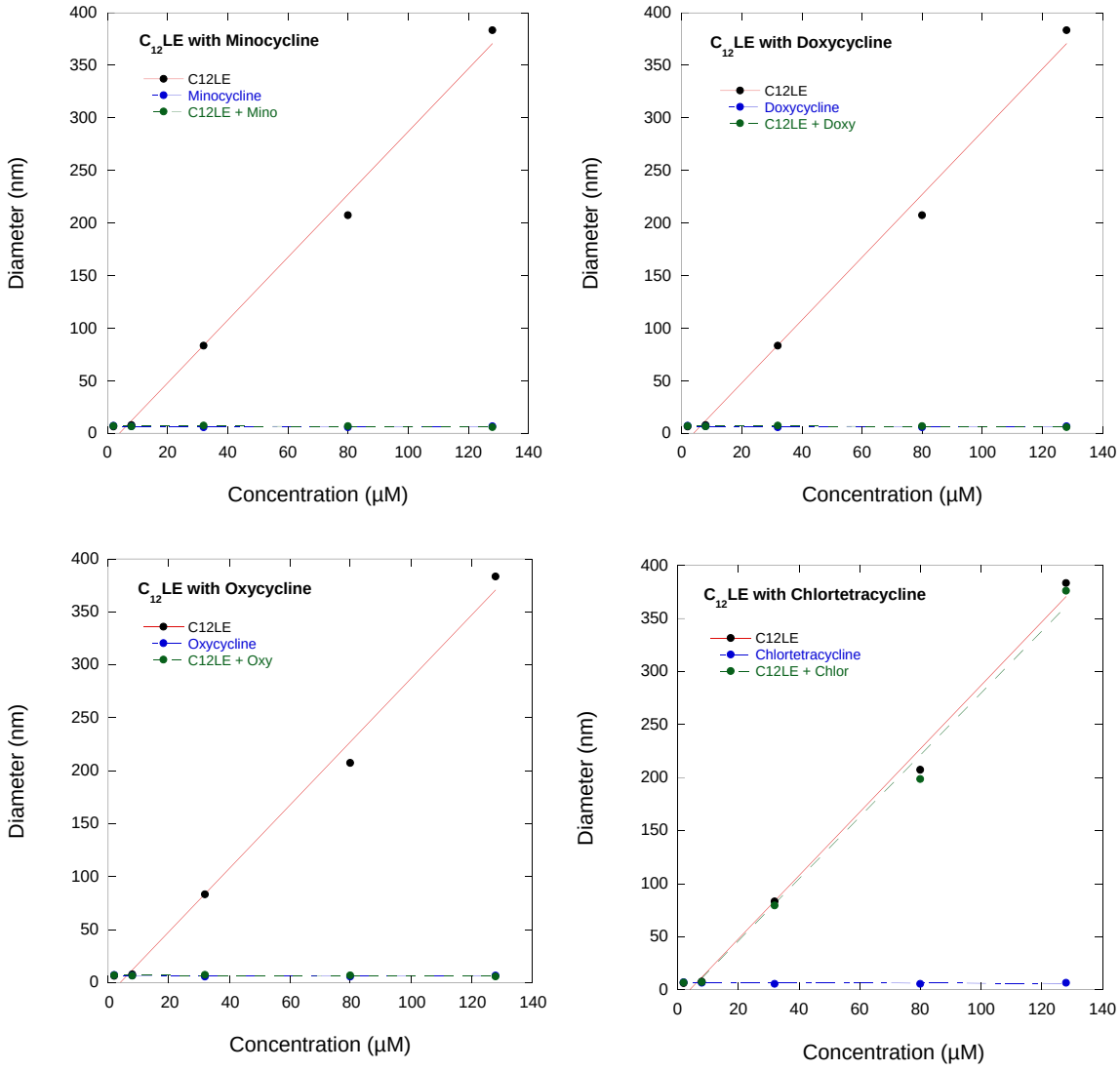

Figure 2-20. Particle size analysis of C_{12}LE with tetracycline derivatives in 1x PBS/0.5% DMSO, structures shown in Figure 2-10.

As previously shown, complexation is observed for each tetracycline derivative except for chlortetracycline. Unsurprisingly, the DLS results line up very well with the results from the NMR complexation studies, in that each tetracycline derivative inhibits aggregation except for chlortetracycline. This could be due to the bulky and electronegative chlorine present at the 7-position of the D-ring. These results are duplicated for the C_{14}LE, which showed the same complexation pattern.

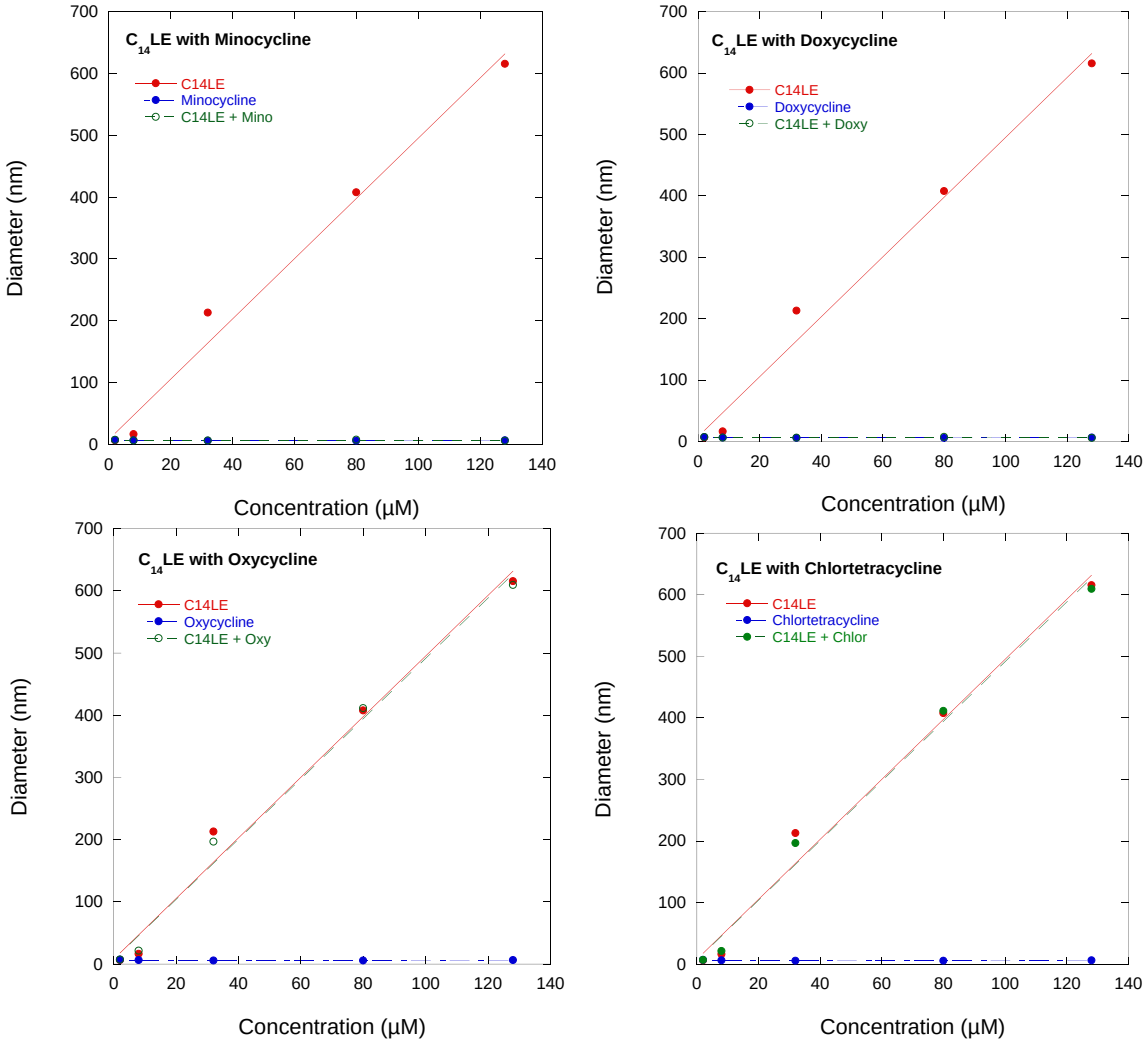

Figure 2-21. Particle size analysis of C_{14}LE with tetracycline derivatives in 1x PBS/0.5% DMSO, shown in Figure 2-10.

Based on the apparent partial complexation of several antimicrobials with lariat ethers, it seemed possible that some aggregation might be observed in experiments similar to those described above. Indeed, the following graphs show that this is precisely what does occur (Figure 2-22).

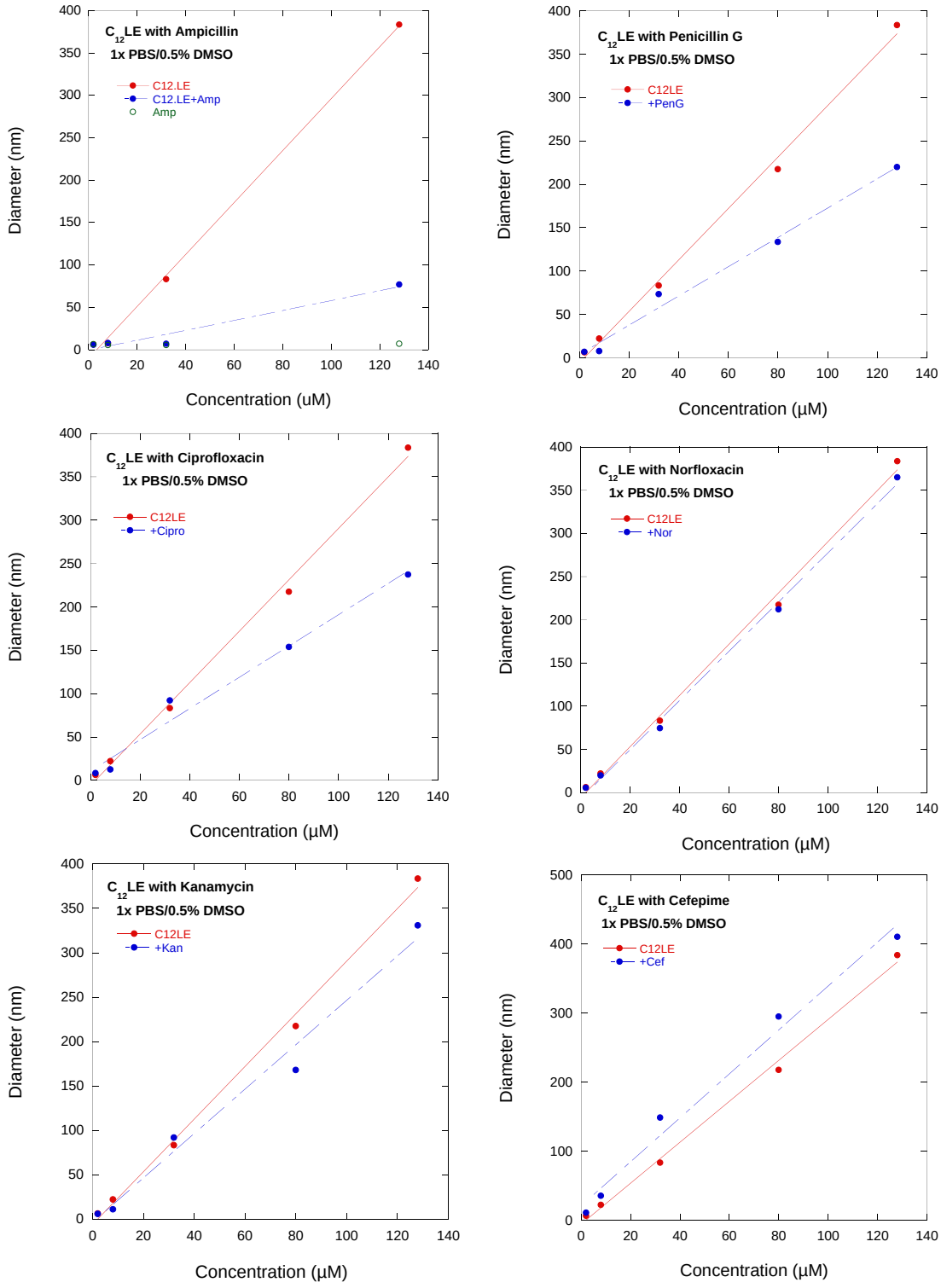

Figure 2-22. Particle size analysis of C_{12}LE with antibiotics that showed partial complexation.

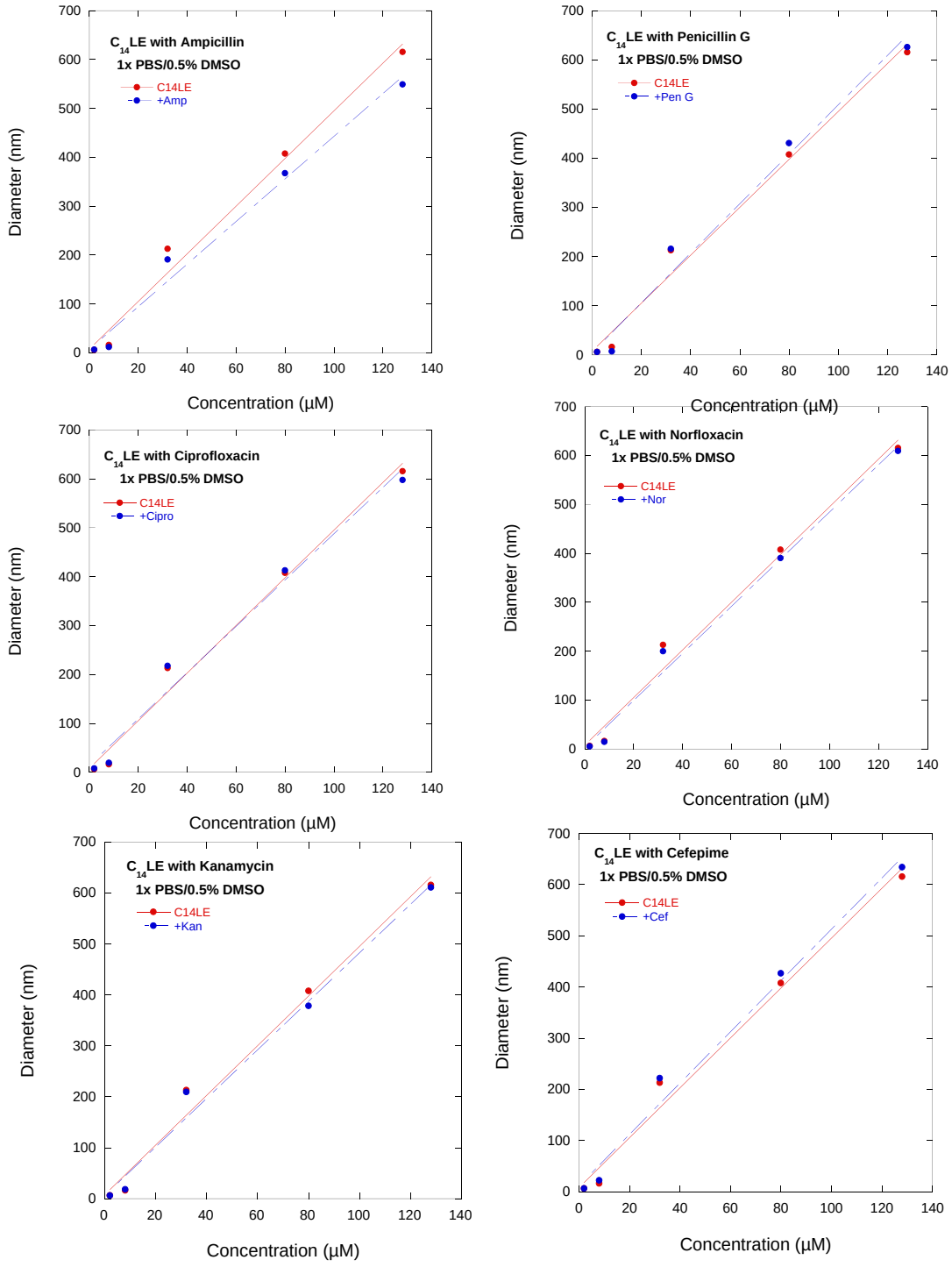

Figure 2-23. Particle size analysis of C_{14}LE with antibiotics that showed partial complexation.

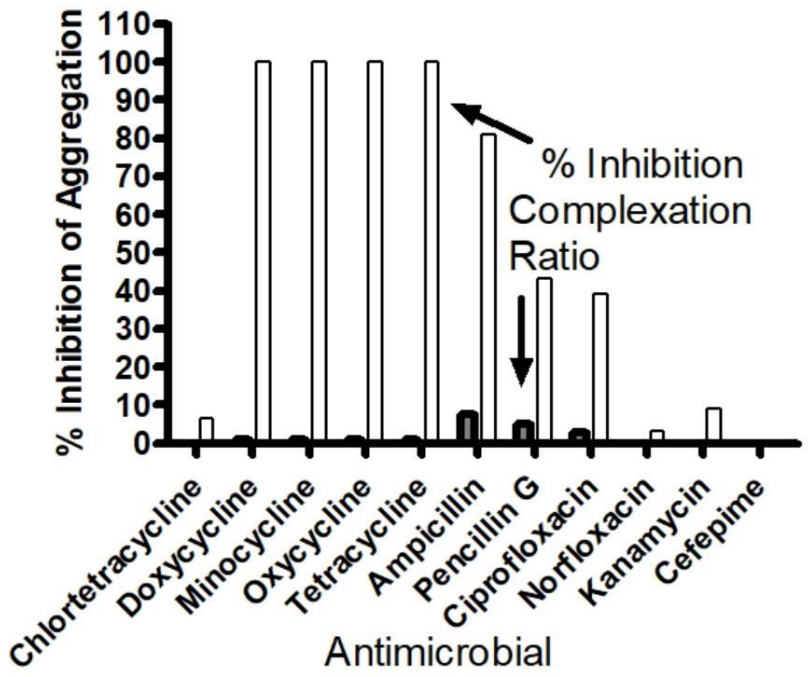

Figure 2-24. Inhibition of LE aggregation by a library of antimicrobials.

The degree to which LE aggregation is inhibited is shown graphically in Figure 2-24. In this figure, it is clear that complexation strength correlates with the degree of aggregation inhibition. The four tetracyclines which showed the most selective complexation completely inhibit aggregation; whereas ampicillin and penicillin, which were less selective, only partially inhibit aggregation.

Antimicrobial Activity against Resistant Bacteria Two species of AMR bacteria were selected to screen with the LEs and their salts: methicillin-resistant *S. aureus* (MRSA, BAA-1720) and *K. pneumoniae* (BAA-2146). This particular strain of MRSA (MRSA-1720) is a hospital-acquired clinical isolate which is resistant by expressing a penicillin-binding protein with a low affinity for synthetic penicillins.[77,78] *Klebsiella pneumoniae* (Kpn2146) was the first isolate of this species to express NDM-1 (New-Delhi metallo-ß-lactamase-1) along with many other resistance determinants. In fact, this strain was resistant against 34 antimicrobial and antimicrobial/adjuvant combinations.[79] Minimum inhibitory concentrations

were determined for the library of antibiotics used in NMR complexation experiments (Table 2-6), as well as for the C_{10}, C_{12}, and C_{14} LEs and salts (Table 2-7).

Table 2-6. MICs of antibiotic library against wildtype (K12) and resistant bacteria.

Antibiotic	**Minimum Inhibitory Concentration (μM)**		
	E. coli K12	Kpn2146	MRSA-1720
Tetracycline	2	≥128	0.025
Minocycline	4	≥128	≤0.063
Ampicillin	16	≥128	≥128
Penicillin G	128	≥128	128
Ciprofloxacin	0.015	≥128	64
Norfloxacin	0.125	≥128	≥128
Kanamycin	4	≥128	≥128
Cefepime	128	≥128	≥128

Table 2-7. MICs of lariat ethers and their salts against wildtype and resistant bacteria.

Lariat Ether	Minimum Inhibitory Concentration (μM)		
	E. coli K12	Kpn2146	MRSA-1720
C_{10}LE	32	≥128	>128
C_{10}LE.2HCl	8	≥128	4
C_{10}LE.2MeI	4	32	2
C_{12}LE	>128	≥128	>128
C_{12}LE.2HCl	>128	≥128	2
C_{12}LE.2MeI	4	4	2
C_{14}LE	n.d.	≥128	≥128
C_{14}LE.2HCl	n.d.	≥128	>128
C_{14}LE.2MeI	n.d.	64	2

In the wildtype bacteria (*E. coli* K12), the freebases and both salts show activity; however, against the resistant strains, only the salts are active. Further, only the methiodide salts are active against the Kpn2146, whereas both salts are active against MRSA-1720.

Because of the enrichment of resistance determinants in Kpn2146, this strain was selected to screen for combination activity between the methiodide salts and the library of antibiotics. The LE.2MeIs were administered at sub-lethal concentrations. The enhancement of antibiotic potency by LE methiodide salts is summarized in Table 2-8.

Table 2-8. Combination activity between methiodide salts and antibiotic library against *K. pneumoniae* BAA-2146.

Drug	LE.2MeI		Antibiotic MIC		Fold Enhancement @ ½ LE MIC
	Sidearm	MIC (μM)	Solo (μM)	Combo (μM)	
Tetracycline	C_{12}	4	>128	32	4x
Minocycline	C_{10}	32	>128	2	64x
	C_{12}	4	>128	8	16x
	C_{14}	64	>128	16	8x
Ciprofloxacin	C_{14}	64	>128	16	8x
Norfloxacin	C_{10}	32	>128	8	16x
Kanamycin	C_{12}	4	>128	2	64x
Cefepime	C_{10}	32	>128	64	2x
	C_{12}	4	>128	8	16x

As previously mentioned, *K. pneumoniae* is an ESKAPE pathogen. It is a priority for AMR research with good reason. This species of bacteria are commonly resistant to polymyxins, carbapenems, fluoroquinolones, cephalosporins, aminoglycosides, and tetracyclines.[13] Clinical isolates of this species have been cultured and classified as "pan-drug resistant", meaning that they are resistant to all antimicrobial agents in all categories.[80] There is about a 10-fold increase in potency for the tested antibiotics, except penicillin derivatives; however, the most significant are for minocycline and kanamycin. Each of these drugs were increased in potency

64-fold with the C_{10}LE.2MeI. This is significant because current treatments for resistant *K. pneumoniae* include new generations of aminoglycosides and synthetic tetracyclines.[81,82] Although kanamycin and minocycline are not novel antibiotics, this is promising as the enhancement of potency could extend to other structures in these families.

2.4 Mechanistic Information and Speculation

An obvious question concerning the enhancement of antimicrobial potency by lariat ethers concerns the mechanism. There are four things that are unequivocally known about the dialkyl lariat ethers themselves. (1) The macroring binds cations. (2) Because the dialkyl lariat ethers are amphiphilic, they can enter membranes. As noted above, neutron reflectance confirms this. (3) Dialkyl lariat ethers having side arms of sufficient length can form aggregates either in the presence or absence of alkali metal cations. (4) Dialkyl lariat ethers can transport cations across membranes either by a carrier or pore-formation mechanism.

The complexation and solubilization of such antibiotics as tetracycline hydrochloride occur with the neutral lariat ethers and not with the corresponding hydrochlorides and methiodides. One-to-one complexation is observed with four of the five tetracycline hydrochloride derivatives examined. Less well-defined complexation occurs with other classes of antimicrobials. However, in some cases compounds that are closely related structures, such as ciprofloxacin and norfloxacin, show some or no complexation, just as observed with tetracycline and chlortetracycline. Further, complexation is more effective with di-n-decyl-diaza-18-crown-6 (C_{10}LE) than it is with the dodecyl (C_{12}LE) derivative. The trend continues for C_{14}LE (Table 2-3). Studies with these three LEs showed that no complexation occurred when the lariat ethers were present either as their hydrochlorides or methiodide derivatives, so no trend could be discerned.

The supramolecular interaction between, for example, tetracycline hydrochloride and C_{10}LE is certain based on the solubilization experiments (visual and NMR). It is confirmed by the diminished aggregation ability of the LEs in the presence of those antimicrobials to which they complex. When no complexation was observed in a solution study, aggregation of the LE was unhindered by the presence of the antibiotic.

The inference we draw from this is that a supramolecular complex is forming that depends on the presence of the antimicrobial's hydrochloride component. The NMR spectra of the complexes show that the most shifted protons are those present on the macrocycle's nitrogen atoms. This suggests a hydrogen bonding interaction between the macrocycle and the antimicrobial. An examination of Corey-Pauling-Koltun (CPK) molecular models suggests that the presence of the chloride in chlortetracycline hinders complexation. This is a steric effect that prevents the formation of two hydrogen bonds. The H-bonds could span from the protonated dimethylamino group in tetracycline's A-ring and the C-ring hydroxyl group. This is illustrated in in 2D in Figure 2-25.

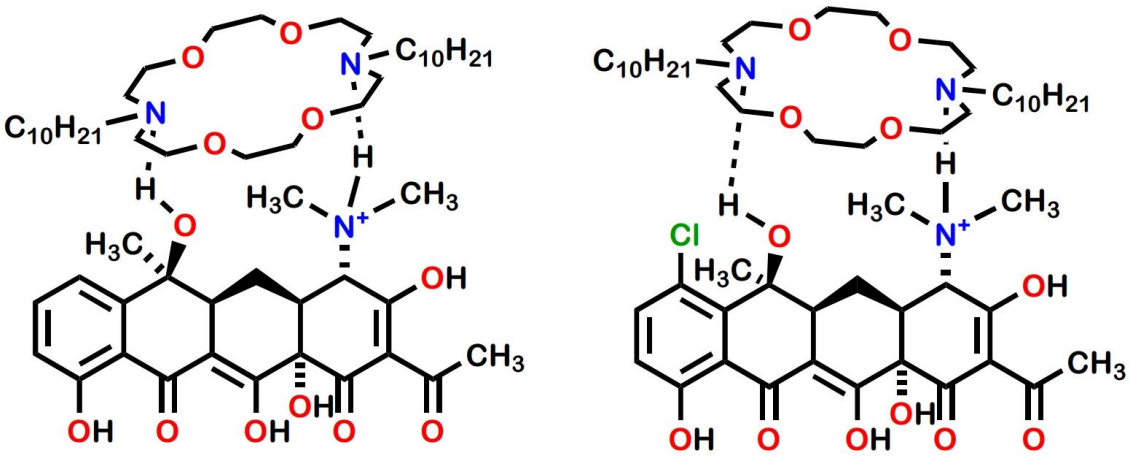

Figure 2-25. Proposed hydrogen bonding between C_{10}LE and tetracycline and chlortetracycline.

Framework models of 18-crown-6 ether and tetracycline were made and overlayed in an attempt visualize possible structures of the supramolecular complex. A photo of this overlay is shown in Figure 2-26. The gray framework model represents the crown ether, while the black model represents tetracycline. Our initial hypothesis was that hydrogen bonds could form between the diaza groups in the crown and the protonated dimethylamino group of the A ring and the C ring hydroxyl. The dimethylamino group of the A ring is well-positioned to form a hydrogen bond with one of the diaza groups of the crown, the C ring hydroxyl is not. Instead, the D ring hydroxyl is in a more favorable position. The locations of suspected hydrogen bonds are indicated with yellow arrows.

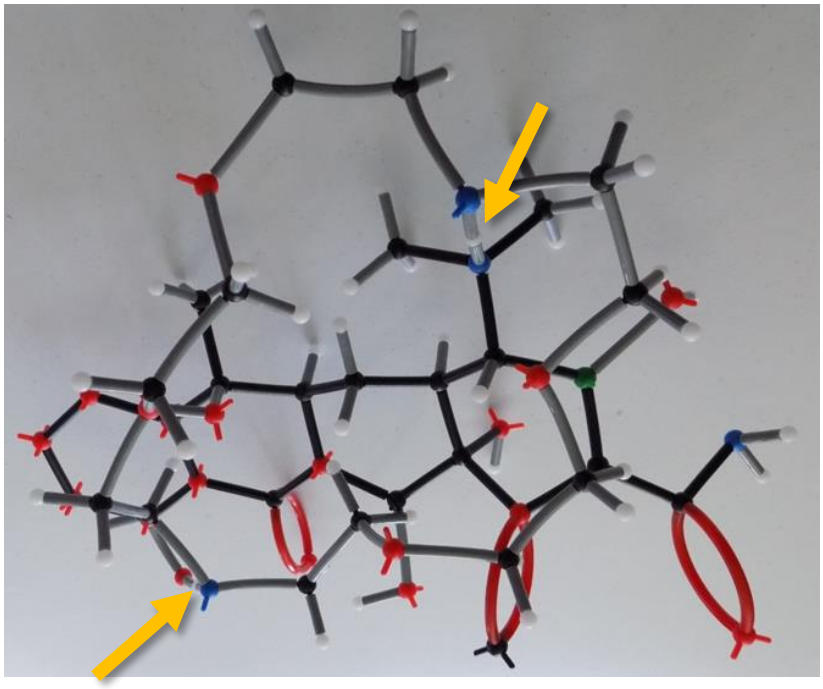

Figure 2-26. Framework model of Crown:Tet complex.

This structural representation is speculative. It is supported by the facts of complexation and the NMR chemical shifts of the protons near macroring nitrogen. However, the molecular models do not show any clear “puzzle-piece” fit.

2.5 Conclusions

N,N-dialkyl-18-crown-6 lariat ethers have been of interest in the Gokel Laboratory due to their bactericidal activity and ion conductance properties. We have previously established that the lariat ethers function both as ion carriers and ion channels. These compounds show individual biological activity, as well as synergy with clinically relevant antibiotics. To improve solubility and stability, hydrochloride and methiodide salts were also prepared and examined for antimicrobial activity. The salts proved to be more potent than the freebases, and subsequent *in vitro* studies employing fluorescence microscopy suggested that the salts differed in mechanism compared to the freebase.

One of the antibiotics which showed synergy with the lariat ethers was tetracycline. In fact, tetracycline resistance was reversed in Tet^R *E. coli*. Through collaboration with Dr. Harshit Kumari, we found that lariat ethers enhance membrane penetration of tetracycline. The lariat ethers are expected to associate with bilayer membranes in some fashion, which could reduce the membrane's integrity leading to increased permeability. However, the enhanced membrane penetration of tetracycline in the presence of LEs could also be due to the formation of a supramolecular complex.

This was investigated with nuclear magnetic resonance (NMR) by examining the solubility of tetracycline in a non-polar solvent in the presence and absence of LEs. The solvent was selected to mimic the hydrophobic interior of a bilayer membrane. We showed that a 1:1 complex forms between the C_{10}LE and tetracycline. In fact, this selectivity was maintained for four other tetracycline derivatives. Only one tetracycline derivative did not form a complex with any LE: chlortetracycline. After examining crystal structures of each tetracycline derivative, we concluded that increased torsion angles in chlortetracycline inhibit contact with the LE in such a way that prevents complexation. Biological synergy was observed for other antibiotic and lariat ether combinations, so a library of antibiotics was

screened for complexation by NMR. They revealed that weaker, more transient complexes form with penicillin derivatives and ciprofloxacin. We suspected that the crown facilitated most of the interactions between LEs and antibiotics, which caused a surprise when we compared complexation ratios for LEs of varying sidearm lengths. The best results were obtained with the *n*-decyl sidearms, while the *n*-dodecyl and *n*-tetradecyl showed weaker complexation. This suggests that while the crown dominates the intermolecular interactions, the sidearms also contribute.

Next, we sought to better understand the nature of the complexes being formed. It was previously established that the lariat ethers spontaneously formed aggregates in aqueous solution. The crown moiety is polar enough to serve as a headgroup, and the alkyl sidearms orient to form hydrocarbon tails. Although CPK models could not illuminate a likely conformation, we suspected that the supramolecular complex is largely held together by hydrogen bonds which would only be possible in the crown moiety. Based on peak broadening observed in the NMR, it was hypothesized that most interactions must be centered around the crown. Aggregation of the LEs alone and in concert with antibiotics was examined with dynamic light scattering (DLS). This revealed that when a complex was formed, aggregation was inhibited. This correlated well with the degree of complexation observed in NMR spectra. Where we saw 1:1 complexation, aggregation was completely inhibited. Where there was transient/weak complexation, aggregation was partially inhibited. Where there was no evidence of complexation, aggregation was unaffected. This suggests that complex formation alters the amphiphilicity of the LEs to an extent that aggregation is disfavored.

The potency of lariat ethers, and their salts, individually make them good candidates for novel antibiotics. They alter permeability of cell membranes and disrupt ion regulation, while remaining non-cytotoxic. Combined with their synergy to multiple classes of clinically relevant antibiotics, they become even more attractive

drug candidates. The results described here highlight the selectivity of lariat ethers for the tetracycline class of antibiotics, as well as explore the nature of supramolecular complexes formed.

Chapter 3

Structure Activity Relationship of Bis-Tryptophans

3.1 Introduction

The Gokel Lab has studied crown ether derivatives and their applications in ion conductance, notably by dint of membrane channel formation for more than 20 years. This has led to the question: what are the minimum requirements for a unimolecular transmembrane channel? Sequence analysis of transmembrane proteins shows an enrichment of tryptophan residues at the bilayer interface.[83] Previous work done by our lab involved the preparation of *N*-alkylindoles (structures shown in Figure 3-1). The cholestanyl derivative was substituted at the two position. These were prepared and analyzed by dynamic light scattering (DLS). The data are shown below in Table 3-1.[60]

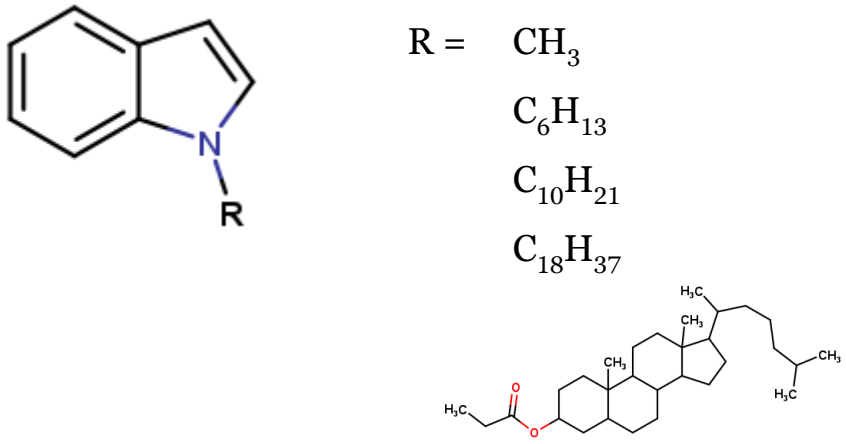

Figure 3-1. Structure of *N*-alkylindoles.[60]

Table 3-1 Laser light scattering data for aggregates formed from *N*-substituted indoles.

R	Unimodal diameter (Å)	Cumulative distribution (Å)	
		by intensity	by weight
CH_3 [a]	*b*	*b*	*b*
Hexyl [a]	*b*	*b*	*b*
Decyl [a]	2720 ± 430	2840 ± 470	2900 ± 450
Octadecyl [a]	3130 ± 1000	3880 ± 2100	4550 ± 2200
Octadecyl [c]	1380[d]	1980 ± 1210	688[d]
Cholestanyl [c]	2180 ± 740	2600 ± 1000	2570±1300

[a] Vesicles prepared by reverse-phase method. [b] No aggregates detected. [c] Vesicles prepared by lipid hydration method. [d] Standard deviation broad.

The formation of aggregates requires a polar headgroup attached to a nonpolar tail. Traditionally, indole is not regarded as having polar character; however, the data clearly show that when substituted with an alkyl moiety of suitable length, indole functions as a headgroup to form stable vesicles.[61] A control experiment was conducted to verify that a polar head group was necessary for aggregate formation using *N*-decylbenzene. This compound showed no evidence of aggregation, as expected. Together, these results suggest that the *N*-alkylindoles are very simple molecules with the potential to be membrane active.

Tryptophan is one of three aromatic proteinogenic amino acids, with the other two being phenylalanine and tyrosine. Due to the electron-rich nature of the indole group, tryptophan is highly fluorescent and solvatochromic.[59] It also has the lowest frequency of the 20 naturally occurring proteinogenic amino acids. Despite having a low frequency in proteins, tryptophan often appears in very interesting locations in proteins and peptides.[83,84] For example, the KcsA voltage gated potassium channel is

enriched with tryptophan along the bilayer interface.[30] Similarly, the antimicrobial pore former, gramicidin, contains a series of Leu-Trp repeats that is thought to orient the peptide for dimerization.[85] These all suggest that tryptophan often functions as a membrane anchor.

It was hypothesized that bola-amphiphiles consisting of terminal tryptophan residues with varying alkyl spacers would show biological activity. It was expected that the indole groups could help the compound to interact with a biological membrane, while the strong amphiphilic nature might facilitate its incorporation into the membrane. An initial library of compounds, referred to as bis-tryptophans (BTs), were prepared and screened for biological activity against bacteria. Their structures are shown in Figure 3-2.[63]

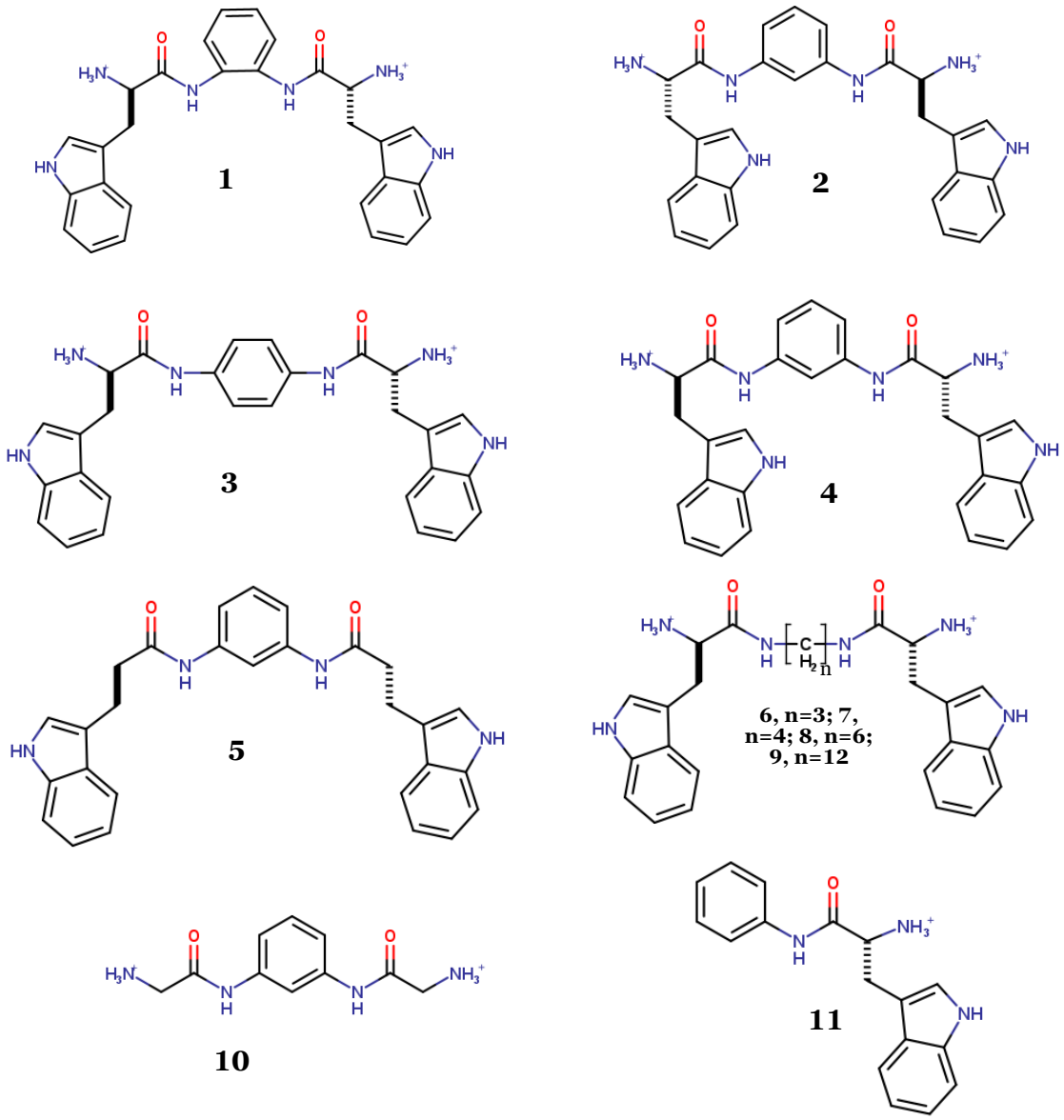

Figure 3-2. Structures of the first suite of bis-tryptophans.[63],[3]

Initial focus was placed on a variety of simple aliphatic and aromatic linkers. The aromatic BTs consisted of *o/m/p*-phenylene linkers (compounds **1**, **2**, **3**), while the aliphatic BTs derived from propylene, butylene, hexylene, and dodecylene linkers (compounds **6**, **7**, **8**, and **9**). Additionally, compounds were prepared that varied only in stereochemistry. Compound **2** has the L,L-stereochemistry, while compound

[3] The previously synthesized BTs were prepared by Joseph Meisel and Michael McKeever.

4 is the D,D-isomer. Three controls compounds were also prepared: one which lacked the terminally charged amines (**5**), one which substituted the tryptophans for glycine residues (**10**), while the last control was monosubstituted (**11**).

These compounds were screened to determine their minimum inhibitory concentrations (MICs) against Gram +/- bacteria according to methods dictated by the National Committee for Clinical Laboratory Standards.[73] The data shown in Table 3-2 reflects the concentrations at which bacterial growth is inhibited by 80%. It is important to note that concentrations above 128 μM were not tested, as compounds active above this concentration are not clinically relevant.

Table 3-2. Minimum inhibitory concentrations of initial BT library.[63]

Cmpd	Linker	*E. coli* K12[a]	*E. coli* Tet^R (μM) [a]	*S. aureus* [a]
1	*ortho*-Ph (L-Trp)	64	56±8	32
2	*meta*-Ph (L-Trp)	64	48±8	32
3	*para*-Ph (L-Trp)	128	120±14	128
4	*meta*-Ph (D-Trp)	64	28±4	32
5	*meta*-Ph (IPA)[b]	>128	>128	>128
6	$(CH_2)_3$	>128	>128	>128
7	$(CH_2)_4$	>128	>128	>128
8	$(CH_2)_6$	>128	>128	>128
9	$(CH_2)_{12}$	8	10±2	4
10	*meta*-Ph (Gly)	>128	>128	>128
11	C_6H_5-L-Trp-NH_2	>128	>128	>128

[a] All concentrations given in μM. [b] 3-(3-Indolyl) propanoic acid.

Escherichia coli K12 and *Staphylococcus aureus* were selected as representative Gram -/+ organisms, respectively. The Tet^R strain of *E. coli* was transformed in house to express the TetA efflux pump, which confers tetracycline

resistance upon the bacterium.[29] It was concluded that both the ammonium and indole moieties were required for activity, based on the inactivity of **5** and **10**. Additionally, the symmetric design proved to be essential for activity, given that the mono-tryptophan (**11**) was inactive. Although the aromatic BTs were modestly active, the *ortho*- and *meta*-phenyl linkers were slightly more potent than the *para*-phenyl, particularly in the Gram + and the resistant strain. Additionally, the aliphatic BTs' potencies clearly show a length dependence, with the C_{12} spacer being most active.

Membranes are a ubiquitous organelle found in every living cell, which presents a danger when designing membrane active drugs. The BTs were designed specifically to interact with biological membranes; however, to be a useful drug candidate, they must be non-cytotoxic. Cell viability against compounds **2**, **4, 6,** and **9** was examined using an XTT assay against three mammalian cell lines: human embryonic kidney (HEK 293), human cervix epithelial (HeLa), and *Cercopithecus aethiops* kidney (COS-7). It was concluded from the results in Figure 3-3 that although the aliphatic BTs are more cytotoxic than the aromatics, the BT class exhibits minimal cytotoxicity at their respective MICs.

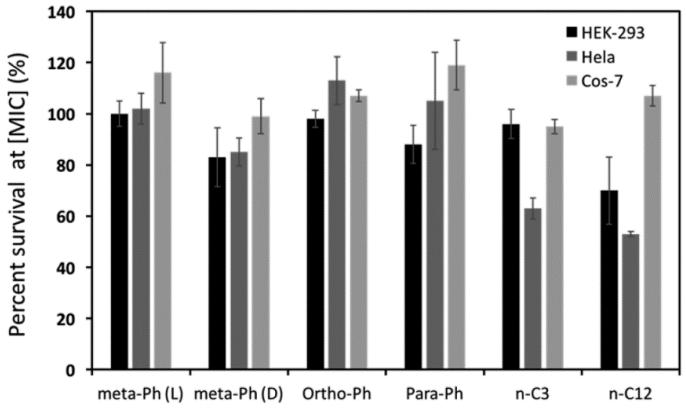

Figure 3-3. Cytotoxicity of select BTs (**1, 2, 3, 4, 6,** and **9**) against three mammalian cell lines.

Despite being biologically active on their own, the BTs were subsequently analyzed for their ability to recover antibiotic potency in resistant bacteria, particularly bacteria harboring efflux pumps. Administering the BTs at sub-MIC concentrations would ensure that the compounds did not affect bacterial growth. It was hypothesized that if the BTs were membrane-active, they could recover antibiotic potency in cases of efflux-pump mediated resistance. As previously mentioned, Tet^R *E. coli* was transformed in-house. This strain of bacteria expresses the TetA efflux pump, is resistant to tetracycline, and has a MIC for tetracycline of 900 μM.[86] As shown in Table 3-3, the BTs cause a remarkable reduction in the tetracycline MIC.

Table 3-3 Recovery of tetracycline potency in Tet^R *E. coli*.

Cmpd.	Linker	[cmpd] μM	MIC [Tet] μM	Fold recovery
	None	0	900	n.a.
2	*meta*-Ph (L-Trp)	24 [1/2 MIC]	56.25	16-fold
2	*meta*-Ph (L-Trp)	12 [1/4 MIC]	112.5	8-fold
4	*meta*-Ph (D-Trp)	14 [1/2 MIC]	112.5	8-fold
4	*meta*-Ph (D-Trp)	7 [1/4 MIC]	225	4-fold
1	*ortho*-Ph (L-Trp)	28 [1/2 MIC]	112.5	8-fold
1	*ortho*-Ph (L-Trp)	14 [1/4 MIC]	225	4-fold
3	*para*-Ph (L-Trp)	60 [1/2 MIC]	112.5	8-fold
3	*para*-Ph (L-Trp)	30 [1/4 MIC]	225	4-fold
6	$(CH_2)_3$	60 [1/2 MIC]	112.5	8-fold
6	$(CH_2)_3$	30 [1/4 MIC]	112.5	8-fold
9	$(CH_2)_{12}$	5 [1/2 MIC]	225	4-fold
9	$(CH_2)_{12}$	2.5 [1/4 MIC]	450	2-fold

Despite seeing modest individual activity, the aromatic BTs induce consistent 8-fold enhancement in tetracycline potency. Although the C_{12}BT was the most active compound on its own, it showed the lowest recovery of tetracycline potency.

The *m*-phenylene and dodecylene BTs became the two most interesting compounds, so their ability to permeabilize membranes was investigated further. Tet^R *E. coli* was employed for this study and was stained with fluorescein diacetate (FDA) and propidium iodide (PI), following treatment with **2** and **9**. FDA is readily permeable to cells; however, it will only fluoresce in viable cells capable of hydrolyzing its diester bonds. Propidium iodide fluoresces when it intercalates with DNA; however, it is impermeable to intact membranes. Co-staining with these two fluorophores allows us to identify cells in which viability is maintained although membrane integrity is compromised.

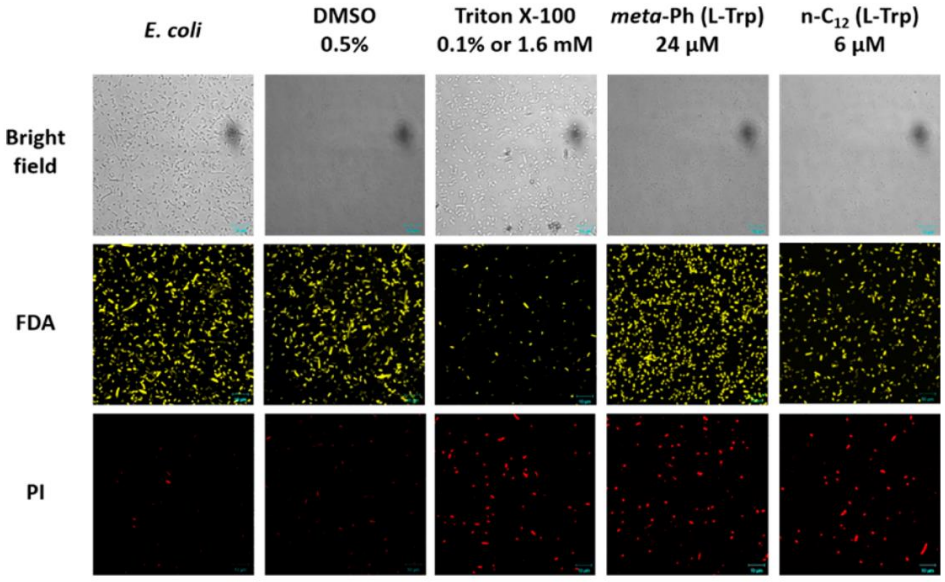

Figure 3-4. Membrane permeability of **2** and **9** at ½ MIC.[63]

The recovery of tetracycline potency and the changes in membrane permeability suggest a mechanism in which the BTs infiltrate the bacterial

membranes and permit more facile entry of the antimicrobial. The images of Figure 3-4 also show that cell viability is maintained.

As previously mentioned, the BTs were prepared with the expectation that they would be membrane active. Although their length is significantly shorter than a typical bilayer membrane, the tryptophan may still serve as a membrane anchor and partial insertion is possible. A planar bilayer voltage clamp (BLM) experiment was used to assess the biologically active BTs (**1, 2, 3, 4,** and **9**) for their membrane insertion and ion conductance. These experiments were conducted in a planar soybean azolectin bilayer membrane. Figure 3-5 shows the classic open-close behavior indicative of channel formation obtained from the *m*-phenyl BT, **4**.[87]

Figure 3-5. Open-close channel behavior or *m*-phenyl BT, **4**, applied voltage = 30 mV, 10 mM HEPES, 450 mM KCl.[87]

This channel activity was observed for each of the aromatic BTs; however, neither **7** (hexylene) nor **9** (dodecylene) showed such activity. Of course, the planar bilayer experiment is challenging and not every experiment yields results. However, assuming that the efforts with **7** and **9** were not simply experimental failures, this suggests that the aromatic and aliphatic BTs may be biologically active through different mechanisms. The aromatic compounds show significant membrane penetration and ion conductance, while the aliphatic compounds appear only to insert into the membrane.

3.2 Target Structures and Experimental Details

One of the goals of the research described in this dissertation was to expand the existing library of BTs. The aliphatic category was missing most of the odd-

numbered linkers, and the aromatic category was limited to three isomers. The structures shown in Figure 3-6 were identified as the most interesting candidates for further exploration and given priority.

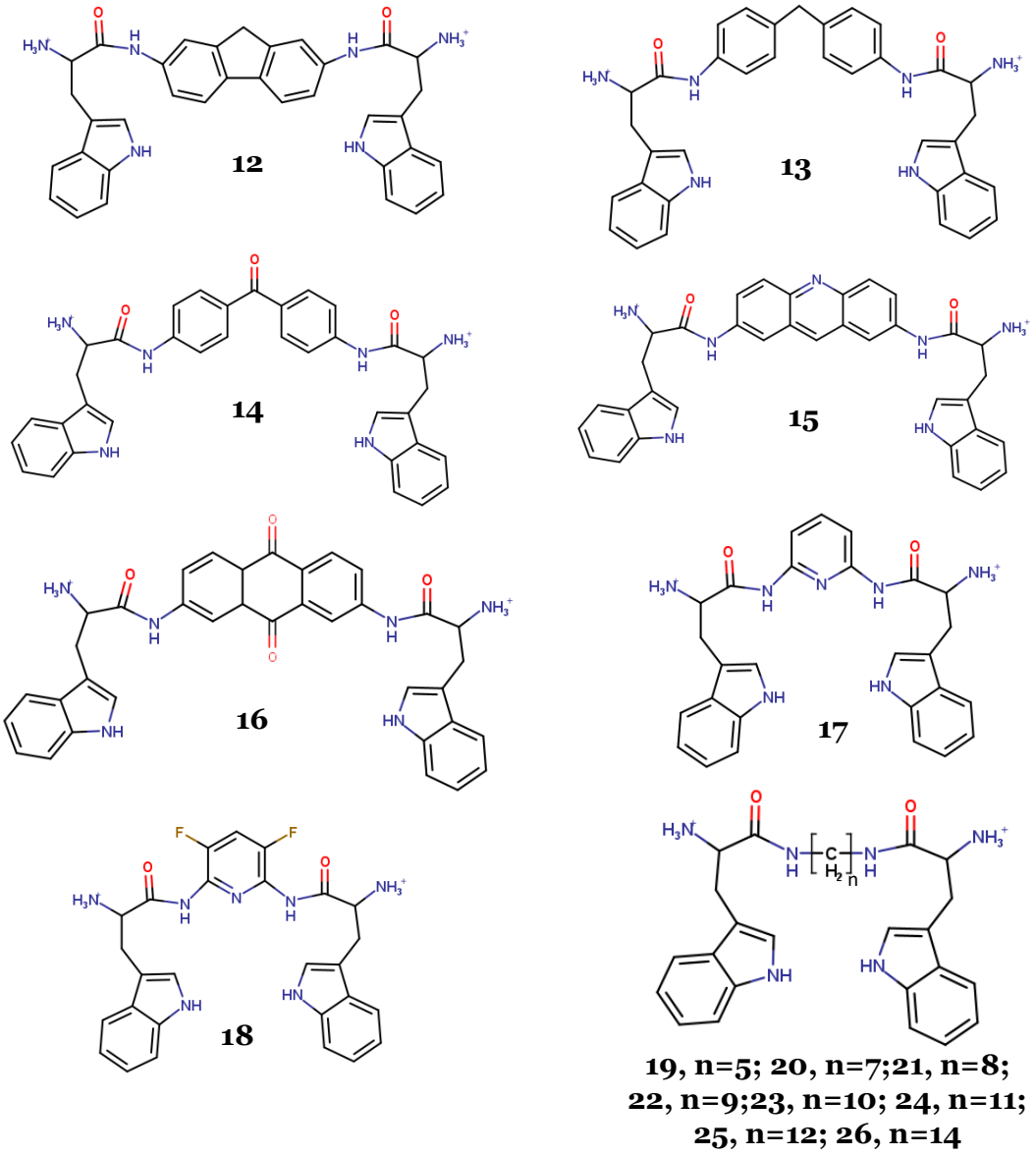

Figure 3-6. Proposed structures to expand BT library.[4]

[4] Compounds 21, 23, and 26 were originally prepared by Michael McKeever, although I performed their synthesis myself.

The synthesis of bis-tryptophans is a straightforward process. Initially, the *t*-butyl carbamate protected tryptophan was dissolved in *N, N*-dimethylformamide (DMF) along with 2-(1 H-benzotriazol-1-yl)-1,1,3,3-tetramethyluronium hexafluorophosphate (HBTU, Hexafluorophosphate Benzotriazole Tetramethyl Uronium) (2.1 equivalents) and diisopropylethylamine (DIPEA) (4.0 equivalents for neutral diamines and 6.0 equivalents for dihydrochlorides). This reaction mixture stirred for ~1/2 an hour before the diamine, dissolved in either DMF or DMSO, was added. The reaction was allowed to run until there was no visible change observed by using thin-layer chromatography (TLC). Next, the reaction was diluted with ethyl acetate and washed three times each with 1M $NaHSO_4$, 5% $NaHCO_3$, and brine. The resulting organic layer was filtered through $MgSO_4$/Celite, the solvent evaporated. In most cases, the protected crude material appeared as a light yellow/tan solid. This reaction is shown in Scheme 3-1.[63]

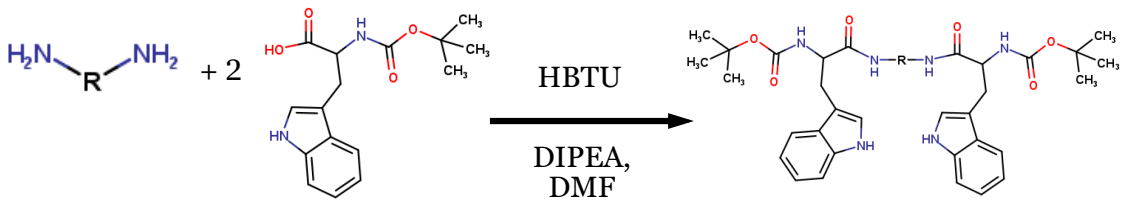

Scheme 3-1. Synthesis of *N*-Boc protected product.

To remove the Boc protecting group, the crude product was dissolved in a minimal volume of 1,4-dioxane. Next, HCl in dioxane (4 M) was added and allowed to stir for two-to-three hours. During this time, the deprotected product precipitated from solution. It was subsequently filtered and dried over a high vacuum. This reaction is shown in Scheme 3-2.

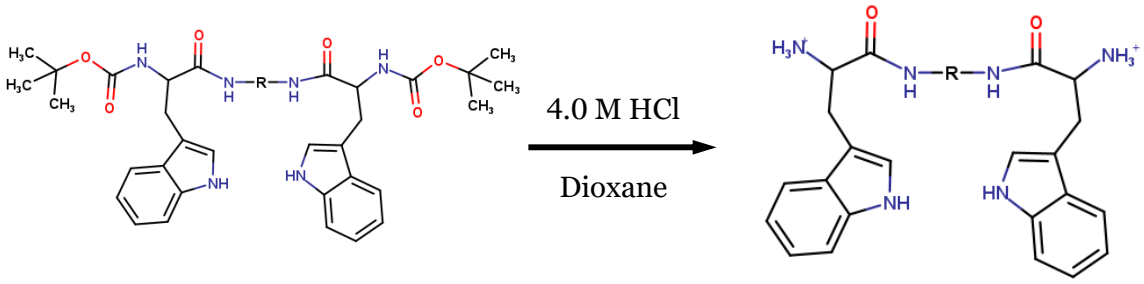

Scheme 3-2. Deprotection of crude product to yield dihydrochloride product.

3.3 Results and Discussion

Rational Design of Target Structures The aromatic linkers shown in Figure 3-6 were selected because no other aromatic compounds beyond the phenylenes had yet been prepared. Further, the presence of an extended aromatic system might provide an entity with greater fluorescent response than observed for tryptophan alone. It was also unclear whether any heteroatoms could successfully be incorporated into the BT framework. Thus, compounds **14**-**18** were proposed.

The simple aromatic BTs (*o*/*m*/*p*-PhBTs), while biologically active, were not very potent antimicrobials. There was a question of whether increasing the size of the aromatic linker would improve or diminish the antimicrobial activity. For this reason, several structures incorporating poly-ring systems were proposed, some with fused rings and others with a more flexible methylene linker. Notably, **12** (fluorenyl), **15** (acridine), and **16** (anthraquinone) were designed with other applications in mind. Compounds **12** and **15** contain fluorene and acridine linkers. These two motifs are commonly found in commercial fluorophores. It was hypothesized that by incorporating them into a bis-tryptophan scaffold, the resulting compound could be a highly permeable cell stain. Compound **16** was imagined as a molecular switch because anthraquinone is known to undergo facile redox chemistry and the radical ions are water stable, even if oxygen sensitive.

Unfortunately, there was limited success with the aromatic linkers. Only compounds **12** (fluorenyl) and **13** (diphenylmethyl) were successfully prepared. The reactions where the linker contained a heteroatom simply did not work. Even with longer reaction times, increased temperature, and greater equivalents of DIPEA, the reactions involving **14-18** failed to afford isolable products. It is thought that the presence of heteroatoms decreases the reactivity of the α,ω-amines which prevents it from coupling with tryptophan. In contrast, there was no difficulty in preparing the odd-chain aliphatic BTs.

Aliphatic Bis-Tryptophans The design of bis-tryptophans was based on previous work in the Gokel Lab showing that tryptophan can serve as a polar head group in the context of an amphiphile.[84] As such, it was assumed that the resultant amphiphiles (technically bola-amphiphiles) would interact with membranes. To assess the likelihood that a compound will interact with membranes, our lab has utilized dynamic light scattering (DLS) to assess aggregate size. If a compound spontaneously forms aggregates in aqueous solution, it is likely that the compound will associate with biological membranes.

Aggregation was monitored for the eleven aliphatic BTs, *n*$C_{3\text{-}12,14}$BT, as well as for the five aromatic BTs: *o/m/p*-phenylene, 2,7-fluorenyl (FBT), 4,4-diphenylmethane (DPM). Stock solutions were prepared fresh in DMSO prior to each experiment. They were subsequently diluted across a range of biologically relevant concentrations, from 10-256 μM, in 1x phosphate buffered saline (PBS) and 0.5% DMSO. Both PBS and DMSO were filtered through a 0.2 μM filter before being used to prepare any solutions. These solutions were thoroughly mixed, then allowed to sit at room temperature on the bench top for two hours before being analyzed with DLS. The particle size of each solution was an average of 10 measurements over 20 minutes. Each compound was analyzed at least in triplicate on different days to obtain aggregate sizes with <10% error.

Particle size analysis of the aliphatic BTs shows that when the linkers are shorter chains, aggregation is not observed as highlighted in Figure 3-7. This is not unexpected, because previous work done by our lab showed that indole functions as a polar headgroup for aggregation only when coupled with a sufficiently sized hydrophobic tail/linker. The minimum length required for aggregation appears to be the *n*-heptyl linker. Aliphatic linkers longer than this all readily form aggregates, even at the lowest concentration studied (10 μM). The results from these DLS experiments are shown in Figure 3-8.

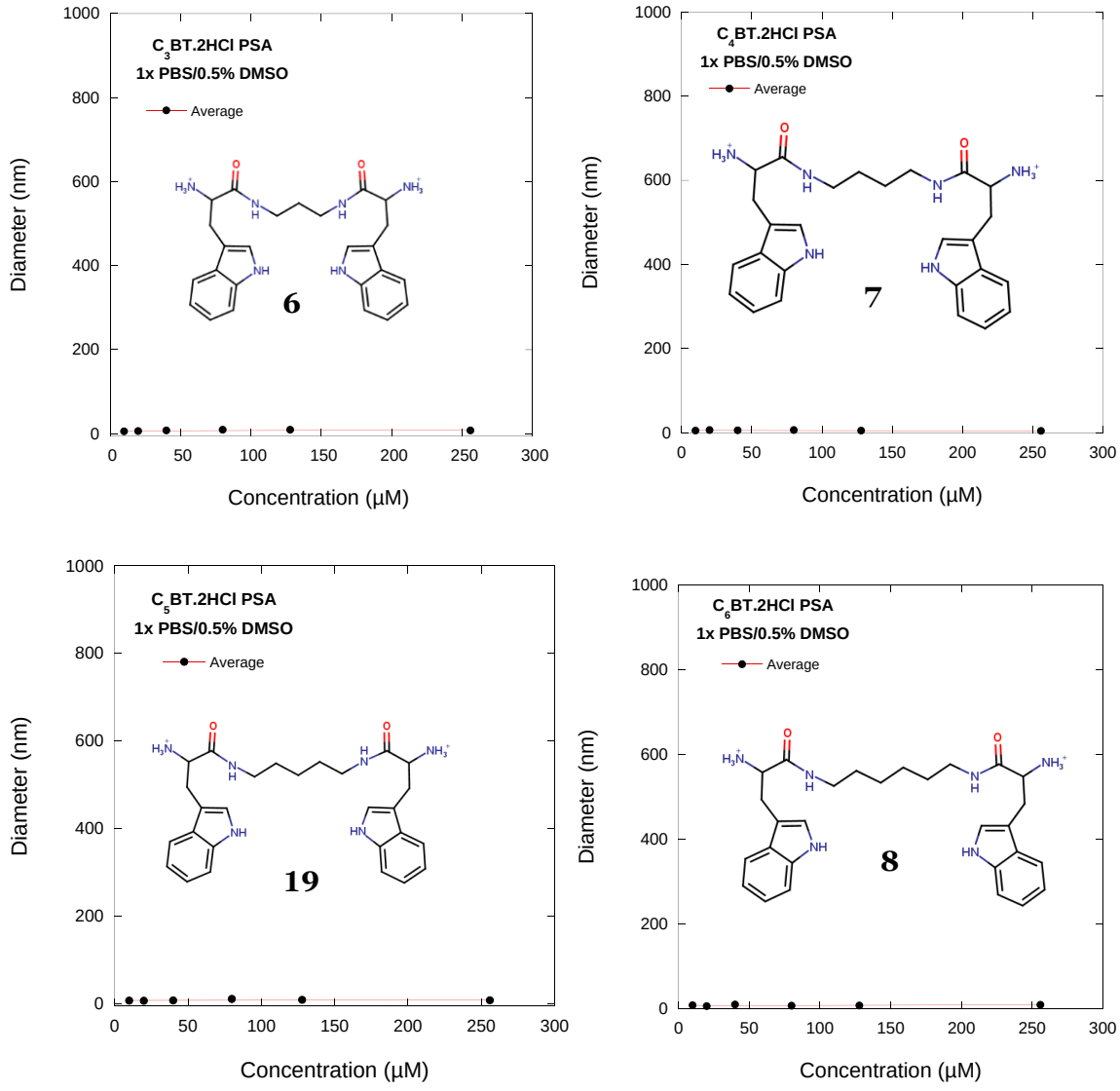

Figure 3-7. Particle size analysis of short chain aliphatic BTs in 1x PBS/0.5% DMSO showing no aggregation for **6, 7, 8,** and **9**.

The situation proved to be entirely different when the BT linkers contained seven or more carbon atoms. Experiments like those, the results of which are graphed in Figure 3-8, showed clear evidence of concentration-dependent aggregation.

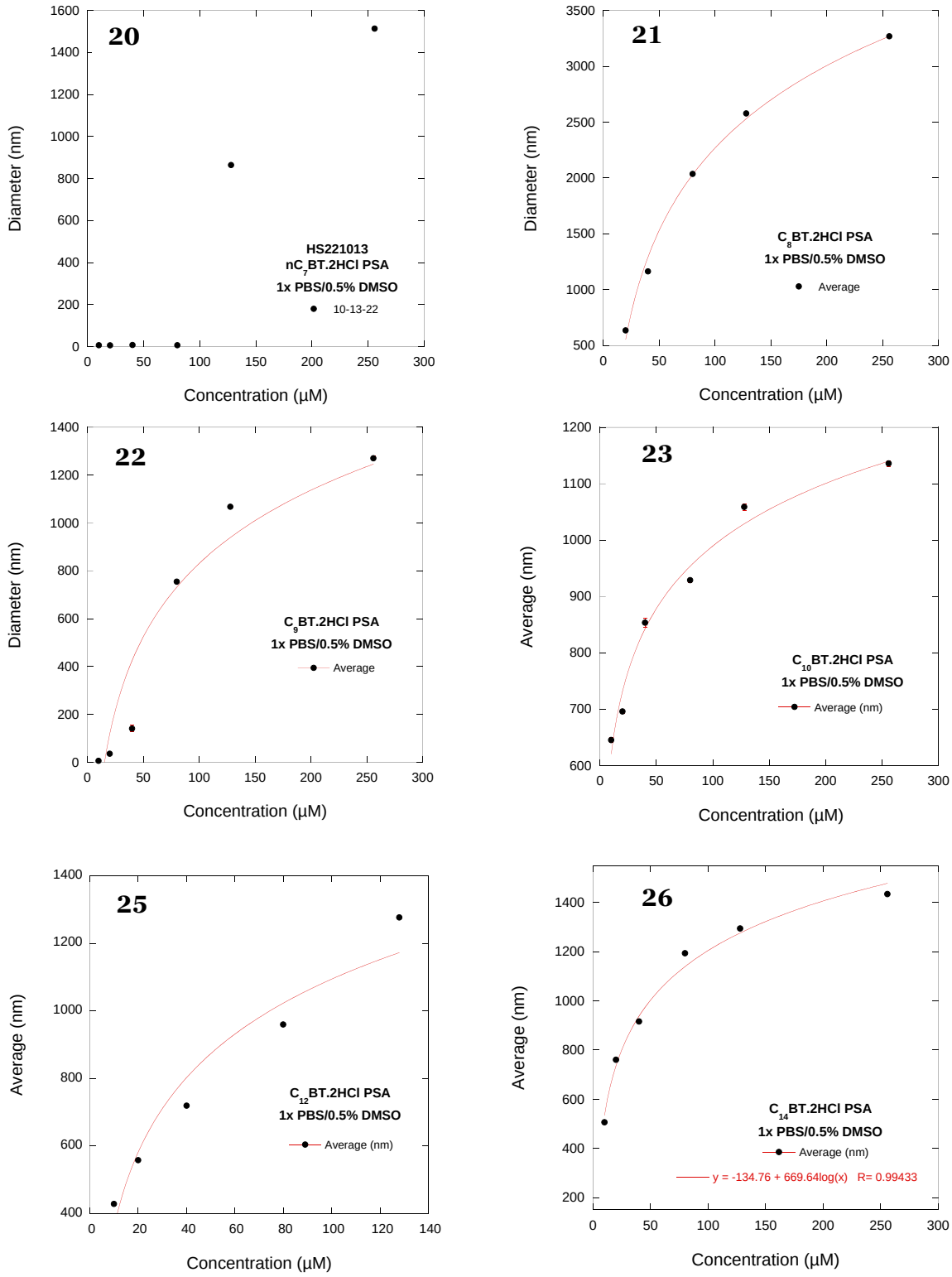

Figure 3-8. Particle size analysis of long chain aliphatic BTs.

Simultaneous with the DLS experiments, the new bis-tryptophans were screened for individual antimicrobial activity against *E. coli* K12, which is a commonly used Gram – bacteria. The bacterial cells were grown in Mueller-Hinton II (MHII) media in accord with the National Committee for Clinical Laboratory Standards protocol for MIC determination.[73] Taken together, it becomes apparent that aliphatic BTs show a relationship between their propensity for aggregation and their antimicrobial activity (Figure 3-9).

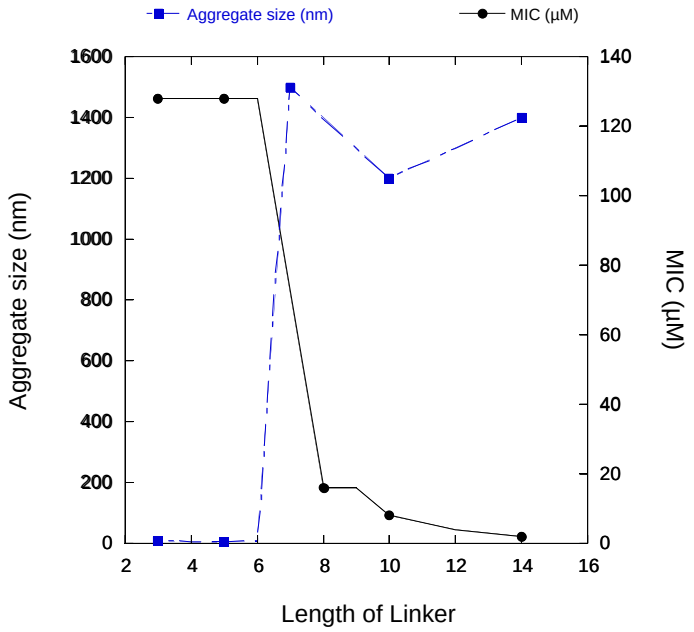

Figure 3-9. Correlation of aggregation in aqueous solution with antimicrobial activity. **23** forms very large aggregates relative to the other BTs; it was intentionally omitted from this graph to not distort it unnecessarily.

The data in Figure 3-9. clearly show that the aliphatic BTs are biologically active only when they form aggregates. The black trace shows the trend of MICs, while the blue trace shows the largest aggregate size at 256 μM.

The partition coefficient, or log P, is a number that describes the ratio of a compound's concentration between two immiscible solvents, typically water and *n*-

octanol.[71] This value is used to predict the hydrophobicity or hydrophilicity of a compound. Lower log P values indicate more hydrophilic character, while higher values indicate the opposite. Log Ps were calculated for all the BTs under study in this dissertation; the values for the aliphatic BTs are listed in Table 3-4, along with their particle sizes and MICs.

Table 3-4 log Ps, particle sizes, and MICs of aliphatic bis-Tryptophans.

Compound	**Log P[a]**	**Particle Size (nm)[b]**	**MIC (μM)[c]**
nC_3BT (**6**)	1.07	n/a	>128
nC_4BT (**7**)	1.59	n/a	>128
nC_5BT (**19**)	2.04	n/a	>128
nC_6BT (**8**)	2.46	n/a	>128
nC_7BT (**20**)	2.96	1500	128
nC_8BT (**23**)	3.37	3300	16
nC_9BT (**21**)	3.81	1300	16
nC_{10}BT (**6**)	4.26	1200	8
nC_{11}BT (**22**)	4.70	TBD	TBD
nC_{12}BT (**9**)	5.15	1300	4
nC_{14}BT (**24**)	6.04	1400	2

[a]Calculator plug-ins were used for log P, Marvin 19.9.0, 201(2019), chemaxon.com. [b]at 256 μM. [c]against *E. coli* K12.

All the inactive BTs (**6, 7, 19,** and **8**) have log Ps of <3, while generally the active BTs (**6, 9, 21-24**) have log Ps >3. The data in Table 3.4 clearly demonstrates that there is a critical transition that occurs around log P = 3. The *n*-heptyl BT (**20**) is the shortest chain BT to spontaneously aggregate in aqueous solution. It also shows modest antimicrobial activity with a MIC against *E. coli* K12 of 128 μM. The

transition that occurs at the *n*-heptylBT is evidenced by the fact that aggregates are not observed until much higher concentrations, relative to the longer chain BTs which aggregate around 10-20 μM. All active aliphatic BTs have log P values of about ≥3. This confirms that an aliphatic BT's propensity for aggregation is a good indicator of its biological activity.

Aromatic Bis-Tryptophans The aromatic BTs follow a similar trend. Although all five aromatic compounds are active at clinically relevant concentrations, the compounds which form larger aggregates are more potent. The particle size analyses of the aromatic BTs are shown in Figure 3-10 and 3-11. These aromatic BTs have been further divided into two categories: single-ring and poly-ring BTs. For the single-ring BTs (phenylene derivatives, **1, 2,** and **3**), aggregation is not observed at low concentrations. Single-ring BTs also do not grow to very large sizes, except for the *o*-phenylene BT, **1**. On the other hand, the poly-ring BTs form large aggregates, on the order of 10^4 nanometers. Interestingly, the poly-ring BTs are significantly more potent than the single-ring BTs.

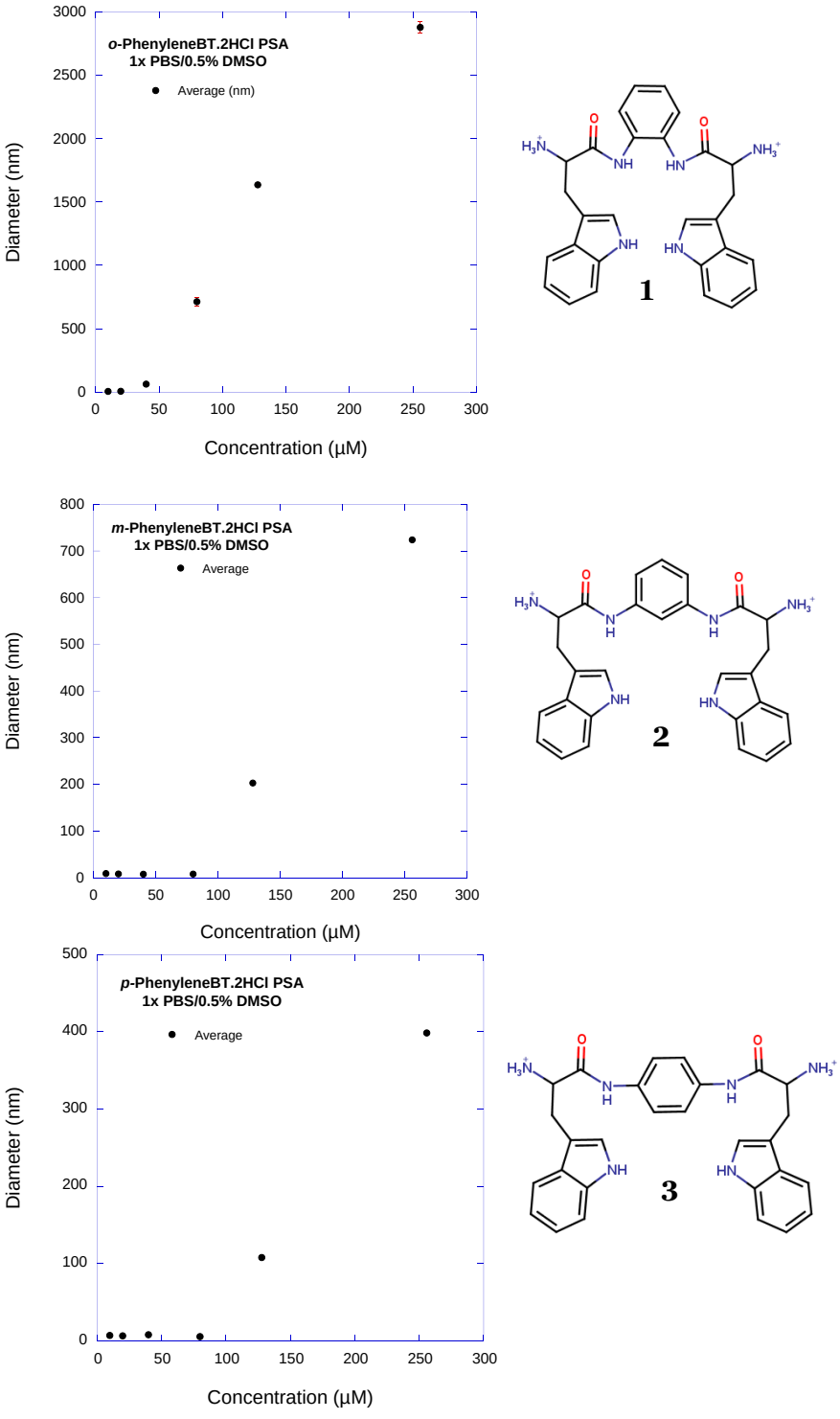

Figure 3-10. Particle size analysis of **1, 2,** and **3** in 1x PBS/0.5% DMSO.

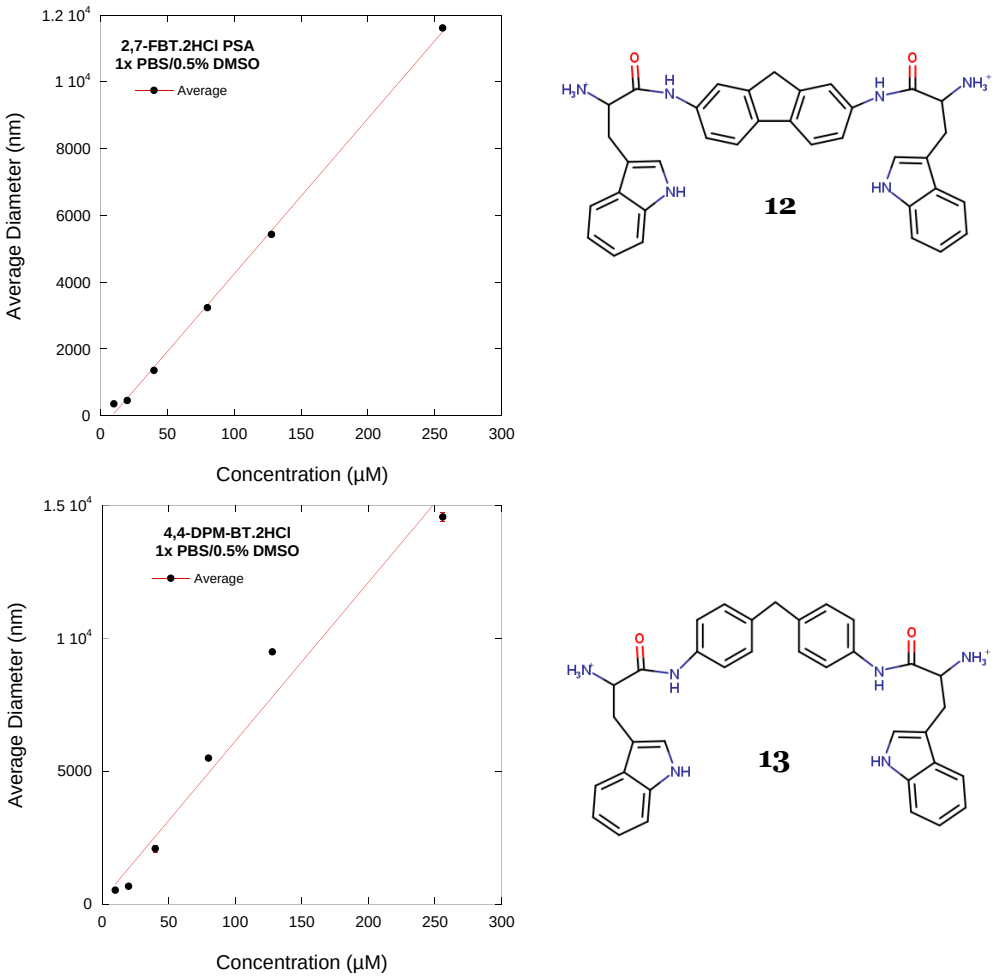

Figure 3-11. Particle size analysis of **12** and **13** in 1x PBS/0.5% DMSO.

Comparing Figures 3-10 and 3-11, it is obvious that the poly-ring aromatic BTs aggregate much more readily than the phenylene isomers. This is reflected in the lower concentrations at which aggregates are first observed, 40 μM compared to ~100 μM.

Both aliphatic and aromatic BTs show a correlation between their spontaneous aggregation and antimicrobial activity. However, aggregation does not seem to be enough for the aromatic BTs. Each of the five aromatic BTs aggregate, but the poly-ring linkers are nearly 10-fold more potent. This lends support to the

hypothesis that the aromatic and aliphatic BTs function through two different mechanisms.

Table 3-5. LogPs, particle sizes, and MICs of aromatic bis-Tryptophans.

Compound	Log P[a]	Particle Size (nm)[b]	MIC (μM) [c]
ortho-Ph (L-Trp) (**1**)	3.25	2900	64
meta-Ph (L-Trp) (**2**)	3.25	700	64
para-Ph (L-Trp) (**3**)	3.25	400	128
2,7-FBT (**12**)	5.01	11,600	8
4,4-DPM (**13**)	5.34	14,600	8

[a]Calculator plug-ins were used for log P, Marvin 19.9.0, 201(2019), chemaxon.com.

[b]at 256 μM. [c]against *E. coli* K12.

3.4 Conclusions

Our lab has been interested in minimalistic ion channels for several decades. The initial focus was on crown ether derivatives, which were quite successful given the activity and potency of both lariat ethers and hydraphiles. However, their synthesis is somewhat complicated and low yielding. As stated in the introduction, tryptophan has low abundance relative to the other proteinogenic amino acids; however, it is enriched at protein/bilayer interfaces. We had previously shown that indole functioned as a polar head group when attached to a sufficient non-polar tail, so the bola-amphiphiles known as bis-tryptophans were designed. This symmetrical design is easily accessible synthetically, and in high yields (70-90%). The early BTs proved to be active at low micromolar concentrations, and some even showed channel-like activity in planar bilayer experiments. The recovery of antibiotic potency in resistant bacteria by BTs further emboldened our desire to expand the library of structures.

Desirable linkers for the BTs were identified. Particularly, we were interested in the odd chain aliphatics and more complex aromatic structures. While aliphatic BTs were easily synthesized, aromatic structures containing heteroatoms yielded products that could not be isolated. Nevertheless, two poly-ring aromatic linkers were successful: the 2,7-fluorene and 4,4-diphenylmethane. The suite of bis-tryptophans were assessed for their ability to form aggregates in aqueous solution; this was intended to predict the likelihood that they would associate with a biological membrane. They were also examined for antimicrobial activity. Interestingly, compounds which readily aggregated were also potent against *E. coli* K12, whereas compounds which did not aggregate were nontoxic to the cells.

The relationship of amphiphilicity to activity is clear from an empirical point of view. The presumption is that membrane affinity translates to membrane penetration and enhancement of membrane permeability. It also appears that aromatics and aliphatics may differ in mechanism, but no evidence is currently in hand to specify either mechanism or to differentiate them.

Chapter 4

Further Research

We hypothesize that the reversal of tetracycline resistance by lariat ethers is coordinated by two mechanisms: increased tetracycline accumulation within the cell and inhibition of at least the TetA efflux pump. Here, several experiments are proposed to address these mechanisms.

The first experiment addresses to what extent tetracycline accumulates in a membrane-bound vesicle. Neutron reflectance data shows that in the presence of the lariat ether, tetracycline more effectively penetrates a synthetic membrane. Additionally, it showed that tetracycline is more prone to transverse mobility (flip-flopping) between the two leaflets of the membrane when lariat ether is present. Tetracycline and many derivatives have been extensively studied using absorption spectroscopy. This allows the concentration of tetracycline to be quantified using the same technique. I propose forming two types of small unilamellar vesicles (SUV): one that contains only lipids and one that contains both lipids and lariat ether molecules. Next, tetracycline will be introduced to both SUV solutions. Following an equilibration time, the solutions will be placed into dialysis to remove any tetracycline which did not penetrate the vesicles. The SUVs should now be in pure buffer with no contaminating tetracycline. Then the absorption spectra could be collected and quantitated to determine the concentration of tetracycline in both SUV solutions. While we may never be able to construct a completely representative synthetic biological system, comparing the tetracycline concentration between the two solutions could reveal if the lariat ethers significantly increase tetracycline accumulation within a membrane-bound vesicle.

The previously described experiment could work, but there are a few caveats that may obscure the results. For example, how would you know that the tetracycline has fully crossed the SUV membrane into the inner aqueous phase instead of remaining in the membrane with the lariat ether? While the SUVs could be lysed following dialysis, this experiment may not be completely quantitative. However, the

question of increased accumulation of tetracycline across a membrane could be addressed using another experiment, which has been traditionally used to measure ion transport. In the proposed experiment, a U-shaped tube, like the one shown in Figure 2-3, will be initially filled with an organic solution of lariat ether. Into one arm, a concentrated solution of aqueous tetracycline will be added. The other arm (receiving arm) will be filled with pure water. At various time points, the absorbance of the solution in the receiving arm will be measured which will allow the concentration of tetracycline to be quantified. NMR experiments in Chapter 2 have shown that the complex between C_{10}LE and tetracycline forms in both nonpolar and aqueous solution, but this experiment would clarify if the lariat ether enhances tetracycline transport across a liquid membrane.

The next experiment addresses the ability of lariat ethers to inhibit efflux pump activity. Reserpine is an efflux pump inhibitor known to dysregulate the ion gradient required for many efflux pump's activity. Particularly, the Gokel lab has shown that reserpine effectively inhibits the NorA efflux pump, which expels fluoroquinolones and ethidium bromide from cells. When the NorA efflux pump is inhibited and cells are treated with ethidium bromide, a fluorescent signal can be detected. For this reason, reserpine has been identified as a suitable positive control. Previously, the Gokel lab has used this experiment to examine the ability of hydraphiles to inhibit efflux pump activity, where the hydraphiles proved to be slightly more effective inhibitors than existing efflux pump inhibitors. [88] I propose a similar approach for the lariat ethers. Initially, combination studies will be performed to confirm that the lariat ethers can recover the activity of fluoroquinolones or ethidium bromide in NorA expressing cells. Then, bacteria expressing this efflux pump will be exposed to ethidium bromide and the various lariat ethers or reserpine. The fluorescence will immediately be measured using a

Biotek Cytation 5 plate reader, for 20 minutes. This experiment will clarify if the lariat ethers function as efflux pump inhibitors, as do the hydraphiles.

The data presented in Chapter 2 present a conundrum where, generally, only the freebase is an effective antimicrobial complexing agent. Given the structural similarities between the freebase and salts it raises the question of what causes such a stark difference in complexing ability. The two nitrogen atoms located at the 4,13-positions could have differing conformations, particularly when comparing the free base to the methiodide salt. The NMR complexation experiments and the difference in complexation effectiveness among various sidearms suggest that the sidearms likely play a role that more or less holds the antibiotic in an appropriate orientation for complexation. The significance of sidearm length is further confirmed by the diminished complexing effectiveness of the dibenzyl-18-crown-6. The nitrogen atoms in the freebase are ionizable and not held in any permanent position, whereas methylating these nitrogen atoms locks the sidearms into some fixed orientation. The two sidearms could be fixed on the same side of the macrocycle, as we have seen in the crystal structure of the freebase, or they could be fixed in opposite directions.

To address the question, I propose to utilize Förster Resonance Energy Transfer (FRET). This technique can be used to measure intermolecular distances on the scale of 5-10 nm. A pair of fluorophores is required in which the emission of one overlaps with the excitation of the other. By exciting the donor and collecting the emission spectrum of the acceptor, one can measure the energy transfer efficiency and calculate distances between the fluorophores. I propose synthesizing a lariat ether methiodide salt in which the sidearms are short, aliphatic chains terminated by dimethylaminosulfonyl (dansyl) and 2-nitroindole moieties, Figure 4-1.

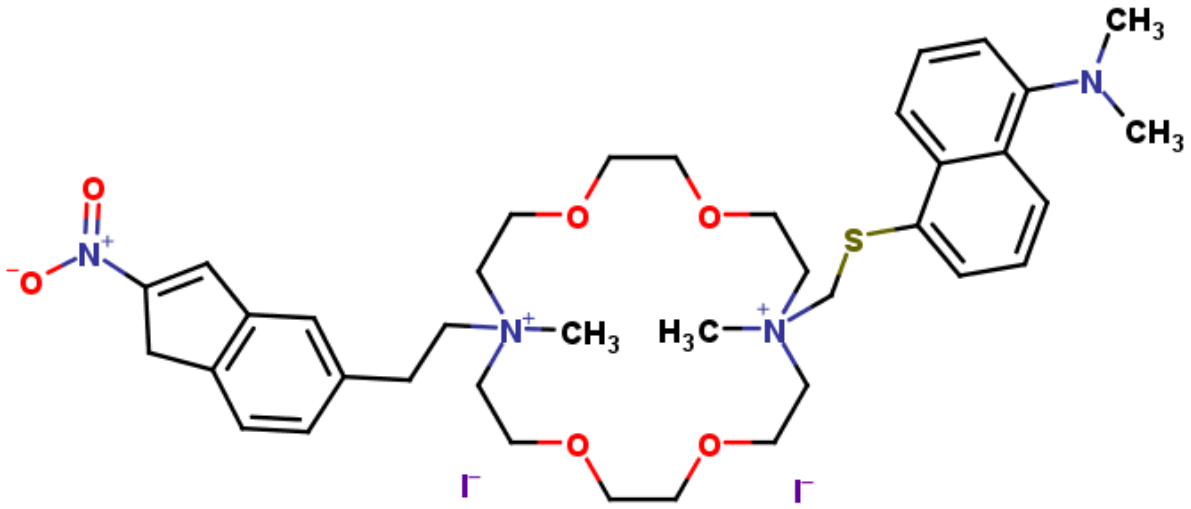

Figure 4-1. Structure of a lariat ether methiodide salt for FRET studies.

The excitation and emission wavelengths for 2-nitroindole are 292 nm and 345 nm, respectively. The values for dansyl are 340 nm and 535 nm, respectively. Given the closeness of the indole emission and dansyl excitation wavelengths, the two fluorophores may make an acceptable FRET pair. If the two sidearms are in *syn* conformation, I would expect to see FRET. However, if the sidearms are in the *anti* conformation, they would likely be too far apart for any energy transfer to occur. However, the synthesis of this compound may present some difficulty, particularly when it comes to the 2-nitroindole. It is not commercially available in a form that would be suitable for this synthesis, so additional preparation of the starting material would be necessary. Nonetheless, this could reveal interesting structural information about the conformation of the sidearms in the methiodide salts.

There is another approach to determining the conformation of the sidearms in lariat ethers where the sidearms are permanently fixed in one position which may be more synthetically accessible. The proposed structure is shown in Figure 4-2.

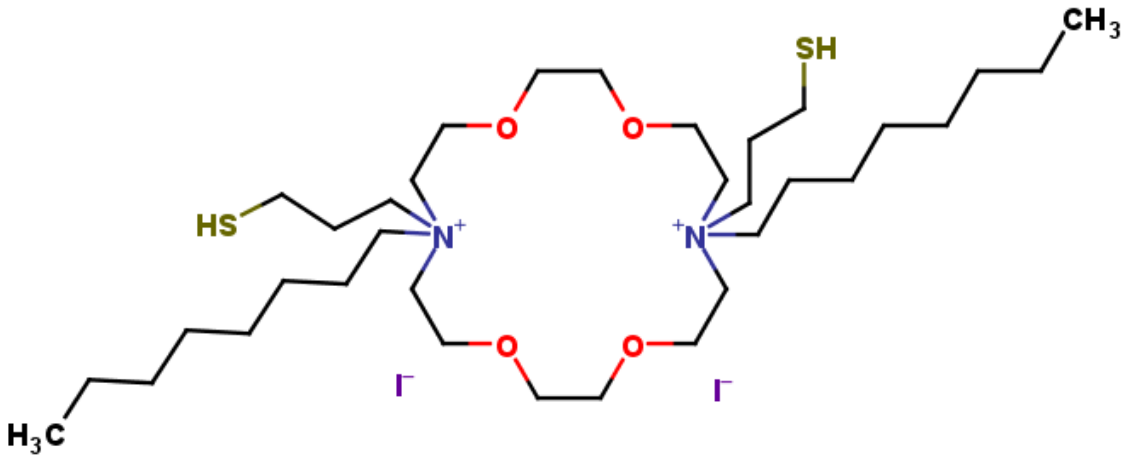

Figure 4-2. Structure of tetrasubstituted diaza-18-crown-6 ether.

By replacing the two methyl groups in the methiodide salts with propanethiol residues, a disulfide could form in oxidizing conditions. If these two moieties are in close enough proximity (*syn* conformation), placing this compound in an oxidizing environment could allow the formation of a disulfide bond. If no disulfide bond forms, then the two thiol substituents must be in the *anti* conformation. Again, synthesis of this compound may be difficult; however, the orientation of sidearms in cases where the nitrogen is not invertible is of particular interest.

Another question raised by the results in Chapter 2 is whether complexation of antimicrobial agents inhibits or diminishes the lariat ether's ionophoretic activity or ability to permeabilize bacterial membranes. To address this question, I propose similar confocal microscopy experiments as have previously been performed for the lariat ethers and their salts. Co-staining with propidium iodide and fluorescein diacetate is a method which allows the visualization of cells where membrane permeability is diminished while maintaining cell viability. DLS experiments have shown that the C_{10}LE and tetracycline form complexes at sub-lethal concentrations, and previous work in the Gokel lab shows that membrane permeabilization by lariat ethers also occurs at sub-lethal concentrations. Co-administering the lariat ethers

with tetracycline at non-inhibitory concentrations, then staining with propidium iodide and fluorescein diacetate should reveal if the LE:Tet complex permeabilized membranes to the same extent as LE individually. Similarly, the fluorophore $DiBAC_4(3)$ has been used to measure membrane depolarization. I propose treating cells with sub-lethal concentrations of LE and tetracycline, then staining with $DiBAC_4(3)$ and visualizing with confocal microscopy. These two experiments could reveal whether the lariat ethers mechanism is altered by complexation with antimicrobial agents.

Since the bis-tryptophans are significantly newer than the lariat ethers, we know less about their mechanism. We know that some of them show ion channel activity, but not to the same extent as lariat ethers. Additionally, the correlation between aggregation and antimicrobial activity further confirms the hypothesis that the BTs are membrane active. Taken together, we hypothesize that the BTs are active through similar mechanisms as the lariat ethers: some combination of membrane permeabilization and disruption of ion homeostasis. For this reason, the same confocal microscopy experiments are proposed for the bis-tryptophans. Co-staining with propidium iodide and fluorescein diacetate and staining with $DiBAC_4(3)$ will reveal whether membrane permeability or ion homeostasis are altered by bis-tryptophans.

The Gokel lab has previously reported that BTs enhance antibiotic potency of FDA approved antimicrobial agents; however, the mechanism for this enhancement is unknown. It is possible that a supramolecular could form between the antibiotics and BTs. For this reason, similar complexation experiments as described in Chapter 2 should be attempted. The NMR solubilization experiments are unlikely to yield results, due to poor solubility of the BTs in nonpolar solvents. However, for the lariat ethers, DLS studies proved to reflect the same results, although in a qualitative

manner. If solubility issues become a problem for NMR complexation experiments, qualitative results may be obtained with DLS.

The results in Chapter 3 correlate a BT's ability to form aggregates in aqueous solution with the antimicrobial activity. However, it is unknown if the BT monomers or aggregates are the active form of the compound. DLS studies were conducted over the same range of concentrations as the antibacterial experiments; however, determining the critical aggregate concentration may be useful to address this question. For this type of experiment, solutions of BT would be prepared with smaller steps in the concentration gradient rather than the two-fold steps used in Chapter 3. Comparing the critical aggregate concentration with the minimum inhibitory concentration could shed light on which form is active for the bis-tryptophans.

Another approach to this question would employ scanning electron microscopy. Previously the Gokel lab used this technique when investigating hydraphiles. In these experiments, bacterial cells were treated with the hydraphile for 10 minutes prior to loading on the filter membrane. The cells were then fixed using glutaraldehyde, then washed and stained with osmium tetroxide. The samples were serially dried with increasing v/v concentrations of ethanol, before being sputter coated with gold and imaged. These experiments with hydraphiles revealed that the compounds aggregated on the surface of the bacterial cell before inserting into the membrane. Additional physical changes in membrane topology were observed, such as membrane smoothening. Repeating a similar experiment with the bis-tryptophans would also establish whether the monomer or aggregated form is active.

While the exact mechanism of both classes of compounds described in this thesis is still unclear, particularly the mechanism by which they enhance antibiotic

potency of antimicrobial agents, the further experiments described in this chapter would greatly expand our knowledge and understanding thereof.

Chapter 5

Experimental Details

4.1 Dynamic Light Scattering

Measurements were performed on a Brookhaven Instruments Corp. ZetaPALS instrument at 25°C using a 660 nm laser and correlating scattering at 90°. Samples were prepared by initially dissolving the amphiphile in filtered DMSO obtained from ThermoFisher. Next, they were diluted into 1x PBS such that DMSO was fixed at 0.5% in 15 mL sterile conical tubes. 10x PBS was obtained commercially, then diluted 10-fold in MQ H_2O. The mixture was vortexed and incubated at room temperature for two hours, then transferred to a clean quartz cuvette and equilibrated in the instrument for ten minutes at 25°C. Ten measurements consisting of two-minute runs were made on each sample. The average effective diameter was calculated with standard error reported for at least three trials.

4.2 Synthesis and Characterization

The *tert*-butyl carbamate protected (Boc-protected) tryptophan was coupled to the diamine linkers using a uronium-based coupling reagent HBTU in *N,N*-dimethylformamide (DMF) with diisopropylethylamine (DIPEA). After workup, the Boc-protected *bis*(aminoamide) product was deprotected using 4.0 M HCl in 1,4-dioxane.

General procedure A: coupling with HBTU

The Boc-protected tryptophan and HBTU (2.1 equivalents) were dissolved in about 10 mL of anhydrous DMF with DIPEA (4.0 equivalents for neutral diamines; 6.0 equivalents for diamine dihydrochlorides). This was allowed to stir for 30 minutes in an ice bath, under an inert atmosphere. After 30 minutes, the diamine dissolved in DMF was added to the reaction vessel and placed back under an inert atmosphere. The reaction was allowed to run until there was no observable change via thin-layer chromatography (TLC); this was no longer than two days. The reaction

mixture was taken up in 50 mL ethyl acetate, then washed three times each with 1 M $NaHSO_4$, 5% $NaHCO_3$, and brine. The organic layer was dried by filtration through a $MgSO_4$/celite plug, and the solvent removed *in vacuo*. Deprotection was carried out on Boc-protected products without any further purification.

General procedure B: Boc deprotection with HCl/dioxane

The Boc-protected *bis*(aminoamide) deprotection was carried out using 10 equivalents of HCl in dioxane. The Boc-protected product was dissolved in 10 mL 1,4-dioxane, then combined with 3.5 mL of 4.0 M HCl in dioxane. The reaction was placed under argon and stirred for two hours, during which time the deprotected product precipitated. Cold hexane was added dropwise to recover any product still in solution. The solid was filtered and dried under high vacuum.

Di-tert-butyl (2S,2'S) -(2,7-fluorenylbis(azanediyl))bis(3-(1H-indol-3-yl)-1-oxopropane-2,1-diyl))dicarbamate (12a) was prepared according to general procedure A using 2,7-fluorenyldiamine (245 mg, 1.25 mmol) and Boc-L-Tryp-OH. ^{1}H-NMR (300 MHz, DMSO-d6): δ 1.41 (s, 18H, 2(CH_3)$_3$), 2.98-3.20 (ABX, 4H, 2CH_2ß), 4.54 (ABX, 2H, CHα), 6.84-6.95 (t, 4H, indole H5 and H6), 7.15 (d, 2H, fluorenyl H4 and H5), 7.30 (d, 2H, indole H7), 7.44 (d, 2H, fluorenyl H3 and H6), 7.56 (d, 2H, indole H4), 7.79 (s, 2H, fluorenyl H1 and H8).

(2S,2'S) -(2,7-fluorenylbis(azanediyl))bis(3-(1H-indol-3-yl)-1-oxopropane-2,1-diyl))dicarbamate (12) was prepared using 12a according to general procedure B. ^{1}H-NMR (300 MHz, DMSO-d6): δ 2.98-3.20 (ABX, 4H, 2CH_2ß), 4.54 (ABX, 2H, CHα), 6.84-6.95 (t, 4H, indole H5 and H6), 7.15 (d, 2H, fluorenyl H4 and H5), 7.30 (d, 2H, indole H7), 7.44 (d, 2H, fluorenyl H3 and H6), 7.56 (d, 2H, indole H4), 7.79 (s, 2H, fluorenyl H1 and H8) HRMS (FAB+) calc'd ($C_{35}H_{33}N_6O_2^+$) 568.681 Found: 569.2660

Di-tert-butyl (2S,2'S) -(4,4-diphenylmethylbis(azanediyl)) bis(3-(1H-indol-3-yl)-1-oxopropane-2,1-diyl))dicarbamate (13a) was prepared according to general procedure A using 4,4-diphenylmethyl (DPM) diamine (245 mg, 1.25 mmol) and Boc-L-Tryp-OH. ^{1}H-NMR (300 MHz, DMSO-d6): δ 1.41 (s, 18H, 2(CH_3)$_3$), 2.98-3.20 (ABX, 4H, 2CH_2ß), 4.54 (ABX, 2H, CHα), 6.29-6.41 (t, 4H, indole H5 and H6), 6.52 (d, 4H, DPM H2), 6.59 (s, 2H, indole H2), 6.67 (d, 2H, indole H7), 6.82 (d, 4H, DPM H3) 7.03 (d, 2H, indole H4).

(2S,2'S) -(4,4-diphenylmethylbis(azanediyl)) bis(3-(1H-indol-3-yl)-1-oxopropane-2,1-diyl))dicarbamate (13) was prepared using 13a according to general procedure B.^{1}H-NMR (300 MHz, DMSO-d6): δ 2.98-3.20 (ABX, 4H, 2CH_2ß), 4.54 (ABX, 2H, CHα), 6.29-6.41 (t, 4H, indole H5 and H6), 6.52 (d, 4H, DPM H2), 6.59 (s, 2H, indole H2), 6.67 (d, 2H, indole H7), 6.82 (d, 4H, DPM H3) 7.03 (d, 2H, indole H4) HRMS (FAB+) calc'd ($C_{35}H_{36}N_6O_2^+$) 570.701 Found: 571.2816

Di-tert-butyl (2S,2'S) -(pentane-1,5-diylbis(azanediyl)) bis(3-(1H-indol-3-yl)-1-oxopropane-2,1-diyl))dicarbamate (19a) was prepared according to general procedure A using 1,5-diaminopentane (219 mg, 1.25 mmol) and Boc-L-Tryp-OH. ^{1}H-NMR (300 MHz, DMSO-d6): δ 1.41 (s, 18H, 2(CH_3)$_3$), 1.24 (m, 6H, $\underline{CH_2}\underline{CH_2}CH_2NH$-), 2.89 (m, 4H, $CH_2CH_2\underline{CH_2}NH$-), 2.98-3.20 (ABX, 4H, 2CH_2ß), 4.54 (ABX, 2H, CHα), 6.99-7.07 (t, 4H, indole H5 and H6), 7.21 (s, 2H, indole H2), 7.34-7.65 (d, 4H, indole H4 and H7).

(2S,2'S) -(pentane-1,5-diylbis(azanediyl)) bis(3-(1H-indol-3-yl)-1-oxopropane-2,1-diyl))dicarbamate (19) was prepared using 19a according to general procedure B. ^{1}H-NMR (300 MHz, DMSO-d6): δ 1.24 (m, 6H, $\underline{CH_2}\underline{CH_2}CH_2NH$-), 2.89 (m, 4H, $CH_2CH_2\underline{CH_2}NH$-), 2.98-3.20 (ABX, 4H, 2CH_2ß), 4.54 (ABX, 2H, CHα), 6.99-7.07 (t, 4H, indole H5 and H6), 7.21 (s, 2H, indole H2),

7.34-7.65 (d, 4H, indole H4 and H7). HRMS (FAB+) calc'd ($C_{27}H_{36}N_6O_2^+$) 547.530 Found: 548.1284

Di-tert-butyl (2S,2'S) -(heptane-1,7-diylbis(azanediyl)) bis(3-(1H-indol-3-yl)-1-oxopropane-2,1-diyl))dicarbamate (20a) was prepared according to general procedure A using 1,5-diaminoheptane (163 mg, 1.25 mmol) and Boc-L-Tryp-OH. ^{1}H-NMR (300 MHz, DMSO-d6): δ 1.41 (s, 18H, 2(CH_3)$_3$), 1.24 (m, 10H, $\underline{CH_2CH_2CH_2}CH_2NH$-), 2.89 (m, 4H, $CH_2CH_2CH_2\underline{CH_2}NH$-), 2.98-3.20 (ABX, 4H, 2CH_2ß), 4.54 (ABX, 2H, CHα), 6.99-7.07 (t, 4H, indole H5 and H6), 7.21 (s, 2H, indole H2), 7.34-7.65 (d, 4H, indole H4 and H7).

(2S,2'S) -(heptane-1,7-diylbis(azanediyl)) bis(3-(1H-indol-3-yl)-1-oxopropane-2,1-diyl))dicarbamate (20) was prepared using 20a according to general procedure B. ^{1}H-NMR (300 MHz, DMSO-d6): δ 1.24 (m, 10H, $\underline{CH_2CH_2CH_2}CH_2NH$-), 2.89 (m, 4H, $CH_2CH_2CH_2\underline{CH_2}NH$-), 2.98-3.20 (ABX, 4H, 2CH_2ß), 4.54 (ABX, 2H, CHα), 6.99-7.07 (t, 4H, indole H5 and H6), 7.21 (s, 2H, indole H2), 7.34-7.65 (d, 4H, indole H4 and H7). HRMS (FAB+) calc'd ($C_{29}H_{40}N_6O_2^+$) 575.583 Found: 575.2698

Di-tert-butyl (2S,2'S) -(nonane-1,9-diylbis(azanediyl)) bis(3-(1H-indol-3-yl)-1-oxopropane-2,1-diyl))dicarbamate (22a) was prepared according to general procedure A using 1,9-diaminononane (198 mg, 1.25 mmol) and Boc-L-Tryp-OH. ^{1}H-NMR (300 MHz, DMSO-d6): δ 1.41 (s, 18H, 2(CH_3)$_3$), 1.24 (m, 10H, $\underline{CH_2CH_2CH_2}CH_2NH$-), 2.89 (m, 4H, $CH_2CH_2CH_2\underline{CH_2}NH$-), 2.98-3.20 (ABX, 4H, 2CH_2ß), 4.54 (ABX, 2H, CHα), 6.99-7.07 (t, 4H, indole H5 and H6), 7.21 (s, 2H, indole H2), 7.34-7.65 (d, 4H, indole H4 and H7)

(2S,2'S) -(nonane-1,9-diylbis(azanediyl)) bis(3-(1H-indol-3-yl)-1-oxopropane-2,1-diyl))dicarbamate (22) was prepared using 22a according to general procedure B. ^{1}H-NMR (300 MHz, DMSO-d6): δ 1.24 (m, 10H,

$\underline{CH_2CH_2CH_2}CH_2NH$-), 2.89 (m, 4H, $CH_2CH_2CH_2\underline{CH_2}NH$-), 2.98-3.20 (ABX, 4H, $2CH_2ß$), 4.54 (ABX, 2H, CHα), 6.99-7.07 (t, 4H, indole H5 and H6), 7.21 (s, 2H, indole H2), 7.34-7.65 (d, 4H, indole H4 and H7) HRMS (FAB+) calc'd ($C_{31}H_{42}N_6O_2^+$) 530.7170 Found: 531.3442

Di-tert-butyl (2S,2'S) -(undecane-1,11-diylbis(azanediyl)) bis(3-(1H-indol-3-yl)-1-oxopropane-2,1-diyl))dicarbamate (24a) was prepared according to general procedure A using 1,11-diaminoundecane (233 mg, 1.25 mmol) and Boc-L-Tryp-OH. ^{1}H-NMR (300 MHz, DMSO-d6): δ 1.41 (s, 18H, $2(CH_3)_3$), 1.24 (m, 14H, $\underline{CH_2CH_2CH_2CH_2CH_2}CH_2NH$-), 2.89 (m, 4H, $CH_2CH_2CH_2CH_2CH_2\underline{CH_2}NH$-), 2.98-3.20 (ABX, 4H, $2CH_2ß$), 4.54 (ABX, 2H, CHα), 6.99-7.07 (t, 4H, indole H5 and H6), 7.21 (s, 2H, indole H2), 7.34-7.65 (d, 4H, indole H4 and H7).

(2S,2'S) -(undecane-1,11-diylbis(azanediyl)) bis(3-(1H-indol-3-yl)-1-oxopropane-2,1-diyl))dicarbamate (24) was prepared using 24a according to general procedure B. ^{1}H-NMR (300 MHz, DMSO-d6): δ 1.41 (s, 18H, $2(CH_3)_3$), 1.24 (m, 14H, $\underline{CH_2CH_2CH_2CH_2CH_2}CH_2NH$-), 2.89 (m, 4H, $CH_2CH_2CH_2CH_2CH_2\underline{CH_2}NH$-), 2.98-3.20 (ABX, 4H, $2CH_2ß$), 4.54 (ABX, 2H, CHα), 6.99-7.07 (t, 4H, indole H5 and H6), 7.21 (s, 2H, indole H2), 7.34-7.65 (d, 4H, indole H4 and H7). HRMS (FAB+) calc'd ($C_{33}H_{48}N_6O_2^+$) 631.70 Found: 632.2571

4.3 Bacterial Cultures and MIC Determination

All bacteria were grown in Mueller Hinton II (MHII) media. The cells were grown overnight from one colony forming unit (CFU) in 2 mL media. On the day of the experiment, the bacteria were knocked back to $O.D._{600}$=0.100 and incubated at 37°C until they reached $O.D._{600}$=0.500 (4×10^8 CFU/mL). These cells were then diluted 100-fold in MHII media. The diluted cells were then added to each well in a 96-well plate, yielding a final concentration of about 4×10^5 CFU/mL after addition of media and drug.

Compounds were dissolved in either DMSO or dH_2O, then serially diluted into 1.5 mL microcentrifuge tubes to generate stock solutions. These solutions were prepared such that the final concentration in the wells was no more than 0.5% DMSO.

In a 96-well plate, first the media was added followed by the compound of interest. Each well had a final volume of 200 µL. The contents of each well were mixed by pipetting up and down three times. Empty wells were filled with buffer to minimize evaporation, and the edges of the plates were taped to further this end. They were incubated at 37°C overnight, and the results were collected by measuring the $O.D._{600}$ on a BioTek Cytation 5 plate reader. Percent inhibition was calculated by comparing the well to growth of cells alone. MIC was identified as the concentration which resulted in 90% growth inhibition.

4.4 Checkerboard Experiments

In a checkerboard experiment, each column contains a different amphiphile concentration and each row has a different concentration of antibiotic. In both cases, the concentrations vary by a factor of two. Four controls were employed on each checkerboard plate: full growth (only cells), no growth (only media), and then a column for each drug alone to accurately reflect their individual MIC. The concentrations of amphiphile and antibiotic tested were ½, ¼, 1/8, 1/16, and 1/32 of the [MIC]. Preparation of the stock solutions and plates were done using the same method described in 4.3.

Chapter 5

References

1. Shlaes, D. M. Resistance. in *Antibiotics* 15–28 (2010).
2. Davies, J. & Davies, D. Origins and evolution of antibiotic resistance. *Microbiol. Mol. Biol. Rev.* **74**, 417–433 (2010).
3. De Schweinitiz, D. A. The War with the Microbes. *Science (80-.).* **5**, 561–570 (1897).
4. Prestinaci, F., Pezzotti, P. & Pantosti, A. Antimicrobial resistance: A global multifaceted phenomenon. *Pathog. Glob. Health* **109**, 309–318 (2015).
5. Services, U. S. D. of H. and H. Antibiotic resistance threats in the United States, 2019. *Centers Dis. Control Prev.* 1–113 (2019).
6. CDC. Covid-19 U.S. Impacty on Antimicrobial Resistance. *Antimicrob. Resist.* 1–44 (2022).
7. Prestinaci, F., Pezzotti, P. & Pantosti, A. Antimicrobial resistance: A global multifaceted phenomenon. *Pathog. Glob. Health* **109**, 309–318 (2015).
8. Organization, W. H. WHO Coronavirus (Covid-19) Dashboard. https://covid19.who.int/ (2022).
9. Organization, W. H. *World health statistics 2022 (Monitoring health of the SDGs)*. (2022).
10. CDC. Covid-19 U.S. Impacty on Antimicrobial Resistance. *Antimicrob. Resist.* 1–44 (2022).
11. Murray, C. J. *et al.* Global burden of bacterial antimicrobial resistance in 2019: a systematic analysis. *Lancet* **399**, 629–655 (2022).

12. Tacconelli, E. *et al.* Discovery, research, and development of new antibiotics: the WHO priority list of antibiotic-resistant bacteria and tuberculosis. *Lancet Infect. Dis.* **18**, 318–327 (2018).

13. De Oliveira, D. M. P. *et al.* Antimicrobial resistance in ESKAPE pathogens. *Clin. Microbiol. Rev.* **33**, (2020).

14. Lowe, J. Mechanisms of Antibiotic Resistance. *Annu. Rep. Med. Chem.* **17**, 119–127 (1982).

15. Høiby, N., Bjarnsholt, T., Givskov, M., Molin, S. & Ciofu, O. Antibiotic resistance of bacterial biofilms. *Int. J. Antimicrob. Agents* **35**, 322–332 (2010).

16. Nickel, J. C., Ruseska, I., Wright, J. B. & Costerton, J. W. Tobramycin resistance of Pseudomonas aeruginosa cells growing as a biofilm on urinary catheter material. *Antimicrob. Agents Chemother.* **27**, 619–624 (1985).

17. Hill, D. *et al.* Antibiotic susceptibilities of Pseudomonas aeruginosa isolates derived from patients with cystic fibrosis under aerobic, anaerobic, and biofilm conditions. *J. Clin. Microbiol.* **43**, 5085–5090 (2005).

18. Egorov, A. M., Ulyashova, M. M. & Rubtsova, M. Y. Bacterial enzymes and antibiotic resistance. *Acta Naturae* **10**, 33–48 (2018).

19. Naas, T. *et al.* Beta-lactamase database (BLDB)–structure and function. *J. Enzyme Inhib. Med. Chem.* **32**, 917–919 (2017).

20. Abraham, E. P. & Chain, E. An Enzyme from Bacteria Able to Destroy Penicillin. *Nature* **146**, 837 (1940).

21. Yocum, R. R., Rasmussen, J. R. & Strominger, J. L. The mechanism of action of penicillin. Penicillin acylates the active site of Bacillus stearothermophilus D-alanine carboxypeptidase. *J. Biol. Chem.* **255**, 3977–3986 (1980).

22. Krause, K. M., Serio, A. W., Kane, T. R. & Connolly, L. E. Aminoglycosides : An Overview. *Cold Spring Harb. Lab. Press* **6**, a027029 (2016).

23. Costello, S. E., Deshpande, L. M., Davis, A. P., Mendes, R. E. & Castanheira, M. Aminoglycoside-modifying enzyme and 16S ribosomal RNA methyltransferase genes among a global collection of Gram-negative isolates. *J. Glob. Antimicrob. Resist.* **16**, 278–285 (2019).

24. Blondeau, J. M. Fluoroquinolones: Mechanism of action, classification, and development of resistance. *Surv. Ophthalmol.* **49**, 1–6 (2004).

25. Munita, J. M. & Arias, C. A. Mechanisms of antibiotic resistance. *Virulence Mech. Bact. Pathog.* 481–511 (2016) doi:10.1128/9781555819286.ch17.

26. Laws, M., Jin, P. & Rahman, K. M. Efflux pumps in Mycobacterium tuberculosis and their inhibition to tackle antimicrobial resistance. *Trends Microbiol.* **30**, 57–68 (2022).

27. Chopra, I. & Roberts, M. Tetracycline Antibiotics: Mode of Action, Applications, Molecular Biology, and Epidemiology of Bacterial Resistance. *Microbiol. Mol. Biol. Rev.* **65**, 232–260 (2001).

28. Kumar, S. & Varela, M. F. Biochemistry of bacterial multidrug efflux pumps. *Int. J. Mol. Sci.* **13**, 4484–4495 (2012).

29. Stavropoulos, T. A. & Strathdee, C. A. Expression of the tetA(C) tetracycline efflux pump in Escherichia coli confers osmotic sensitivity. *FEMS Microbiol. Lett.* **190**, 147–150 (2000).

30. Armstrong, C. M. The Na/K pump, Cl ion, and osmotic stabilization of cells. *Proc. Natl. Acad. Sci. U. S. A.* **100**, 6257–6262 (2003).

31. Pedersen, C. J. Cyclic Polyethers and Their Complexes with Metal Salts. *J. Am.*

Chem. Soc. **89**, 7017–7036 (1967).

32. Outreach, N. P. Charles J. Pedersen. (2022).

33. Schultz, R. A., White, B. D., Dishong, D. M., Arnold, K. A. & Gokel, G. W. 12-, 15-, and 18-membered-ring nitrogen-pivot lariat ethers: syntheses, propertis and sodium and ammonium cation binding properties. *J. Am. Chem. Soc.* **107**, 6659–6668 (1985).

34. Gokel, G. W., Dishong, D. M. & Diamond, C. J. Lariat ethers. Synthesis and cation binding of macrocyclic polyethers possessing axially disposed secondary donor groups. *J. Chem. Soc. Chem. Commun.* 1053–1054 (1980) doi:10.1039/c39800001053.

35. White, B. D. *et al.* Syntheses and cation binding properties of 12-membered ring nitrogen-pivot lariat ethers. *Tetrahedron Lett.* **26**, 151–154 (1985).

36. Dietrich, B., Lehn, J. M. & Sauvage, J. P. Les Cryptates. *Tetrahedron Lett.* **10**, 2889–2892 (1969).

37. Gokel, M. R. *et al.* Crown ethers having side arms: a diverse and versatile supramolecular chemistry. *J. Coord. Chem.* **74**, 14–39 (2021).

38. Berezin, S. K. Valinomycin as a Classical Anionophore: Mechanism and Ion Selectivity. *J. Membr. Biol.* **248**, 713–726 (2015).

39. Hasani, M. & Shamsipur, M. Conductance study of the thermodynamics of ammonium ion complexes with several crown ethers in acetonitrile solution. *J. Solution Chem.* **23**, 721–734 (1994).

40. Echegoyen, L. *et al.* Dynamics of Crown and Lariat Ether Cation Complexation Assessed by 13C NMR Relaxation Times. *J. Am. Chem. Soc.* **106**, 5100–5103 (1984).

41. De Wall, S. L., Barbour, L. J. & Gokel, G. W. Solid-state bilayer formation from a dialkyl-substituted lariat ether that forms stable vesicles in aqueous suspension. *J. Phys. Org. Chem.* **14**, 383–391 (2001).

42. Echegoyen, L. E., Hernandez, J. C., Kaifer, A. E., Gokel, G. W. & Echegoyen, L. Aggregation of steroidal lariat ethers: The first example of nonionic liposomes (niosomes) formed from neutral crown ether compounds. *J. Chem. Soc. Chem. Commun.* 836–837 (1988) doi:10.1039/C39880000836.

43. Negin, S., Patel, M. B., Gokel, M. R., Meisel, J. W. & Gokel, G. W. Antibiotic Potency against E. coli Is Enhanced by Channel-Forming Alkyl Lariat Ethers. *ChemBioChem* **17**, 2153–2161 (2016).

44. Murillo, O. *et al.* Synthetic transmembrane channels: Functional characterization using solubility calculations, transport studies, and substituent effects. *J. Am. Chem. Soc.* **119**, 5540–5549 (1997).

45. Pressman, B. C., Harris, E. J., Jagger, W. S. & Johnson, J. H. Antibiotic-mediated transport of alkali ions across lipid barriers. *Proc. Natl. Acad. Sci. U. S. A.* **58**, 1949–1956 (1967).

46. Leevy, W. M. *et al.* Correlation of bilayer membrane cation transport and biological activity in alkyl-substituted lariat ethers. *Org. Biomol. Chem.* **3**, 1647–1652 (2005).

47. Djedovič, N. K., Ferdani, R., Schlesinger, P. H. & Gokel, G. W. Aggregation of lariat ethers attached to a membrane anchoring unit. *Tetrahedron* **58**, 10263–10268 (2002).

48. Pajewski, R. *et al.* Pore formation in and enlargement of phospholipid liposomes by synthetic models of ceramides and sphingomyelin. *Bioorganic Med. Chem.* **13**, 29–37 (2005).

49. Zakharian, E. Recording of Ion Channel Activity in Planar Bilayer Experiments. *Methods Mol. Biol.* 109–118 (998) doi:10.1007/978-1-62703-351-0.

50. Singer, S. J. & Nicolson, G. L. The fluid mosaic model of the structure of cell membranes. *Science (80-.).* **175**, 720–731 (1972).

51. Yang, N. J. & Hinner, M. J. Getting across the cell membrane: an overview for small molecules, peptides, and proteins. *Methods Mol. Biol.* 29–53 (2015) doi:10.1007/978-1-4939-2272-7.

52. Gokel, G. W. & Negin, S. Synthetic membrane active amphiphiles. *Adv. Drug Deliv. Rev.* **64**, 784–796 (2012).

53. Patel, M. B. *et al.* Hydraphiles enhance antimicrobial potency against Escherichia coli, Pseudomonas aeruginosa, and Bacillus subtilis. *Bioorganic Med. Chem.* **24**, 2864–2870 (2016).

54. Gokel, G. W. Hydraphiles: Design, synthesis and analysis of a family of synthetic, cation-conducting channels. *Chem. Commun.* 1–9 (2000) doi:10.1039/a903825f.

55. Doyle, D. A. *et al.* The structure of the potassium channel: Molecular basis of K+ conduction and selectivity. *Science (80-.).* **280**, 69–77 (1998).

56. Abel, E. *et al.* Hydraphile Channels : Structural and Fluorescent Probes of Position and Function in a Phospholipid Bilayer. 9043–9052 (1999).

57. Atkins, J. L., Patel, M. B., Cusumano, Z. & Gokel, G. W. Enhancement of antimicrobial activity by synthetic ion channel synergy. *Chem. Commun.* **46**, 8166–8167 (2010).

58. Smith, B. A. *et al.* In vivo cell death mediated by synthetic ion channels. *Chem.*

Commun. **47**, 7977–7979 (2011).

59. De Planque, M. R. R. *et al.* Interfacial anchor properties of tryptophan residues in transmembrane peptides can dominate over hydrophobic matching effects in peptide-lipid interactions. *Biochemistry* **42**, 5341–5348 (2003).

60. Abel, E., Fedders, M. F. & Gokel, G. W. Vesicle Formation from N-Alkylindoles: Implications for Tryptophan—Water Interactions. *J. Am. Chem. Soc.* **117**, 1265–1270 (1995).

61. Gokel, G. W. Indole , the aromatic element of tryptophan , as a pi-donor and amphiphilic headgroup. **1304**, 1–14 (2007).

62. Patel, M. *et al.* Bis (Tryptophan) Amphiphiles Form Ion Conducting Pores and Enhance Antimicrobial Activity against Resistant Bacteria. *Antibiotics* 1–18 (2021).

63. Meisel, J. W., Patel, M. B., Garrad, E., Stanton, R. A. & Gokel, G. W. Reversal of Tetracycline Resistance in Escherichia coli by Noncytotoxic bis(Tryptophan)s. *J. Am. Chem. Soc.* **138**, 10571–10577 (2016).

64. Mckeever, M. Bis(Tryptophan) Amphiphiles: Design, Synthesis and Efficacy as Antimicrobial Agents. (2022).

65. Gandour, R. D. *et al.* Solid-State Structural Chemistry of Lariat Ether and BiBLE Cation Complexes: Metal Ion Identity and Coordination Number Determine Cavity Size. *J. Am. Chem. Soc.* **108**, 4078–4088 (1986).

66. Çiçek, B., Çakir, Ü. & Azizoglu, A. The associations of macrocyclic ethers with cations in 1,4-dioxane/ water mixtures; Potentiometric Na + and K + binding measurements and computational study. *J. Incl. Phenom. Macrocycl. Chem.* **72**, 121–125 (2012).

67. Delgado, M. *et al.* Contrasting One- and Two-Cation Binding Behavior in syn-

and anti-Anthraquinone Bibracchial Podand (BiP) Mono- and Dianions Assessed by Cyclic Voltammetry and Electron Paramagnetic Resonance Spectroscopy. *J. Am. Chem. Soc.* **110**, 119–124 (1988).

68. Kudrevatykh, A. A., Nenaeva, D. A., Martyanov, T. P. & Klimenko, L. S. Effect of substituents on cation-receptor properties of crown-containing 1-hydroxyanthraquinone imines. *Russian* **68**, 623–627 (2019).

69. Pressman, B. C. Ionophorous antibiotics as models for biological transport. *Fed Proc* **6**, 1283–1288 (1968).

70. Daschbach, M. M., Negin, S., You, L., Walsh, M. & Gokel, G. W. Aggregation and supramolecular membrane interactions that influence anion transport in tryptophan-containing synthetic peptides. *Chem. - A Eur. J.* **18**, 7608–7623 (2012).

71. Schönsee, C. D. & Bucheli, T. D. Experimental Determination of Octanol-Water Partition Coefficients of Selected Natural Toxins. *J. Chem. Eng. Data* **65**, 1946–1953 (2020).

72. American Chemical Society. Common solvents used in organic chemistry:Table of properties. (2005).

73. Ferraro, M. J. & National Committee for Clinical Laboratory Standards. *Methods for dilution antimicrobial susceptibility tests for bacteria that grow aerobically: approved standard*. (2000).

74. Etter, M. C., Jahn, D. A. & Frye, J. S. Solid-State Structural Characterization of 1,3-cyclohexanedione and of a 6:1 cyclohexanedione:benzene cyclamer, a novel host-guest species. *J. Am. Chem. Soc.* **108**, 5871–5876 (1986).

75. Wall, S. L. De *et al.* Azacrown Ethers as Amphiphile Headgroups : Formation of Stable Aggregates from Two- and Three-Armed Lariat Ethers. **3263**, 6784–

6791 (1997).

76. Corporation, W. T. Liposome Characterization by DLS. 2005 (2005).

77. Ito, T. *et al*. Classification of staphylococcal cassette chromosome mec (SCCmec): Guidelines for reporting novel SCCmec elements. *Antimicrob. Agents Chemother.* **53**, 4961–4967 (2009).

78. Buntaran, L., Hatta, M., Sultan, A. R., Dwiyanti, R. & Sabir, M. Sccmec type II gene is common among clinical isolates of methicillin-resistant Staphylococcus aureus in Jakarta, Indonesia. *BMC Res. Notes* **6**, 0–6 (2013).

79. Hudson, C. M., Bent, Z. W., Meagher, R. J. & Williams, K. P. Resistance determinants and mobile genetic elements of an NDM-1-encoding Klebsiella pneumoniae strain. *PLoS One* **9**, (2014).

80. Zowawi, H. M. *et al*. Stepwise evolution of pandrug-resistance in Klebsiella pneumoniae. *Sci. Rep.* **5**, 1–8 (2015).

81. Paterson, D. L. *et al*. Antibiotic therapy for Klebsiella pneumoniae bacteremia: Implications of production of extended-spectrum β-lactamases. *Clin. Infect. Dis.* **39**, 31–37 (2004).

82. Snydman, D. R. *et al*. Evaluation of the in vitro activity of eravacycline against a broad spectrum of recent clinical anaerobic isolates. *Antimicrob. Agents Chemother.* **62**, (2018).

83. Hu, W., Lee, K. C. & Cross, T. A. Tryptophans in Membrane Proteins: Indole Ring Orientations and Functional Implications in the Gramicidin Channel. *Biochemistry* **32**, 7035–7047 (1993).

84. Meisel, J. W. *et al*. Tryptophan in Membrane-active Synthetic Antimicrobials. *J. Explor. Res. Pharmacol.* **2**, 7–15 (2017).

85. Mo, Y., Cross, T. A. & Nerdal, W. Structural Restraints and Heterogeneous Orientation of the Gramicidin A Channel Closed State in Lipid Bilayers. *Biophys. J.* **86**, 2837–2845 (2004).

86. Patel, M. B. *et al.* Resensitization of Resistant Bacteria to Antimicrobials. *Ann. Pharmacol. Pharm.* **2**, 1055 (2017).

87. Patel, M. *et al.* Bis(Tryptophan) amphiphiles form ion conducting pores and enhance antimicrobial activity against resistant bacteria. *Antibiotics* **10**, 1–18 (2021).

88. Patel, M. B. *et al.* Synthetic ionophores as non-resistant antibiotic adjuvants. *RSC Adv.* **9**, 2217–2230 (2019).

Appendix 1

Group 14 Metallafluorenes as Sensitive Luminescent Probes of Surfactants in Aqueous Solution

Journal of Fluorescence (2021) 31:961–969
https://doi.org/10.1007/s10895-021-02730-3

ORIGINAL ARTICLE

Group 14 Metallafluorenes as Sensitive Luminescent Probes of Surfactants in Aqueous Solution

Helena J. Spikes[1] · Shelby J. Jarrett-Noland[1] · Stephan M. Germann[1] · Janet Braddock-Wilking[1] · Cynthia M. Dupureur[1]

Received: 22 February 2021 / Accepted: 23 March 2021 / Published online: 5 April 2021

Abstract

Sila- and germafluorenes containing alkynyl(aryl) substituents at the 2,7- position are strongly emissive with high quantum yields in organic solvents. Provided they are sufficiently soluble in water, their hydrophobic structures have the potential for many biological and industrial applications in the detection and characterization of lipophilic structures. To that end, the emission behaviors of previously synthesized 2,7- bis[alkynyl(biphenyl)]-9,9-diphenylsilafluorene (**1**), 2,7- bis[alkynyl(methoxynaphthyl)]-9,9-diphenylgermafluorene (**2**), 2,7- bis[alkynyl(*p*-tolyl)]-9,9-diphenylsilafluorene (**3**), and 2,7- bis[alkynyl(*m*-fluorophenyl)]-9,9-diphenylsilafluorene (**4**) were characterized in aqueous solution and in the presence of various surfactants. Despite a high degree of hydrophobicity, all of these metallafluorenes (MFs) are soluble in aqueous solution at low micromolar concentrations and luminesce in a common aqueous buffer. Further, the 2,7 substituent makes the emission behavior tunable (up to 30 nm). Fold emission enhancements in the presence of various surfactants are highest toward Triton X-100 and CTAB (ranging from 5 to 25 fold) and are lowest for the anionic surfactants SDS and SDBS. These enhancements are competitive with existing probes of surfactants. Quantum yields in buffer range from 0.11 to 0.34, competitive with many common fluorophores in biological use. Strikingly, MF quantum yields in the presence of TX-100 and CTAB approach 100 % quantum efficiency. MF anisotropies are dramatically increased only in the presence of TX-100, CTAB, and CHAPS. Coupled with the above data, this suggests that MFs associate with neutral and charged surfactant aggregates. Interactions with the anionic surfactants are weaker and/or leave MFs solvent exposed. These properties make metallafluorenes competitive probes for surfactants and their properties and behaviors, and thus could also have important biological applications.

Keywords Metallafluorene · Emission · Surfactant · Quantum yield · Anisotropy

Introduction

Sila- and germa-fluorenes, also known as dibenzosiloles or dibenzogermoles, are a class of photoluminescent compounds with high quantum yields in organic solvents [1, 2]. Interest in their potential applications as OLEDs recently drove us to synthetically explore 2,7-alkynyl(aryl) substitutions (Fig. 1a), which could be exploited to tune spectral behavior by extending the high degree of conjugation [1, 2]. Such substitutions can also attenuate solubility in various solvents.

✉ Cynthia M. Dupureur
cdup@umsl.edu

[1] Department of Chemistry & Biochemistry, University of Missouri St. Louis, St. Louis, MO 63121, USA

These optical properties and the hydrophobic nature of the structures suggest that if they are sufficiently soluble in aqueous solution, the utility of these compounds could be expanded to detect surfactants, common contaminants in wastewater [3–5], and could also have applications in the probing of lipid structures and behaviors [3–6].

There are a number of known fluorescent indicators of surfactants (Fig. 1b). They include the cationic pyridinium derivative [4-((1E,3E)-4-(4-(dimethylamino)phenyl)buta-1,3-dien-1-yl)-1-methylpyridin-1-ium (DABP)] [5]; 2,3-substituted naphthalimide dye derivatives DMN-Bu [7] and diethyl 6-(dimethylamino)naphthalene-2,3-dicarboxylate (DMNDC) [8]; the cationic polythiophene derivative poly[3-(1,1′ -dimethyl-4-piperidinemethylene)thiophene-2,5-diyl chloride] (PDPMT-Cl) [9]; and N-n-octyl-4-(1-methylpiperazine)-1,8-naphthalimide iodide [C_8ndi]I [3]. The degree of

characterization of the behaviors of these compounds varies widely, but a typical working concentration for these compounds is 10 μM [3, 5, 7]. Fold enhancements upon the addition of surfactants also vary, but typically they range from a few-fold to 10–20 fold [4, 7, 10].

Metallafluorenes (MFs) of sufficient solubility in aqueous solution and sensitivity to surfactants would represent a new class of fluorescent detectors for the detection and study of surfactants and relevant biological structures. Here we characterize the aqueous solution emission behaviors of four previously synthesized metallafluorenes [1, 2] and their interactions with a variety of surfactant solutions. Indeed, we demonstrate here that these MFs are soluble in aqueous solution at low μM concentrations and luminesce under these conditions with competitive quantum yields. Further, dramatic spectral changes, increases in quantum yield and anisotropies occur in the presence of some surfactants, which demonstrate their potential as fluorescent probes of lipophilic structures in aqueous environments.

Materials and Methods

Materials

Coumarin-102 dye (99 %), Triton X-100, sodium dodecylbenzenesulfonate (SDBS), and hexadecyltrimethylammonium bromide (C-TAB) were purchased from Sigma-Aldrich (St. Louis, MO). Dodecyl sulfate sodium salt (SDS) was purchased from Fisher Scientific (Waltham, MA). CHAPS was purchased from Anatrace (Maumee, OH) and 200 proof ethanol was purchased from Decon Labs (King of Prussia, PA). All chemicals used were of reagent grade and were used as received without further purification.

Preparation of Metallafluorenes

Fluorescent 2,7-disubstituted sila- and germafluorenes **1**–**4** were synthesized as previously described using an appropriate ethynyl aryl precursor in a palladium-catalyzed Sonagashira cross-coupling reaction [1, 2].

Spectroscopy

Absorbance spectra were recorded on a Shimadzu 1800 with slits set to 1 nm.

Luminescence experiments were performed in acid-washed quartz cuvettes at 10 mM Tris, pH 8.0 on a T-formatted Fluorolog-3 (SPEX) spectrofluorimeter equipped with a polarization assembly. The temperature was maintained 25 °C with a thermostatted cell holder equipped with a magnetic stirrer. All intensities were repeated at least three times on different days and the results averaged.

For fluorescence anisotropy, at least three readings were collected over a 0.1 s integration time each and averaged. Anisotropy values were obtained in triplicate and automatically calculated from Eq. 1:

$$A = \frac{I_{\parallel} - I_{\perp}}{I_{\parallel} + 2I_{\perp}} \quad (1)$$

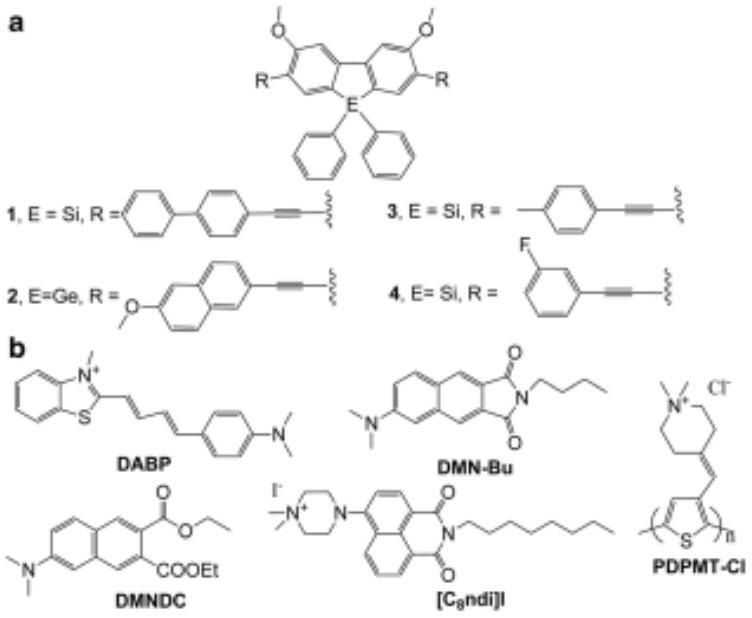

Fig. 1 a Structures of metallafluorenes in this study. b Examples of fluorescent surfactant indicators [3, 7–9]

where I is the recorded intensity at the indicated polarizer orientations and A is the anisotropy. This experiment was repeated at least three times on different days and the results averaged.

Emission spectra collected in the presence of salts (Na_2HPO_4, K_2HPO_4, $CaCl_2$, $ZnCl_2$, NH_4Cl, $(NH_4)_2SO_4$, $MgSO_4$) were conducted at 1 mM salt (a common concentration used in the literature [6] and 1 μM MF. $ZnCl_2$ results in MF precipitation and therefore these data were not reported.

Quantum yield was measured using the previously reported relative method [11] at an excitation wavelength of 350 nm using a range of absorbances. Absorbances were kept below 0.1 to minimize non-linear effects [12]. The fluorescence spectra were recorded from 375 nm to 625 nm at the excitation wavelength of 350 nm. An excitation and emission slit width of 1.0 nm was used. The spectra of the reference standard and the unknown were measured under identical conditions. The slope of the integrated fluorescence intensity versus absorbance was used to calculate the quantum yield using Eq. 2. Coumarin 102 dye in ethanol, with a ϕ_f of 0.764 [13], was used as the reference standard for all determinations.

$$\phi_{unknown} = \phi_{standard}\left(\frac{m_{unknown}}{m_{standard}}\right)\left(\frac{n_{unknown}}{n_{standard}}\right)^2 \quad (2)$$

where ϕ is the quantum yield, m is the slope of integrated fluorescence intensity against absorbance, and n is the refractive index of the solvent.

Results and Discussion

Structural Features of Metallafluorenes in This Study

The available, previously reported metallafluorenes provide for an initial exploration of aqueous solution behavior (Fig. 1a). MFs with both Si (**1**, **3** and **4**) and Ge centers (**2**) are included; both mono (**3**, **4**) and bicyclic (**1**, **2**), fused (**2**) and not fused (**1**) 2,7 substituents are represented. Importantly for aqueous applications, there is variety in the polarity of this group among these compounds. Of particular interest is **2**, which features a 6-methoxy naphthyl substitution, as naphthyl groups are common in fluorophores that interact with surfactants [3, 4, 7, 8].

Group 14 Metallafluorenes are Soluble and Luminescent in Aqueous Solution

Stock solutions of compounds **1**–**4** were prepared in DMSO as determined by mass. Extinction coefficients were calculated from absorbance spectra and confirmed from the slope of a line fit to absorbance data as a function of concentration. See Table 1. These extinction coefficients were then used to prepare solutions for the remainder of the study. Despite significant hydrophobic character, if dispensed from a DMSO stock near 1 mM, these MFs are water soluble in the low micromolar range, sufficient for spectroscopic work.

Table 1 Optical properties of metallafluorenes 1–4 in aqueous solution

Compd	ε^a M^{-1} cm^{-1}	Abs $\lambda_{max}{}^b$ nm	Em $\lambda_{max}{}^b$ nm	Stokes Shift nm
1	28,300	387	453	66
2	73,400	390	483	87
3	59,700	376	465	89
4	56,400	376	464	88

[a] In DMSO at Abs λ_{max}. [b] Conditions: 10 mM Tris, 5 % DMSO, pH 8.0, 25 °C

From DMSO stocks, aqueous solutions were prepared in 10 mM Tris buffer, pH 8.0 (a common biological buffer) with 5 % or less of DMSO and both absorbance and emission spectra obtained. It is clear from Fig. 2 that the 2,7 substituent provides an optical tunability of spectra in aqueous solution of up to 14 nm (376–390 nm) at absorption. The same is true of emission, but here the range is 30 nm. **1** is the most blue shifted of the group, while **2** is the most red shifted. Indeed, using https://www.molinspiration.com/cgi-bin/properties to compute logP for the 2,7 substituents confirms that the biphenyl substituent is the most lipophilic (hydrophobic) with a logP of 4.31 and the tolyl and phenylfluorine substituents are the least lipophilic (2.96 and 2.65, respectively). While the methoxynaphthyl substituent has a high logP value (3.73), it is the only one of this series with a Ge center. Stokes shifts range from 66 to 89 nm. Spectroscopic parameters are summarized in Table 1.

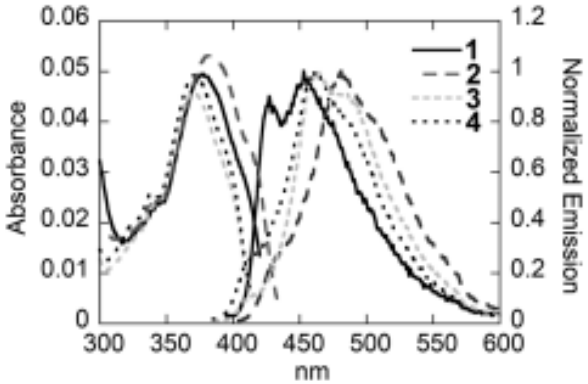

Fig. 2 Absorption and emission spectra of **1**–**4** in aqueous solution. Conditions: 10 mM Tris, pH 8.0, 0.5–0.8 % DMSO, 25 °C. All MF concentration are 1 μM, but due to lower ε, the absorbance of **1** is adjusted mathematically for easy comparison. Excitation wavelengths were at the absorption maximum with 1 nm slitwidth (Table 1)

Metallafluorene Spectroscopic Behavior in the Presence of Surfactants

Absorption Behavior

The hydrophobicity of the MFs suggests that they could interact with detergents/surfactants. To explore this, absorption spectra were collected for **1**–**4** in the presence of 5 surfactants that vary with respect to charge at a concentration above their respective CMC values (TX, CHAPS, CTAB, SDS, and SDBS; see Table S1 for a summary of properties). In all cases, the spectrum of the surfactant itself is subtracted from that of the mixture (Fig. 3). TX elicited the largest enhancements in absorbance, and in the case of **2** and **3**, the absorbance approached that obtained in DMSO. The spectral absorbance changes are the most interesting with **2** and **4**. For these MFs, changes in peak shape are also observed. CTAB introduces scatter for **4** (see intensity between 425 and 450 nm) relative to CTAB itself, the contribution of which has been subtracted. This suggests a change in particle size and thus a direct interaction that affects both the MF and the surfactant (see "Probing Metallafluorene-surfactant Interactions" section for more detail). In contrast, the spectral responses to the anionic surfactants SDS and SDBS were very small to insignificant for all four MFs. This is typical among fluorescent surfactant indicators [3–5, 9].

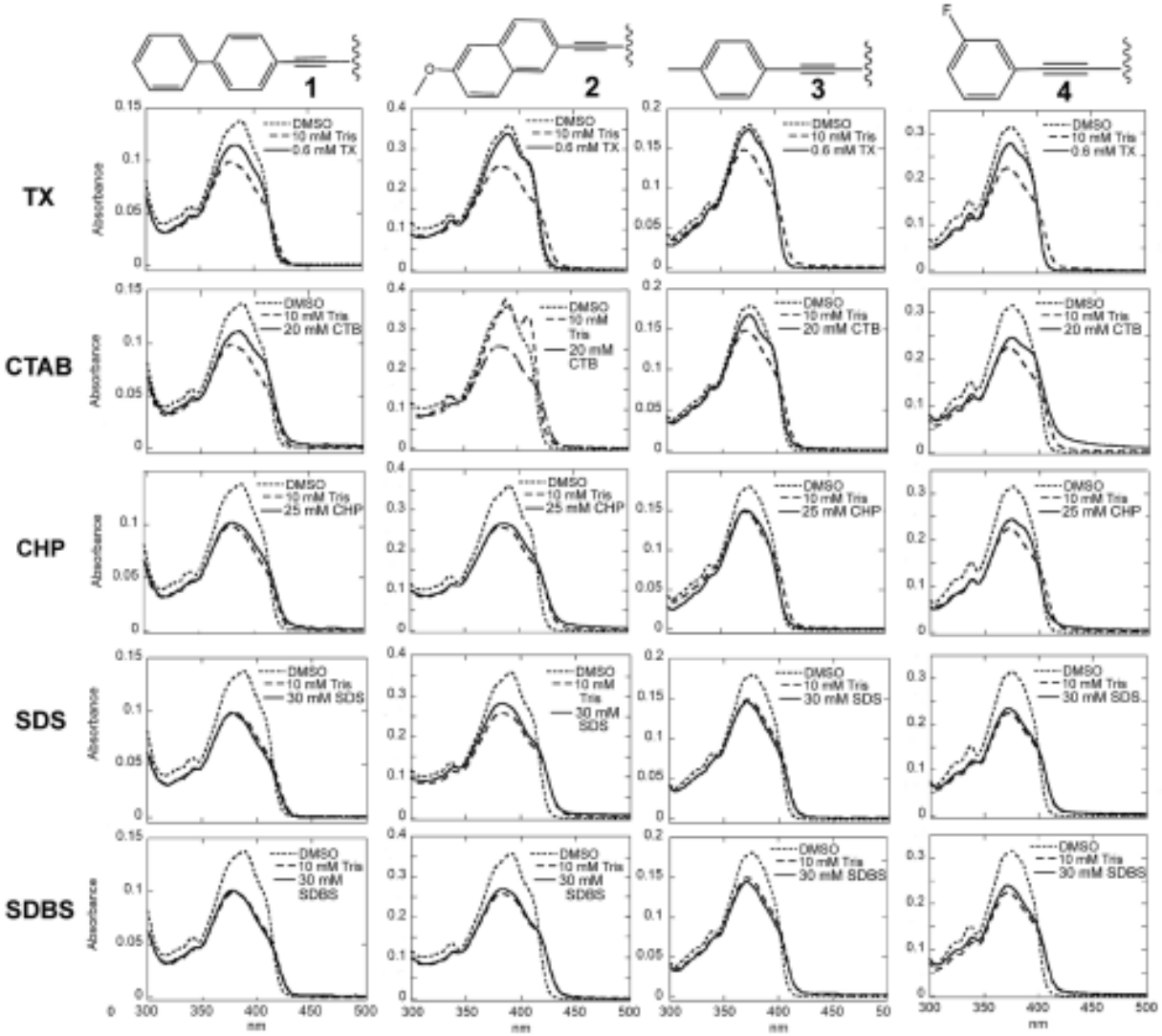

Fig. 3 Absorption spectral behavior of **1**–**4** in aqueous solution upon the addition of surfactants. Conditions: 5 μM MF, 10 mM Tris, pH 8.0, 0.5 % DMSO, 25 °C, 0.6 mM TX, 25 mM CHAPS, 20 mM CTAB, 30 mM SDS, and 10 mM SDBS

Emission Behavior

Figure 4 visually summarizes the effects of various surfactants (above their CMC) on the emission behavior of **2**. Using emission in buffer and DMSO as references, it is clear that for this MF, CTAB and TX induce the greatest emission enhancements upon excitation at 350 nm, while the anionic detergents show little enhancement.

This is reflected in the spectral data summarized in Figs. 5 and 6, and Table 2 for all four compounds. In general, the spectral responses to TX are the most dramatic: a large blue shift is observed in all cases (37–63 nm of lambda max), which is consistent with an interaction between the MF and the surfactant that reduces exposure to aqueous solvent and its relaxation effects. In addition, probably due to the same effect, the electronic transitions are quite distinct in the spectra. Further, the fold emission enhancements are large (6–19 fold). Given that TX is a neutral and aromatic surfactant, this seems reasonable and is comparable to that observed with other indicators [8, 14].

Similar effects are also observed for **2** and **3** towards CHAPS and CTAB, and fold enhancements are similar to that for TX. A standout is **1**, which shows a 25-fold enhancement in the presence of CTAB. In contrast, λ_{max} shifts and emission enhancements are small or negligible upon the addition of anionic surfactants SDS and SDBS to all compounds. This is consistent with the literature [4, 6, 9, 10].

Effect of Surfactants on Metallafluorene Quantum Yields

Quantum yields (ϕ) were measured using coumarin 102 in ethanol as a standard as described in Materials and Methods section. As summarized in Table 3, ϕ values in Tris buffer range from 0.09 to 0.34. On the low end are **2** and **4**. ϕ values for these in water fall in a similar range with common probes 8-Anilinonaphthalene-1-sulfonic acid (ANS; 0.004; [15]), tryptophan (0.13; [16]), and coumarin (0.09; [17]), as well as with DMNDC (0.01; [8]). However, for **3** and **4**, ϕ in water is relatively high (near 0.3). Common xanthene dyes like Rhodamine B and Texas Red have quantum yields of 0.31 and 0.35 in water [18], which is considered respectable for biological probes. **4** has a comparable quantum yield to this family of dyes and a greater quantum yield than dyes like Cy3 and Cy5 (quantum yields 0.04 and 0.27, respectively) [19] and the surfactant indicator N-n-octyl-4-(1-methylpiperazine)-1,8-naphthalimide iodide (0.24; [3]).

ϕ values are at almost 100 % quantum efficiency in the presence of TX and CTAB, indeed higher than in the organic solvent DCM, and ϕ values for all but **2** are above 0.8 in CHAPS. The ϕ values in the presence of anionic surfactants are much lower (0.38–0.55), but all of these are higher than any observed in buffer alone.

Effect of Ions on Metallafluorene Emission Behavior

To address specificity of emission enhancements induced by surfactants, the effects of various ions on MF emission were examined. As summarized in Fig. 7, generally very small reductions in emission were observed. And while they are the same scale as the enhancements observed in the presence of anionic surfactants, they are dwarfed by the changes upon the addition of TX, CTAB, and CHAPS. Thus the response to ions is very small and in an opposite direction to those observed for surfactants, indicating a high degree of specificity toward surfactants.

Probing Metallafluorene-surfactant Interactions

The above data suggest an interaction between MFs and surfactant micelles. To probe this possibility, MF anisotropies

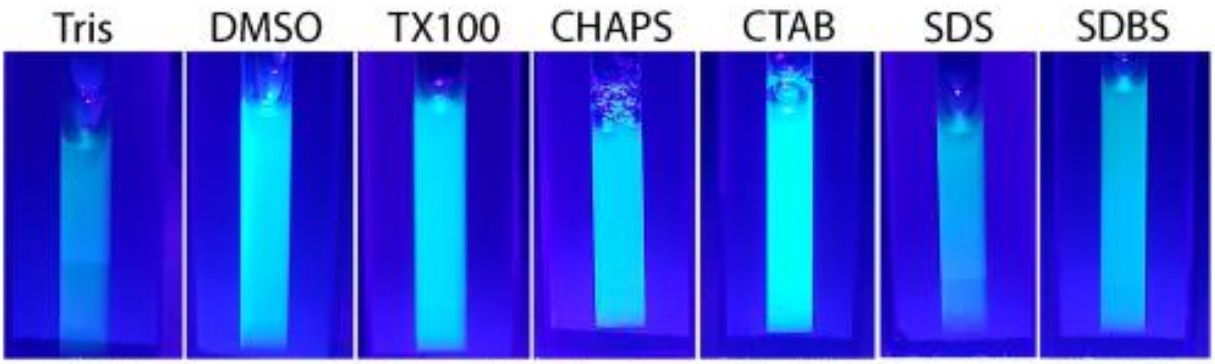

Fig. 4 Visible luminescence upon excitation at 350 nm of 5 μM of **2** in 10 mM Tris buffer pH 8 and 0.5 % DMSO alone and also in the presence of various surfactants at room temperature: TX, 0.6 mM; CHAPS: 25 mM; CTAB, 20 mM; SDS, 30 mM; SDBS, 10 mM. All of these surfactant concentrations are above their respective CMC values

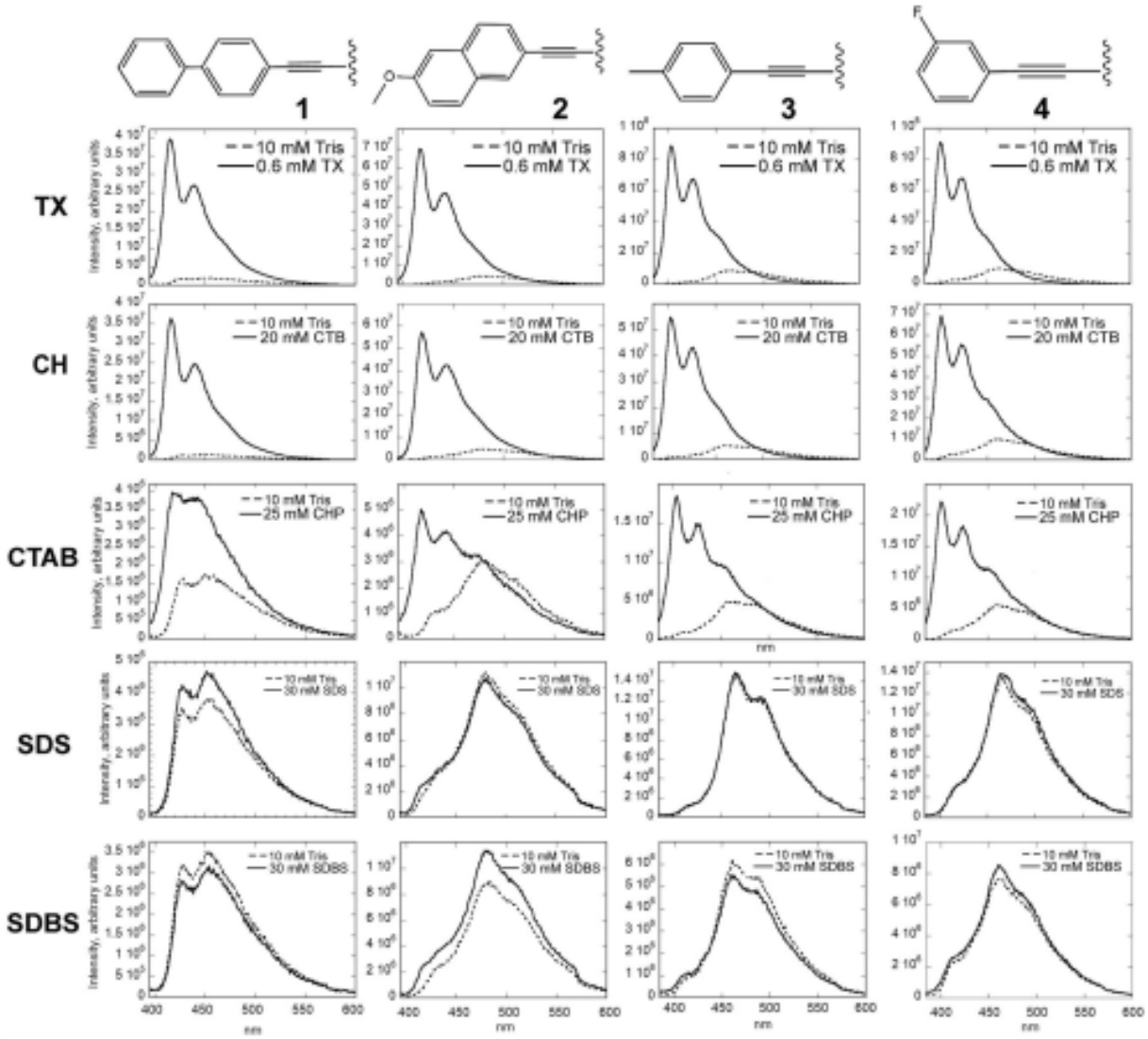

Fig. 5 Effect of Various surfactants on metallafluorene emission spectra. 1 mM MF in 10 mM Tris, 0.5 % DMSO, pH 8.0, 25 °C, with as indicated 0.6 mM TX, 25 mM CHAPS, 20 mM CTAB, 30 mM SDS, 10 mM SDBS. All of these surfactant concentrations are above their respective CMC value

Table 2 Effects of surfactants on metallafluorene emission[a]

Comp	TX		CTAB		CHAPS		SDS		SDBS	
#	λ[b]	FE[c]	λ[b]	FE[c]	λ[b]	FE[c]	λ[b]	FE[c]	λ[b]	FE[c]
1	38	19±0	37	25±10	37	2.0±0.6	2	1.1±0.1	2	0.9±0.02
2	63	13±2	63	12±0	63	1.7±0.04	1	1.0±0.2	0	1±0.1
3	58	13±5	58	9±3	62	3.3±0.4	0	0.9±0.2	3	1±0.4
4	60	10±1	60	5±2	2	4.0±0.2	1	1.1±0.2	1	1.1±0.3

[a] Conditions: 1 μM MF, 10 mM Tris pH 8.0; 0.5 % DMSO, 25 °C. TX, 0.6 mM; CHAPS, 25 mM; CTAB, 20 mM; SDS, 30 mM; SDBS, 10 mM. All of these surfactant concentrations are above their respective CMC.[b] Lambda refers to shift in nm of λ_{max} upon the addition of surfactant.[c] Fold enhancement is calculated by dividing the maximum emission with surfactant by the maximum emission in the absence of surfactant with a 3 min incubation

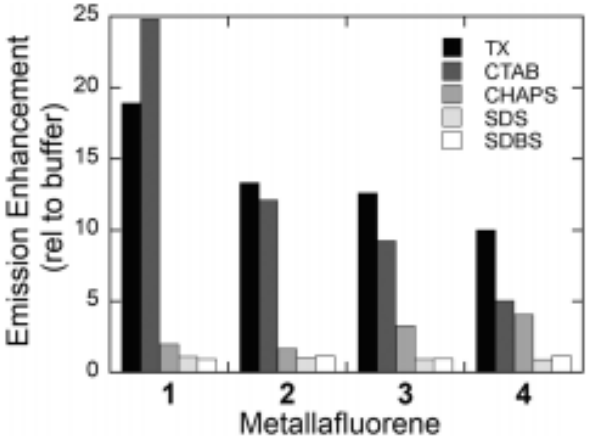

Fig. 6 Summary of emission metallafluorene enhancements induced by surfactants. 1 μM MF, 10 mM Tris, 0.5 % DMSO, pH 8.0, 25 °C. Conditions as in Table 2

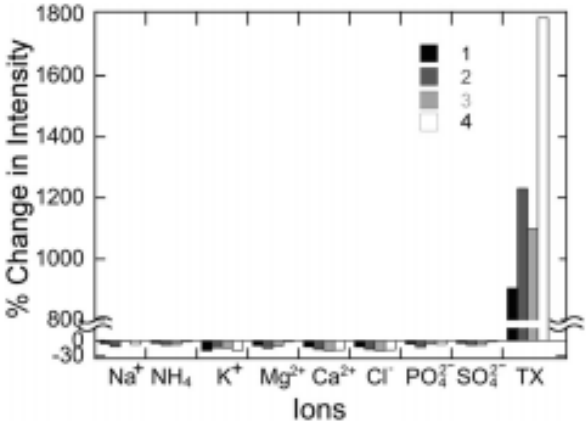

Fig. 7 Effects of ions on metallafluorene fluorescence. Conditions: 1 μM MF, 1 mM salt, 10 mM Tris, pH 8.0, 0.5 % DMSO, 25 °C. TX concentration is 0.6 mM

were collected in the presence and absence of surfactant (Fig. 8). When MFs are added to TX, CHAPS, and CTAB, there is an obvious large increase in anisotropy. This is consistent with association of MF with the surfactant micelle. Coupled with spectral changes (blue shifts), fold enhancements and quantum yields, these data are consistent with substantial protection of MFs from polar solvent and its relaxation effects. This is in sharp contrast to the effect of anionic surfactants, which generally result in lower fold-enhancements, quantum yields, and anisotropies. This latter pattern is consistent with either weak interactions with aggregates or an association with smaller surfactant structures that provide little to no protection from solvent relaxation and no evidence that MFs are highly sequestered in hydrophobic environments.

To better understand the interaction of MF with a surfactant micellar surface, TX was titrated into **4**. As shown in Fig. 9, emission increases dramatically at 200 μM, commonly reported as the CMC of TX [8, 20]. This is also consistent with a sensitivity toward aggregates surfaces and thus a direct interaction with them.

Conclusions

The results here demonstrate the potential of MFs as probes of surfactants. First, substitution at the 2,7 position offers an opportunity to tune desirable properties that could include water solubility as well as electronic properties that could include λ_{max} and quantum yield. Second, they have sufficient water solubility and favorable luminescence behaviors for use in aqueous solution. Third, the differences in MF responses to various surfactants suggest sensitivities to surfactant charge, aggregate size, and CMC [3, 5, 7], any of which could make them useful probes of these properties. **1** exhibits the highest fold enhancements toward neutral and cationic surfactants; **2** exhibits the most distinct spectral responses to the various surfactants. Both have bicyclic 2,7 substituents and suggest a pathway for the development of second-generation MF probes.

We hypothesize that these compounds are intramolecular charge transfer (ICT) dyes that contain an electron rich moiety and electron deficient moiety connected by conjugated bonds. As an ICT dye, they may have future applications as aggregation-induced emission enhancing probes for protein, nucleic acid, and polysaccharide detection [21]. Given their

Table 3 Effect of surfactants on metallafluorene quantum yield ϕ [a]

Compd	10 mM Tris pH 8	TX	CTAB	CHAPS	SDS	SDBS	DCM[b]
1	0.11±0.016	0.94±0.05	0.92±0.08	0.90±0.02	0.49±0.09	0.38±0.13	0.80
2	0.094±0.011	0.85±0.06	0.97±0.03	0.52±0.01	0.38±0.06	0.46±0.006	0.75
3	0.24±0.013	0.97±0.04	1.01±0.11	0.80±0.08	0.53±0.03	0.55±0.01	0.89
4	0.34±0.005	1.00±0.04	0.92±0.08	0.90±0.02	0.49±0.09	0.38±0.13	0.80

[a] Conditions: 1 μM MF, 0.6 mM TX, 20 mM CTAB, 25 mM CHAPS, 30 mM SDS, 10 mM SDBS in 10 mM Tris, pH 8.0, 5 % DMSO, 25 °C. [b] From Hammerstroem et al. [1, 2]

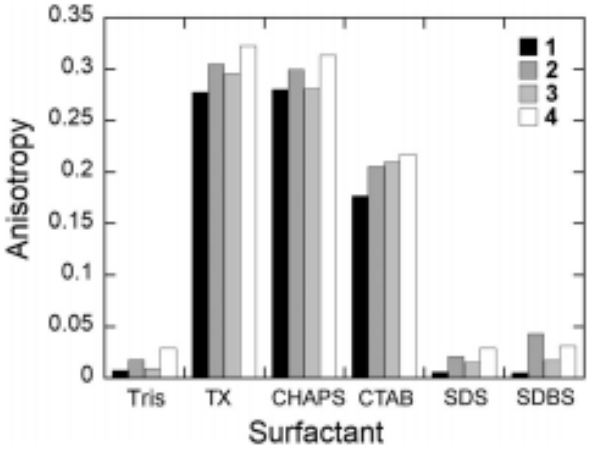

Fig. 8 Anisotropies of metallafluorenes in the presence of surfactants. Conditions: 1 μM MF, 10 mM Tris, pH 8.0, 0.5 % DMSO, 25 °C, 0.6 mM TX, 20 mM CTAB, 25 mM CHAPS, 30 mM SDS, 10 mM SDBS. Anisotropies were collected in triplicate with an error of no more than 10 %

sensitivity to surfactant aggregates, MFs would be especially useful probes of the properties of lipids and biological membranes. This could include detecting changes in local membrane lipid composition in response to a molecular or cellular stimulus [22] as well as imaging cellular structures that have differing lipid compositions [22]. There are also potential applications in probing protein behavior through the detection of conformational changes (that often involve changes in accessible nonpolar surface area) [23]. Finally, through conjugation with a biomolecule of interest, MFs could be used to measure proximity or distance via FRET with chromophores located on biomolecular binding partners (e.g., lipids, proteins, and nucleic acids) [24]. Investigations into the electronic mechanisms of these MFs and their potential applications are ongoing.

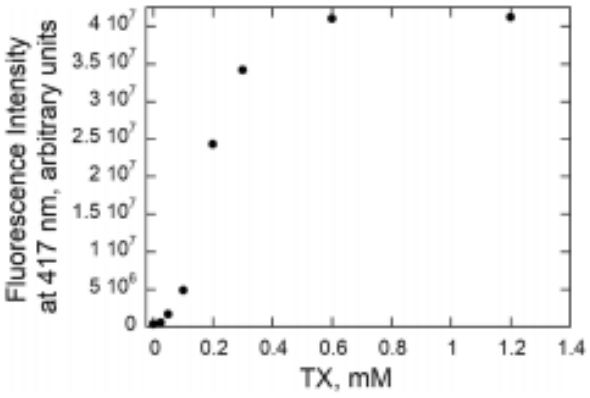

Fig. 9 Equilibrium titration of TX into MF. Conditions: 1 mM **4**, 10 mM Tris, pH 8.0, 0.5 % DMSO, 25 °C

Abbreviations CHAPS, 3-[(3-Cholamidopropyl)dimethylammonio]-1-propanesulfonate; CMC, critical micelle concentration; CTAB, cetyltrimethylammonium bromide; SDS, sodium dodecyl sulfate; SDBS, Sodium dodecylbenzenesulfonate; MF, metallafluorene; TX, Triton X-100

Supplementary Information The online version contains supplementary material available at https://doi.org/10.1007/s10895-021-02730-3.

Author Contributions All authors contributed to the study conception and design. Material preparation, data collection and analysis were performed by Helena Spikes, Shelby Jarrett-Noland and Stephan Germann. The first draft of the manuscript was written by Cynthia Dupureur and all authors commented on previous versions of the manuscript. All authors read and approved the final manuscript.

Funding This work was supported by the National Science Foundation (to Janet Braddock-Wilking) CHE-1362431.

Data Availability The datasets generated during and/or analyzed during the current study are available from the corresponding author on reasonable request.

Declarations

Conflict of Interest The authors have no conflicts of interest to declare that are relevant to the content of this article.

References

1. Hammerstroem DW, Braddock-Wilking J, Rath NP (2016) Synthesis and characterization of luminescent 2,7-disubstituted silafluorenes. J Organomet Chem 813:110–118
2. Hammerstroem DW, Braddock-Wilking J, Rath NP (2017) Luminescent 2,7-disubstituted germafluorenes. J Organomet Chem 830:196–202
3. Zhao Y, Li X (2014) Detecting themicellization of anionic surfactants by a colorimetric and fluorescent probe based on electrostatic attraction. Colloid Polym Sci 292:1577–1584
4. Zhao Y, Li X (2015) Colorimetric and fluorometric detection of anionic surfactants withwater soluble sensors. Sens Actuators B Chem 209:258–264
5. Vasu A, Kanvah S (2017) Red-emitting cationic fluorophore as a probe for anionic surfactants. Dyes Pigm 142:230–236
6. Qian J, Qian X, Xu Y (2009) Selective and sensitive chromo- and fluorogenic dual detection of anionic surfactants in water based on a pair of "On–Off–On" fluorescent sensors. Chem Eur J 15:319–323
7. Mallick S, Arathi A, Koner AL (2017) Customized tuning of aggregation-induced emission of a napthalimide dye by surfactants and cyclodextrin. J Coll Interface Sci 499:46–53
8. Mallick S, Pal K, Koner AL (2016) Probing microenvironment of micelle and albumin using diethyl 6-(dimethylamino)naphthalene-2,3-dicarboxylate: An electroneutral solvatochromic fluorescent probe. J Coll Interface Sci 467:81–89
9. Li E, Lin L, Wang L, Pei M, Xu J, Zhang G (2012) Synthesis of a new cationic polythiophene derivative and its application for colorimetric and fluorometric detection of iodide ion and anionic surfactants in water. Macromol Chem Phys 213:887–892
10. Hussain S, Malik A, Iyer P (2015) Highly precise detection, discrimination, and removal of anionic surfactants over the full pH Range via cationic conjugated polymer: an efficient strategy to

facilitate illicit-drug analysis. ACS Appl Mater Interfaces 7:3189–3198
11. Würth C, Grabolle M, Pauli J, Spieles M, Resch-Genger U (2013) Relative and absolute determination of fluorescence quantum yields of transparent samples. Nat Protoc 8:1535–1550
12. Dhami S, de Mello AJ, Rumbles G, Bishop SM, Phillips D, Beeby A (1995) Phthalocyanine fluorescence at high concentration: dimers or reabsorption effect? Photochem Photobiol 61:341–346
13. Rurack K, Spieles M (2011) Fluorescence quantum yields of a series of red and near-infrared dyes emitting at 600 – 1000nm. Anal Chem 83:1232–1242
14. Long S, Qiao Q, Deng F, Miao L, Yoon J, Xu Z (2019) Self-assembling nanoprobes that display two-dimensional fluorescent signals for identification of surfactants and bacteria. Chem Commun 55:969–972
15. Stryer L (1968) Fluorescence spectroscopy of proteins. Science 162:526–533
16. Chen R (1967) Fluorescence quantum yields of tryptophan and tyrosine. Anal Lett 1:35–42
17. Jones I, Rahman G (1994) Fluorescence properties of coumarin laser dyes in aqueous polymer media. chromophore isolation in poly(methacrylic acid) hypercoils. J Phys Chem 98:13028–13037
18. Magde D, Rojas G, Seybold P (1999) Solvent dependence of the fluorescence lifetimes of xanthene dyes. Photochem Photobiol 70:737–744
19. Mujumdar RB, Ernst LA, Mujumdar SR, Lewis CJ, Waggoner AS (1993) Cyanine dye labeling reagents: sulfoindocyanine succinimidyl esters. Bioconjug Chem 4:105–111
20. Mohr A, Talbiersky P, Korth H-G, Sustmann R, Boese R, Blaser D, Rehage H (2007) A new pyrene-based fluorescent probe for the determination of critical micelle concentrations. J Phys Chem B 111:12985–12992
21. Klymchenko AS (2017) Solvatochromic and fluorogenic dyes as environment-sensitive probes: design and biological applications. Acc Chem Res 50:366–375
22. Sezgin E, Levental I, Mayor S, Eggeling C (2017) The mystery of membrane organization: composition, regulation and roles of lipid rafts. Nat Rev Mol Cell Biol 18:361–374. https://doi.org/10.1038/nrm.2017.16
23. Royer CA (2006) Probing protein folding and conformational transitions with fluorescence. Chem Rev 106:1769–1784
24. Algar WR, Hildebrandt N, Vogel SS, Medintz IL (2019) FRET as a biomolecular research tool - understanding its potential while avoiding pitfalls. Nat Methods 16:815–829

Appendix 2

Group 14 Metallafluorenes for Lipid Structure Detection and Cellular Imaging

chemistry proceedings

MDPI

Proceeding Paper

Group 14 Metallafluorenes for Lipid Structure Detection and Cellular Imaging †

Helena J. Spikes, Shelby J. Jarrett-Noland, Stephan M. Germann, Wendy Olivas, Janet Braddock-Wilking and Cynthia M. Dupureur *

Department of Chemistry & Biochemistry, University of Missouri St. Louis, St. Louis, MO 63121, USA; hjs7c5@mail.umsl.edu (H.J.S.); sjdzd@umsystem.edu (S.J.J.-N.); smg8v5@mail.umsl.edu (S.M.G.); olivasw@umsl.edu (W.O.); wilkingj@umsl.edu (J.B.-W.)

* Correspondence: cdup@umsl.edu; Tel.: +1-314-516-4392

† Presented at the 1st International Electronic Conference on Chemical Sensors and Analytical Chemistry, 1–15 July 2021; Available online: https://csac2021.sciforum.net/.

Abstract: Fluorescent compounds have been shown to be useful in probing lipid dynamics, and there is ongoing interest in nontoxic, photostable, and sensitive dyes. Recently, we evaluated a number of 2,7-disubstituted-alkynyl(aryl)-3,6-dimethoxy-9,9-diphenyl sila- and germafluorenes for their potential as cellular fluorescent probes. These compounds exhibit remarkable quantum yields in hydrophobic environments and dramatic increases in emission intensity in the presence of surfactants. Here, we show that they exhibit significant emission enhancements in the presence of small unilamellar vesicles and are nontoxic to *E. coli*, *S. aureus*, and *S. cerevisiae*. Furthermore, they luminesce in *S. cerevisiae* cells with strong photostability and colocalize with the lipid droplet stain Nile Red, demonstrating their promise as lipid probes.

Keywords: fluorescence; lipid; metallafluorene

check for updates

Citation: Spikes, H.J.; Jarrett-Noland, S.J.; Germann, S.M.; Olivas, W.; Braddock-Wilking, J.; Dupureur, C.M. Group 14 Metallafluorenes for Lipid Structure Detection and Cellular Imaging. *Chem. Proc.* 2021, *5*, 83. https://doi.org/10.3390/CSAC2021-10455

Academic Editor: Nicole Jaffrezic-Renault

Published: 30 June 2021

1. Introduction

The introductory understanding of the role of biological membranes is that they are barriers and are used to regulate transport and for energy processes. Only fairly recently has there been a developing understanding that membranes are dynamic in their lipid composition and properties, and that these local differences participate in cellular processes in a profound way and have been linked to disease states [1,2], including cellular stress [3].

Fluorescence spectroscopy is an accessible and powerful tool for the sensing of molecules and their behaviors, including binding interactions, conformational changes, and catalytic activities, in both *in vitro* and *in vivo* via cellular imaging [4]. Due to their ability to respond to changes in molecular environment, molecules that exhibit intramolecular charge transfer (ICT) or excited-state intramolecular proton transfer (ESIPT) are particularly attractive as probes of lipids, their interactions, and dynamics [5,6].

Probes commonly used for such purposes include Nile Red, dansyl, NBD [7], and F2N12S [6]. These vary with respect to relevant properties such as the excitation and extinction wavelength, extinction coefficient, working concentration (sensitivity), photostability, and quantum yield, all of which can impact their utility. When this is coupled with the rapidly expanding research area, it is no surprise that a call for more probes to meet expanding needs is prominently articulated [5].

Recently, we evaluated a small library of sila- and germafluorenes (metallafluorenes or MFs) containing alkynyl(aryl) substituents at the 2,7-position ([8,9]; Figure 1) for their potential as fluorescent probes of surfactants. These compounds are soluble and luminescent in aqueous solution and exhibit high quantum yields and dramatic emission enhancements in the presence of various surfactants (5–25-fold) [10]. These results suggest that MFs could have biological applications. Here, we examine the sensitivity, toxicity, and

photostability of MFs toward lipids both *in vitro* and *in vivo* and demonstrate the potential of these compounds as lipid probes. Indeed, they are sensitive to DOPC small unilamellar vesicles (SUVs) with significant fluorescence enhancements. These dyes show no toxicity to Gram-positive bacteria, Gram-negative bacteria, and yeast cells and demonstrate high photostability. When compared to the commercially available lipid droplet dye Nile Red, these MFs show strong colocalization with more punctate staining, demonstrating their potential as lipid probes.

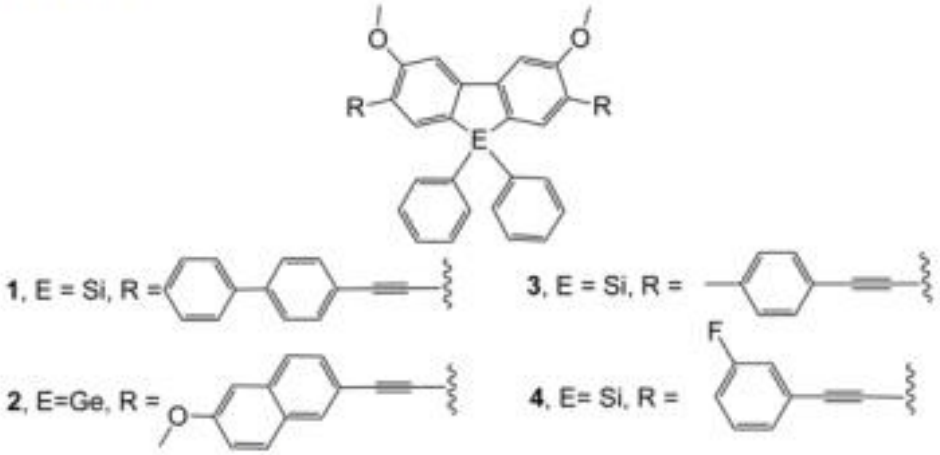

Figure 1. Structures of 2,7-disubstituted sila- and germafluorenes used in this study. 1 silicon based 4-ethynyl-1,1′-biphenyl substitutent; 2 germanium based 2-ethynyl-6-methoxynaphthalene substitutent; 3 silicon based 4-ethynyltoluene substitutent; 4 silicon based 1-ethynyl-3-fluorobenzene substitutent.

2. Materials and Methods

2.1. Materials

Phospholipids were purchased from Avanti Polar Lipids (Alabaster, AL, USA). Two-hundred-proof ethanol was purchased from Decon Labs (King of Prussia, PA, USA). DMSO and Nile Red were obtained from Millipore Sigma (Milkwaukee, WI, USA). p-Xylene was obtained from ThermoFisher (Waltham, MA, USA). All chemicals were of reagent grade and were used as received without further purification. Compounds **1**–**4** were synthesized as previously described using an appropriate alkynyl(aryl) precursor in a palladium-catalyzed Sonagashira cross-coupling reaction [8,9] and dispensed from stocks in DMSO as previously described [10].

2.2. Preparation of Small Unilamellar Vesicles (SUVs)

At 25 °C, a stock concentration of 4.2 mM DOPC was prepared by drying under inert gas and then resuspended in 10 mM Tris buffer. After 30 min, DOPC was sonicated for 27 min at 25 °C until cloudy. The DOPC-SUV solution was then passed through an Avanti Mini Extruder eleven times to make uniformly sized 0.1 µm DOPC-SUVs at 25 °C. DOPC-SUVs were then diluted to 0.1 mM in a quartz cuvette for fluorescence measurements [11,12].

2.3. Spectroscopy

Absorbance spectra were recorded on a Shimadzu 1800 (Kyoto, Japan) with slits (bandpass) set to 1 nm. Emission spectra were collected in an acid-washed quartz cuvette on a Fluorolog-3 (SPEX) spectrofluorimeter (Horiba Scientific, Piscataway, NJ, USA). The temperature was maintained at 25 °C with a thermostatted cell holder equipped with a magnetic stirrer. Emission spectra were collected with the indicated excitation wavelength and slits (bandpass). MF photostability in xylene was observed at the indicated emission maximum.

2.4. Microbial Toxicity

Culture tubes containing LB media or YPD media were inoculated with *Escherichia coli* (Gram-negative), *Staphylococcus aureus* (Gram-positive), or *Saccharomyces cerevisiae*, respectively. Compounds **1–4** were added such that the final DMSO concentration was 2–10% and the MF at its solubility limit in the media. The tubes were incubated at either 37 °C (bacteria) or 30 °C (yeast) overnight and visually inspected for growth.

2.5. Confocal Laser Scanning Microscopy

Samples were prepared by smearing a small amount of cells onto a glass microscope slide and heat-fixed by passing the slide through a flame no more than 5 times. Then, **1–4** or NR was applied to heat-fixed cells at 15 μM and incubated at room temperature for 15 min for MFs and 10 min for Nile Red. Slides were then rinsed with 2–3 mL of deionized water, topped with coverslips, and sealed with clear nail polish. Cells were imaged with a Zeiss LSM 900 (Zeiss, Oberkochen, Germany) confocal microscope with an excitation wavelength of 405 nm. For photostability, the sample was illuminated with 1% laser power and images collected periodically.

3. Results and Discussion

3.1. Spectroscopic Studies

To assess their sensitivity to a biologically relevant membrane, the emission spectra of **1–4** were compared in the absence and presence of DOPC-SUVs. As shown in Figure 2, fold-enhancements range from two- to sevenfold, with **1** and **2** showing the most dramatic changes.

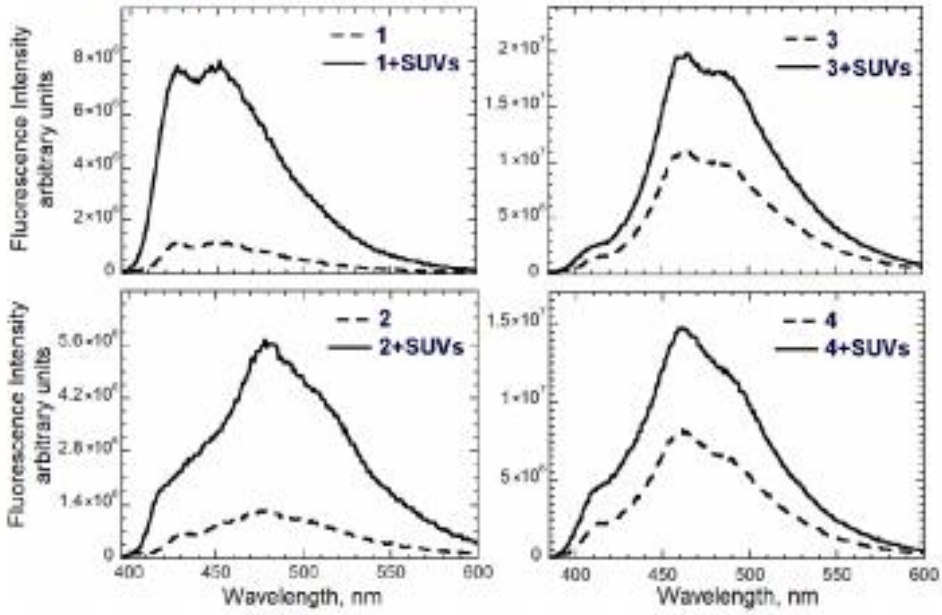

Figure 2. Emission spectra of MFs **1–4** (as numbered in Figure 1) in the absence (dashed) and presence (solid) of 0.1 mM DOPC-SUVs. Conditions: 1 μM MF, 0.1 mM DOPC, 10 mM Tris pH 8, 25 °C. The excitation wavelength was 387 nm and the slits (bandpass) set to 1.0 nm. Three minute incubation.

The photostability of these MFs was initially probed by observing the emission signal as a function of time in xylene, which is used to mimic the interior of membranes [13]. As summarized in Figure 3, these signals are remarkably stable over two hours of continuous excitation. Together, the responsiveness to SUVs and photostability in xylene indicate promise for MFs as probes of lipids *in vivo*.

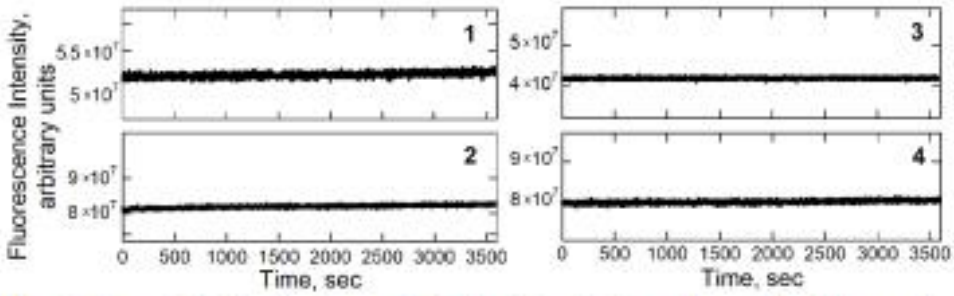

Figure 3. Photostability *in vitro*. Compounds **1**–**4** (as defined in Figure 1) were diluted into p-xylene and excited continuously. Conditions: 1 μM MF, 0.1–0.4% DMSO. 1: excitation at 387 nm, slits 1 nm; 2: excitation at 390 nm, slits 0.8 nm; 3: excitation at 376 nm, slits 0.9 nm; 4: excitation at 376 nm, slits 0.9 nm.

3.2. *Microbial Toxicity Studies*

To assess their potential for use in cellular imaging, MFs were screened for toxicity against microorganisms. For yeast, *E. coli* and *S. aureus*, no inhibition of growth was observed at the MF solubility limit in media (at least 50 μM).

3.3. *Imaging of S. cerevisiae with Metallafluorenes*

To determine if these MFs can be used to stain cells, **1**–**4** were introduced to yeast cells and subsequently imaged using confocal microscopy. Figure 4 illustrates that in all cases, the MF emission intensity is visible inside fixed yeast cells.

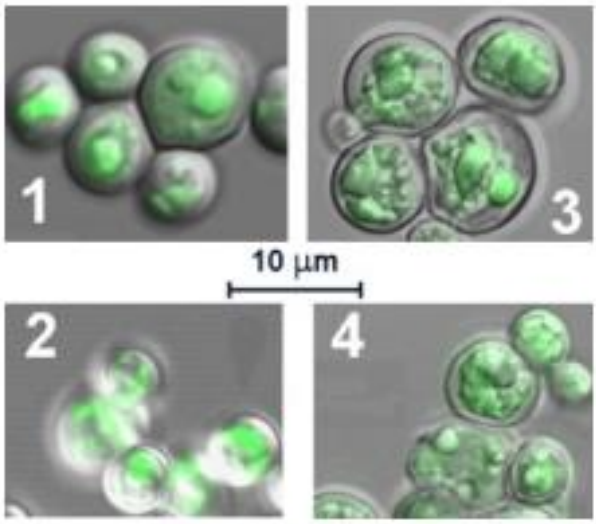

Figure 4. Confocal imaging of MFs **1**–**4** in yeast cells. Conditions: 15 μM MF as indicated, 63×. The excitation wavelength was 405 nm and scan range 400–600 nm. Numbers refer to MFs as defined in Figure 1.

To assess the MF photostability in yeast cells, excitation was applied and fluorescence was observed as a function of time. As summarized in Figure 5 for **1** and **2**, fluorescence persisted for over 2 min, with **2** showing greater photostability. See Supplemental Figure S1 for photostability studies of **3** and **4**.

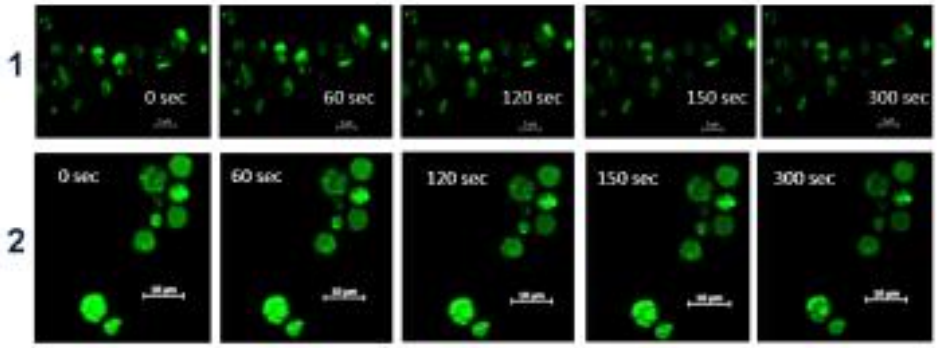

Figure 5. Photostability of 1 and 2 in yeast cells. See Methods for details. *S. cerevisiae* were stained for 15 min with 15 μM 1 or 2 and then imaged periodically during continuous excitation. Magnification is 63×. Numbers at left refer to compounds as defined in Figure 1.

Finally, to determine where these MF localize in yeast, we costained with Nile Red, a well-known lipid droplet stain [14]. As shown in Figure 6, 1 yields more punctate images and colocalizes with this probe, demonstrating clear specificity for *S. cerevisiae* organelles, including the vacuole and possibly lipid granules. See Supplemental Figure S2 for a colocalization study of 2 and 4.

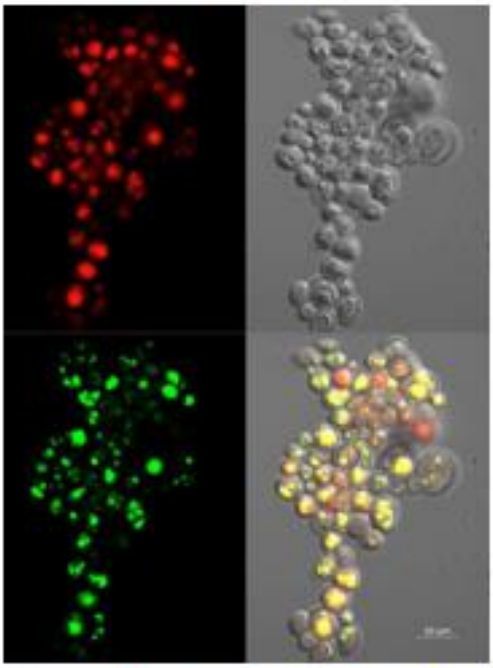

Figure 6. MF 1 colocalizes in yeast with Nile Red. Red, Nile Red; green, 1; top right, transmitted light; bottom right, yellow indicates colocalization. 15 μM probe at 63× magnification.

4. Conclusions

We show here that these metallafluorenes have good photostability and are sensitive to lipid structures *in vitro*, demonstrating impressive fold enhancements in the presence of SUVs. Furthermore, they are non-toxic to cells and can enter cells and colocalize with Nile Red, a lipid probe. In addition, the higher extinction coefficients of MFs and competitive quantum yields [10] make them more sensitive. All of these observations bode well for the application of MFs as lipid probes both *in vitro* and *in vivo*. The synthetic scaffolding of these MFs provides convenient tuning of desired properties by changing the 2,7 substituent.

This feature facilitates designs that incorporate optimal solubility, emission spectra, dipole moment, and solvatochromism for specific applications.

5. Patents

WO/2020/210416; PCT International Patent Application No.: PCT/US2020/027355.

Supplementary Materials: The following are available online at https://www.mdpi.com/article/10.3390/CSAC2021-10455/s1, Figure S1: Photostability of 3 and 4 in Yeast Cells, Figure S2: 2 and 4 Colocalize with Nile Red in Yeast.

Author Contributions: Conceptualization, C.M.D., H.J.S. and S.J.J.-N.; investigation, H.J.S. and S.J.J.-N.; resources, C.M.D., J.B.-W., S.M.G. and W.O.; data curation, S.J.J.-N.; writing—original draft preparation, C.M.D. and H.J.S.; writing—review and editing, C.M.D. and S.J.J.-N.; supervision, C.M.D.; project administration, C.M.D.; funding acquisition, J.B.-W. and C.M.D.; H.J.S. and S.J.J.-N. contributed equally to the preparation of this manuscript. All authors have read and agreed to the published version of the manuscript.

Funding: This work was supported by the National Science Foundation (CHE-1362431 to J.B.-W.).

Data Availability Statement: The data presented in this study are available on request from the corresponding author.

Conflicts of Interest: The authors declare no conflict of interest.

References

1. Levental, I.; Levental, K.R.; Heberle, F.A. Lipid Rafts: Controversies Resolved, Mysteries Remain. *Trends Cell Biol.* 2020, *30*, 341–353. [CrossRef] [PubMed]
2. Carravilla, P.; Nieva, J.L.; Eggeling, C. Fluorescence Microscopy of the HIV-1 Envelope. *Viruses* 2020, *12*, 348. [CrossRef] [PubMed]
3. Ashoka, A.H.; Ashokkumar, P.; Kovtun, Y.P.; Klymchenko, A.S. Solvatochromic Near-Infrared Probe for Polarity Mapping of Biomembranes and Lipid Droplets in Cells under Stress. *J. Phys. Chem. Lett.* 2019, *10*, 2414–2421. [CrossRef]
4. Sedgwick, A.C.; Wu, L.; Han, H.H.; Bull, S.D.; He, X.P.; James, T.D.; Sessler, J.L.; Tang, B.Z.; Tian, H.; Yoon, J. Excited-state intramolecular proton-transfer (ESIPT) based fluorescence sensors and imaging agents. *Chem. Soc. Rev.* 2018, *47*, 8842–8880. [CrossRef] [PubMed]
5. Klymchenko, A.S.; Kreder, R. Fluorescent probes for lipid rafts: From model membranes to living cells. *Chem. Biol.* 2014, *21*, 97–113. [CrossRef] [PubMed]
6. Shynkar, V.V.; Klymchenko, A.S.; Kunzelmann, C.; Duportail, G.; Muller, C.D.; Demchenko, A.P.; Freyssinet, J.M.; Mely, Y. Fluorescent biomembrane probe for ratiometric detection of apoptosis. *J. Am. Chem. Soc.* 2007, *129*, 2187–2193. [CrossRef]
7. Klymchenko, A.S. Solvatochromic and Fluorogenic Dyes as Environment-Sensitive Probes: Design and Biological Applications. *Acc. Chem. Res.* 2017, *50*, 366–375. [CrossRef] [PubMed]
8. Hammerstroem, D.W.; Braddock-Wilking, J.; Rath, N.P. Synthesis and characterization of luminescent 2,7-disubstituted silafluorenes. *J. Organomet. Chem.* 2016, *813*, 110–118. [CrossRef]
9. Hammerstroem, D.W.; Braddock-Wilking, J.; Rath, N.P. Luminescent 2,7-disubstituted germafluorenes. *J. Organomet. Chem.* 2017, *830*, 196–202. [CrossRef]
10. Spikes, H.J.; Jarrett-Noland, S.J.; Germann, S.M.; Braddock-Wilking, J.; Dupureur, C.M. Group 14 Metallafluorenes as Sensitive Luminescent Probes of Surfactants in Aqueous Solution. *J. Fluoresc.* 2021, *31*, 961–969. [CrossRef] [PubMed]
11. Amaro, M.; Filipe, H.A.; Ramalho, J.P.; Hof, M.; Loura, L.M.S. Fluorescence of nitrobenzoxadiazole (NBD)-labeled lipids in model membranes is connected not to lipid mobility but to probe location. *Phys. Chem. Chem. Phys.* 2016, *18*, 7042–7054. [CrossRef] [PubMed]
12. Mazeres, S.; Joly, E.; Lopez, A.; Tardin, C. Characterization of M-laurdan, a versatile probe to explore order in lipid membranes. *F1000Research* 2014, *3*, 172. [CrossRef] [PubMed]
13. Shaya, J.; Collot, M.; Benailly, F.; Mahmoud, N.; Mely, Y.; Michel, B.Y.; Klymchenko, A.S.; Burger, A. Turn-on Fluorene Push-Pull Probes with High Brightness and Photostability for Visualizing Lipid Order in Biomembranes. *ACS Chem. Biol.* 2017, *12*, 3022–3030. [CrossRef] [PubMed]
14. Greenspan, P.; Mayer, E.P.; Fowler, S.D. Nile red: A selective fluorescent stain for intracellular lipid droplets. *J. Cell Biol.* 1985, *100*, 965–973. [CrossRef] [PubMed]